

EVALUATION OF THE REACTIVITY OF ANTHRACITES IN RESPECT TO ITS CHEMICAL AND PETROGRAPHIC CHARACTERISITICS IN AN ILMENITE SMELTING OPERATION

Nirvashnie Bagirathi

A research report submitted to the Faculty of Engineering and the Built Environment, of the University of the Witwatersrand, in partial fulfilment of the requirements for the degree of Master of Science in Engineering.

Johannesburg 2012

DECLARATION

I declare that this research report is my own, unaided work. It is being submitted for the Degree of Masters of Science in the University of the Witwatersrand, Johannesburg. It has not been submitted before for any degree or examination in any University.

Nirvashnie Bagirathi

_____ day of _____ 2012

TABLE OF CONTENTS

ABSTRACT	12
ACKNOWLEDGMENTS	13
1 INTRODUCTION	14
1.1 Background.....	14
1.2 Motivation.....	15
1.3 Objective.....	15
2 LITERATURE REVIEW	16
2.1 Ilmenite reduction.....	16
2.2 Role of anthracite in ilmenite reduction.....	19
2.3 Nature of coal reductants and characterisation	21
3 METHOD OF STUDY	31
3.1 Samples utilised.....	31
3.2 Investigative methodology.....	31
4 EXPERIMENTAL PROCEDURE	33
4.1 Sample preparation.....	33
5 RESULTS AND DISCUSSION.....	37
5.1 Chemical analysis of the different anthracites	37
5.2 Petrographic analysis of the different anthracites	40
5.3 Comparison of mass loss and fractional conversion against time.....	44
5.4 Comparison of the effect of fixed carbon, volatile matter, ash content and ash oxides on anthracite average apparent reactivity	53
5.5 Comparison of rank, vitrinite, volatile matter (dry basis) and inertinite on anthracite average apparent reactivity.....	64
5.6 Comparison of the effect of temperature on anthracite average apparent reactivity	69

5.7	Evaluation of shrinking core model and activation energy	70
6	CONCLUSIONS	79
7	RECOMMENDATIONS.....	82
8	REFERENCES	83
9	APPENDICES	86
9.1	Anthracite size analysis.....	86
9.2	Reflectance histograms.....	91
9.3	Summary of reactivity results	93
9.4	Raw data.....	94

LIST OF FIGURES

Figure 1 Block flow diagram of Heavy mineral concentrate processing via the smelting route (adapted from Rughubir (2011)).....	17
Figure 2 Schematic of smelting mechanism of ilmenite in a DC arc furnace (Pistorius, 2008 in Jordan, 2009).....	19
Figure 3 Characteristic of thermogravimetric reactivity analysis of New Zealand Coal in CO ₂ at 900°C indicated in Shaw et al (1997).....	29
Figure 4 Characteristic of thermogravimetric reactivity of Mequinenza lignite in dry air at 900°C as indicated in Olivella et al (2002).....	30
Figure 5 Thermogravimetric analyser furnace controllers and data output (adapted from Sooful, 2010)	33
Figure 6 Sample preparation procedure.....	34
Figure 7 First stage sample splitter	
Figure 8 Second stage sample splitter	35
Figure 9 Vitrinite % versus Rank (Mean Random Reflectance %).....	43
Figure 10 Total inertinite % versus Rank (Mean Random Reflectance %)	44
Figure 11 Comparison of mass loss against time at 850°C	45
Figure 12 Fractional conversion of fixed carbon against time at 850°C	46
Figure 13 Comparison of mass loss against time at 1100°C	47
Figure 14 Fractional conversion of fixed carbon against time at 1100°C	47
Figure 15 Comparison of mass loss against time at 1350°C	48
Figure 16 Fractional conversion of fixed carbon against time at 1350°C	49
Figure 17 Comparison of mass loss against time at 1600°C	50
Figure 18 Fractional conversion of fixed carbon against time at 1600°C	50
Figure 19 Mass loss comparison of test of SAA anthracite at 1100°C using current study method against the result obtained by Jordan (2009).....	52
Figure 20 Mass loss comparison of test of R anthracite at 1600°C using current study method against the result obtained by Jordan (2009).....	53
Figure 21 Comparison of fixed carbon against average apparent reactivity at 850°C and 1350°C.....	54
Figure 22 Comparison of fixed carbon against average apparent reactivity at 1100°C and 1600°C.....	55
Figure 23 Comparison of percentage volatile matter content against average apparent reactivity 850°C and 1350°C	56

Figure 24 Comparison of percentage volatile matter content against average apparent reactivity at 1100°C and 1600°C	57
Figure 25 Comparison of ash content against average apparent reactivity at 850°C and 1350°C.....	58
Figure 26 Comparison of ash content against average apparent reactivity at 1100°C and 1600°C.....	58
Figure 27 Comparison of calcium oxide (CaO) against average apparent reactivity at 850°C and 1350°C	59
Figure 28 Comparison of percentage calcium oxide (CaO) against average apparent reactivity at 1100°C and 1600°C	60
Figure 29 Comparison of percentage magnesium oxide (MgO) against average apparent reactivity at 850°C and 1350°C	61
Figure 30 Comparison of percentage magnesium oxide against average apparent reactivity at 1100°C and 1600°C	62
Figure 31 Comparison of percentage silica oxide against average apparent reactivity 850°C and 1350°C	63
Figure 32 Comparison of percentage silica oxide (SiO ₂) against average apparent reactivity 1100°C and 1600°C	64
Figure 33 Comparison of rank against average apparent reactivity at 850°C and 1350°C	65
Figure 34 Comparison of rank against average apparent reactivity at 1100°C and 1600°C	66
Figure 35 Comparison of vitrinite against average apparent reactivity at 850°C and 1350°C	67
Figure 36 Comparison of vitrinite against average apparent reactivity at 1100°C and 1600°C.....	67
Figure 37 Comparison of inertinite content against average apparent reactivity at 850°C and 1350°C.....	68
Figure 38 Comparison of inertinite content against average apparent reactivity at 1100°C and 1600°C.....	69
Figure 39 Plot of average apparent reactivity against temperature.....	70
Figure 40 Plot of shrinking core model against time at 850°C	71
Figure 41 Plot of shrinking core model against time at 1100°C	71
Figure 42 Plot of shrinking core model against time at 1350°C	72

Figure 43 Plot of shrinking core model against time at 1600°C	72
Figure 44 Plot of $1-(1-x)^{1/3}$ against time at 850°C to determine reaction constant of each anthracite.....	73
Figure 45 Plot of $1-(1-x)^{1/3}$ against time at 1100°C to determine reaction constant of each anthracite.....	74
Figure 46 Plot of $1-(1-x)^{1/3}$ against time at 1350°C to determine reaction constant of each anthracite.....	75
Figure 47 Plot of $1-(1-x)^{1/3}$ against time at 1600°C to determine reaction constant of each anthracite.....	76
Figure 48 Natural logarithm of rate constant against inverse temperature (Kelvin).....	76
Figure 49 Natural logarithm of $R_{app, ave}$ against inverse temperature	77
Figure 50 Reflectance histogram for Vietnamese anthracite	91
Figure 51 Reflectance histogram for Russian anthracite	91
Figure 52 Reflectance histogram for VLV.....	91
Figure 53 Reflectance histogram for South African Anthracite	92

LIST OF TABLES

Table 1 Reductant characteristics and implications on use (Pinheiro, 2009)	23
Table 2 Reactivity studies using thermogravimetry adapted from Shaw et al (1997)	26
Table 3 Samples submitted for preparation.....	33
Table 4 Proximate and Ultimate analysis of the anthracites (5-8mm size fraction)	38
Table 5 Ash composition analysis of anthracites (wt% on ash) (5-8mm size fraction)	39
Table 6 Composition of oxides in coal (wt% in coal) (5-8mm size fraction)	39
Table 7 Petrographic analysis of the different anthracites (5-8mm size fraction)	41
Table 8 Sub categories for high rank coals: anthracites (SANS ISO 11760:2004)	42
Table 9 Comparison between the activation energy calculated using the shrinking core model rate constant (k) and the average apparent reactivity ($R_{app, ave}$).....	78
Table 10 Vietnamese (V) size analysis	87
Table 11 Russian (R) size analysis	88
Table 12 Vietnamese Low Volatile (VLV) size analysis	89
Table 13 South African Anthracite (SAA) size analysis	90
Table 14 Summary of reactivity results	93
Table 15 Raw data for V at 850°C.....	95
Table 16 Raw data for R at 850°C	96
Table 17 Raw data for VLV at 850°C	97
Table 18 Raw data for SAA at 850°C	98
Table 19 Raw data for V at 1100°C.....	99
Table 20 Raw data for R at 1100°C	100
Table 21 Raw data for VLV at 1100°C	101
Table 22 Raw data for SAA at 1100°C.....	102
Table 23 Raw data for SAA repeat test at 1100°C	103
Table 24 Raw data for V at 1350°C.....	104
Table 25 Raw data for R at 1350°C	105
Table 26 Raw data for VLV at 1350°C	106
Table 27 Raw data for SAA at 1350°C	107
Table 28 Raw data for V at 1600°C.....	108
Table 29 Raw data for R at 1600°C	109
Table 30 Raw data for R repeat test at 1600°C.....	110
Table 31 Raw data for VLV at 1600°C	111

Table 32 Raw data for SAA at 1600°C	112
---	-----

DEFINITIONS AND ABBREVIATIONS

R - Russian

V - Vietnam

VLV - Vietnam low volatile

SAA - South African Anthracite

TGA – Thermogravimetric analyser

NOMENCLATURE

db - Dry basis

daf - Dry ash free basis

C - Fixed carbon mass (dry basis)

w - Mass of sample (dry ash free basis)

t - Time

x - Fractional conversion of carbon

$\tau_{0.5}$ - Time required to reach 50% mass loss

$R_{app, ave}$ - Average apparent reactivity

E_a - Activation energy

k - rate constant

T - Temperature

ABSTRACT

Anthracites are utilised in the reduction of ilmenite in most South African ilmenite processing plants. The smelting mechanism reported by Pistorius (2008) involves the reduction of iron oxide and titanium dioxide, in the ilmenite, using carbon monoxide (generated by the Boudouard reaction) to produce pig iron, titania rich slag and carbon dioxide. The carbon dioxide is converted to carbon monoxide via the Boudouard reaction. The anthracite utilised in the process influences the efficiency of the process. It has been reported that the use of alternative anthracites has affected the smelter operation in the following manner:

- Furnace foaming can occur which results in operational downtime and out of specification product
- Impurities in the reductant can also result in out of specification product
- Smelting reactivity can result in unstable furnace performance and resultant downtime
- Decrepitation of reductant can result in carbon losses and an unstable arc in the furnace with associated resultant downtime

The reasons why different anthracites have a particular effect on the operation have not been determined. The samples evaluated in Jordan (2009) and in the current investigation included a Russian (R), Vietnamese (V), Vietnamese Low Volatile (VLV) and a South African Anthracite (SAA). A representative 5-8mm sample was used for reactivity test in Thermogravimetric Analyser (TGA) at Mintek. Average apparent reactivity was calculated for tests conducted between 850°C and 1600°C (250°C interval). The order of reactivity was that the R most reactive followed by the V, VLV and then the SAA. The Southern hemisphere SAA sample was however comparable to the R and VLV samples at some temperatures. Activation energy was also calculated and it was found that the R anthracite had the highest activation energy followed by the SAA, VLV and V anthracites. Activation energy only indicates the amount of energy required to start the reaction.

ACKNOWLEDGMENTS

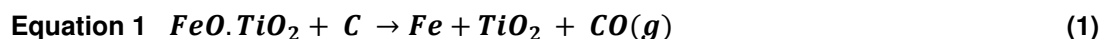
I would like to acknowledge the following individuals or institutions:

- Professor R Falcon for her guidance and supervision during my research
- N Rughubir for the insight into the smelter operational problems
- Mintek for providing resources to complete test work
- V du Cann for the petrographic analysis of samples
- Family and friends for their support during this endeavour

1 INTRODUCTION

1.1 Background

Whilst most Direct Current (DC) operations (open arc steelmaking) are batch processes, ilmenite smelting is a continuous process. Ilmenite smelting is conducted at approximately 1650°C and has two feed materials namely ilmenite and a carbon reductant. The products include titania slag and a pig iron product. The valuable titania slag is produced by the high temperature reduction of ilmenite using carbon and the iron oxide is reduced to metallic iron resulting in a slag that has higher titanium dioxide content than the natural ilmenite. In South Africa, the reductant utilised in the process is anthracite. The fundamental reduction process can be expressed as:



The only desired element in the anthracite is carbon whilst the remaining components (ash content, moisture, volatiles etc) is unwanted as these components utilise energy that should be fully utilised to heat up the furnace contents to the metal and slag temperature. Thus the importance of understanding the reductant that is utilised and the influence on the operation is evident. It is believed that the smelting mechanism is influenced by the Boudouard reaction (Jordan, 2009). Jordan (2009) investigated the link between reductant reactivity and the Boudouard reaction as the Boudouard reaction is believed to influence furnace operation in terms of furnace foaming as well as smelting reactivity.

It should be noted that the basic reductant assessment using proximate and ultimate analyses is not sufficient to predict the performance of a reductant in the furnace. It is therefore essential for research to be conducted to establish criteria beyond the standard analyses such that a carbon material for a specific application can be selected. Characterization of reductants includes an evaluation of the physical, chemical and petrographic characteristics. Reductant characterisation techniques also involve an evaluation of particle size, degree of graphitisation of reductant, porosity, ash analyses, proximate analyses, ultimate analyses and petrography. This study aims specifically to understand the effect of petrographic and chemical characteristics of anthracite on its carbon dioxide reactivity.

1.2 Motivation

As mentioned, the feed to the ilmenite smelter comprises the ilmenite and a reductant such as anthracite. Therefore, anthracite reductants are a major cost driver in an ilmenite smelting operation. In addition, whilst the products include high titania slag and pig iron, the high titania slag is utilised as feed to the chloride process which is used to produce pigments and this process is very sensitive to impurities such as magnesium oxide (MgO) and calcium oxide (CaO). Therefore the quantity of impurities such as CaO and MgO in the reductant is monitored carefully. In addition the selection of the optimum reductant is also important for the following operational reasons (Jordan, 2009):

- Furnace foaming can occur which will result in operational downtime and an out of specification product
- Impurities in the reductant can also result in an out of specification product
- Smelting reactivity can result in unstable furnace performance and resultant downtime
- Decrepitation of reductant can result in carbon losses and in an unstable arc in the furnace resulting in further downtime.

1.3 Objective

The objective of this project is to determine the relationship between the characteristics of four different reductants and their reactivity to carbon dioxide by:

- Evaluating the petrographic and chemical analysis of the anthracite before CO₂ reactivity tests
- Determination of mass loss as a function of time for different anthracites at different temperatures from 850°C to 1600°C (250°C increments) in a CO₂ environment
- Calculation of reactivity as a function of the reactivity model defined in literature
- Comparison of reactivity of the four different anthracites at the different temperatures
- Comparison of calculated reactivity to petrographic and chemical characteristics such as rank, petrographic composition and ash composition.

2 LITERATURE REVIEW

2.1 Ilmenite reduction

Ilmenite is a naturally occurring mineral consisting mainly of titanium and iron oxides and it is one of the main raw materials for the production of white titania pigments. There are two principal chemical processes used for the production of titania pigments and these are known as the sulphate and chloride processes. The sulphate process uses sulphuric acid to remove the iron oxide and other contaminating chemical compounds. The alternative route uses the chloride process to produce high quality titanium dioxide.

Titania slag can be produced by the high temperature reduction (approximately 1650°C) of ilmenite using carbon (indicated in Figure 1). Following physical beneficiation, the magnetic concentrate (rich in ilmenite) is smelted and the non magnetic concentrate is separated. During the ilmenite smelting process the iron oxide is reduced to metallic iron and the resulting slag has higher titanium dioxide content than the natural ilmenite.

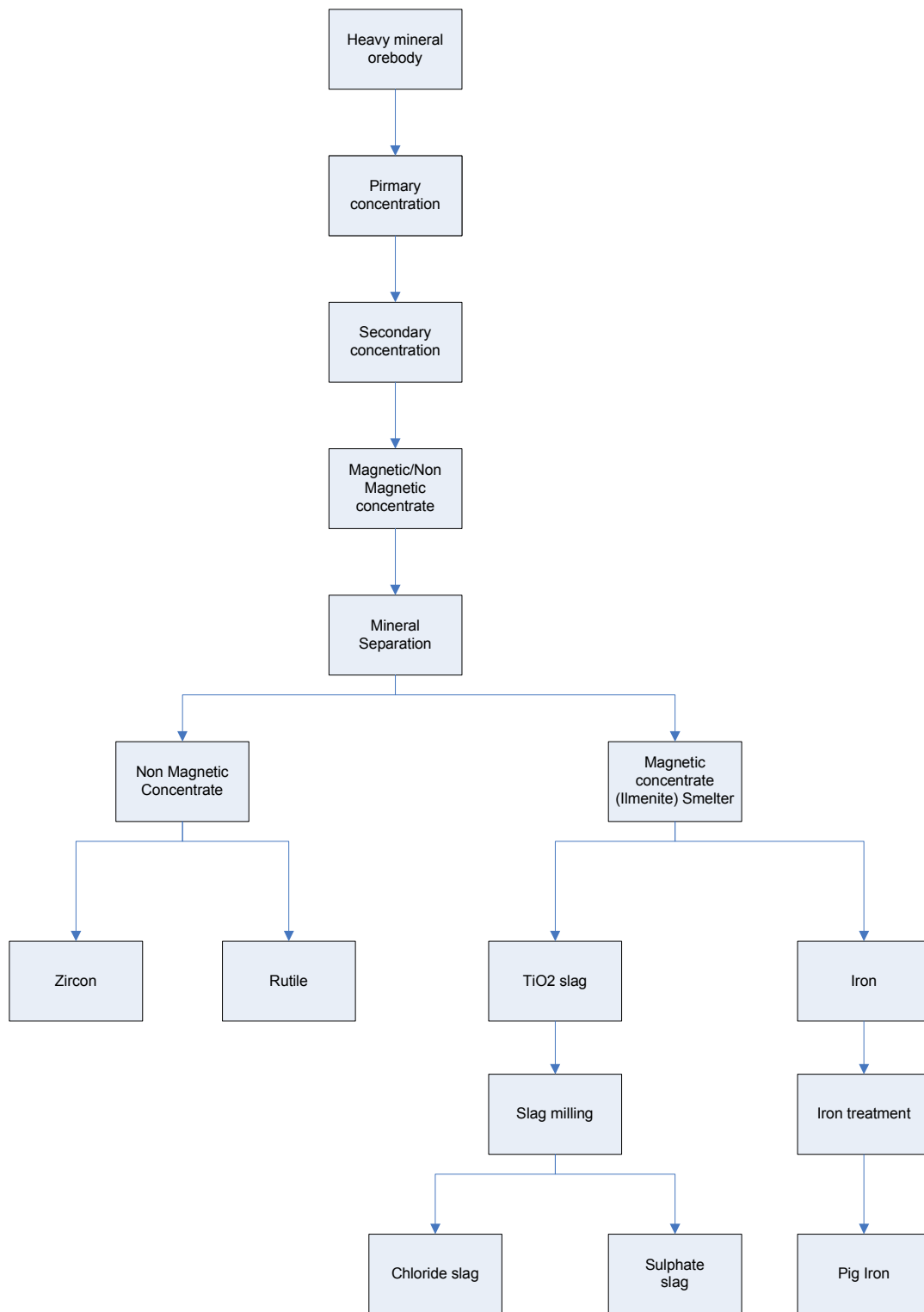
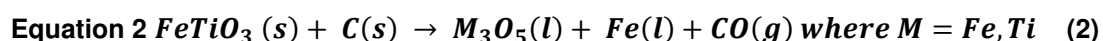


**Figure 1 Block flow diagram of Heavy mineral concentrate processing via the smelting route
(adapted from Rughubir (2011))**

Pistorius (2008) reported on the basics of ilmenite (nominal composition of $\text{FeO} \cdot \text{TiO}_2$) smelting. It was noted that ilmenite can be processed via the synthetic rutile route or by ilmenite smelting for the production of chlorination feedstock. The synthetic rutile route involves the reduction of ilmenite to metallic iron and rutile by solid state reactions (Pistorius, 2008). The iron is then removed via leaching. South African Ilmenite smelters such as Exxaro KZN Sands, Namakwa Sands and Richards Bay Minerals utilize the ilmenite smelting route where ilmenite is smelted at approximately 1650°C in an electric arc furnace and a high titania rich slag and pig iron is produced (Pistorius, 2008). Both anthracite (carbon reductant) and ilmenite are fed to the furnace via a hollow electrode (Kotze et al, 2006).

The unbalanced chemical reaction (Kotze et al, 2006) is indicated below:



Operating constraints of ilmenite smelters

Pistorius (2008) reported that ilmenite smelters have several operating constraints and these include slag composition and process input balance (i.e. power, ilmenite feed rate and reductant feed rate). Slag composition is important as the products of ilmenite smelting are used in the chlorination process which is sensitive to impurities such as magnesium chloride (MgCl_2) and calcium chloride (CaCl_2) which affect the stability of the fluidized bed. Therefore concentrations of magnesium (Mg) and calcium (Ca) in reductants are limited (Pistorius, 2008) and no fluxing agents can be utilized. A balance between power, ilmenite feed rate and reductant feed rate must be maintained such that composition and temperature is maintained. Composition and temperature in the smelter cannot be independently controlled as a freeze lining of solidified slag is used to contain the molten slag because the titania slag is very aggressive against conventional refractories (Pistorius, 2008). The liquid slag is maintained at an M_3O_5 (indicated in Equation 2) composition at the melting point (liquidus temperature of the slag). Gous (2006) reported that the control variables for slag chemistry are:

- Ratio of ilmenite to power
- Ratio of anthracite to ilmenite
- Arc length
- Slag and iron inventory.

According to Gous (2006) the degree of reduction together with the availability of energy are the drivers around which the furnace chemistry is operated.

2.2 Role of anthracite in ilmenite reduction

The smelting mechanism described by Jordan (2009) was adapted from Pistorius (2008). The mechanism is illustrated in Figure 2.

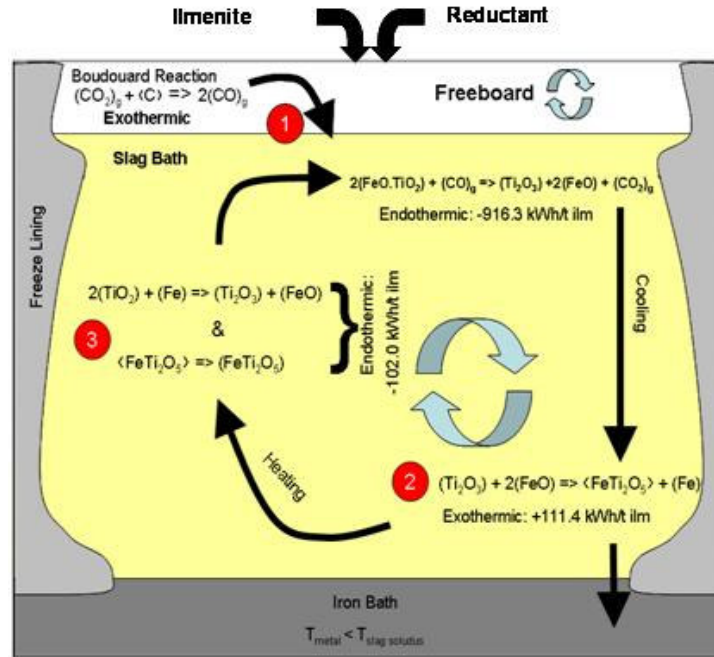
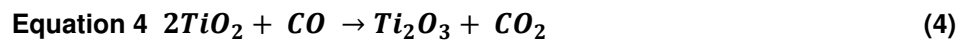


Figure 2 Schematic of smelting mechanism of ilmenite in a DC arc furnace (Pistorius, 2008 in Jordan, 2009)

The reactant, FeTiO_3 , in Equation 1 can be split into iron oxide and titanium dioxide and the reduction can be written as Equation 3 and Equation 4. The proposed smelting mechanism described by Pistorius (2008) includes:

- Reduction of FeO and TiO_2 by



- Mass transfer of CO_2 through gas halo to the reductant
- Regeneration of CO through Boudouard reaction indicated below:

$$\text{Equation 5 } \text{CO}_2 + \text{C} \rightarrow 2\text{CO}$$

(5)

Equation 5 is the Boudouard reaction where carbon is reduced to carbon monoxide with carbon dioxide. Jordan (2009) also reported that some TiO_2 is also reduced to Ti_2O_3 by Fe^0 .

2.2.1 Parameters that can influence the Boudouard reaction rates

Jordan (2009) reported that factors that can influence the Boudouard reaction rate are:

- Environment (temperature, gas composition, gas flow rate and pressure) and this refers to the test or operating environment
- Physical characteristics (size, shape, pores and density) which can be controlled in terms of size and shape of the reductant
- Chemical characteristics (elemental composition, petrography, degree of graphitisation) of anthracite are due to the coal geology, deposition, depositional environment of the original coal deposit and one has little or no control of these factors.

2.2.2 Current reductant analysis

The current reductant analyses conducted at some commercial ilmenite operations includes proximate and ultimate analyses. The reasons why these analyses are monitored is discussed below (Rughubir, 2011):

Moisture - the reductant should contain as little moisture as possible due to following reasons:

- The mass ratio of reductant to ilmenite will have to be adjusted to compensate for the deviation in moisture levels in the reductant as a deviation in the desired quantity of fixed carbon to the furnace can result in out of specification product.
- Excess moisture will be converted to steam by electrical energy (contributes to poor energy efficiency). Any reactions associated with moisture are endothermic and will contribute to energy consumption.
- The presence of steam increases the consumption of carbon.
- Moisture also contributes to an increase in waste gas volume and a decrease in slag temperature. These operating conditions can contribute to slag foaming in the furnace.

Volatile Matter - Volatiles are driven off in the furnace and report to the gas phase as hydrogen and carbon monoxide. Most of the reactions in the furnace are endothermic which inadvertently

contributes to an increase in energy consumption and the volume of waste gas.

Ash - Most of the ash components of the reductant report with the gangue in the ilmenite to the slag. Some elements may report to the metal or off gas however the ash mainly consists of unwanted impurities and results in metal or slag contamination. The quantity of ash in the reductant should be minimised and the ash content should be monitored.

Fixed Carbon - The ilmenite process reduction is achieved by fixed carbon therefore the fixed carbon quantity determines the quantity of reductant required by the process.

Sulphur - Sulphur deportment in coal can occur in different forms. Sulphur can be associated with ash as inorganic sulphur and/or associated with the volatiles as organic sulphur. It is reported that high titania slags do not have good desulphurising properties and the majority of the sulphur reports to the iron and gas phases.

2.2.3 Influence of reductants on slag quality and the overall process

Slag quality is also affected by the ratio of anthracite to ilmenite in the feed mixture (supplied to the furnace). There is an inverse relationship between FeO and TiO₂ as any decrease in the FeO content (due to reduction) will be accompanied by an increase in the TiO₂ content. However, most other slag characteristics involving control of the gangue compounds such as calcium oxide (CaO), manganese oxide (MnO), chromium oxide (Cr₂O₃) etc, can only be changed by altering the quality of the ilmenite and anthracite feed materials. The reductant ratio affects the iron quality as it influences the amount of gangue reporting to the iron product.

2.3 Nature of coal reductants and characterisation

2.3.1 Nature of Southern hemisphere and Northern hemisphere coal

It is important to note that there are distinct differences between the Southern hemisphere and Northern hemisphere coals and these are due to the conditions at the time that the coal was formed and the subsequent geological events (Falcon and Ham, 1988). The Northern hemisphere had hot, humid coastal carboniferous coal forming swamps whilst the Permian swamps in the Southern hemisphere were formed under cold (increasing to warm) temperate conditions associated with the waning of an ice age and these combined conditions lead to variable mineral rich peat forming swamps which developed into widespread, relatively thick coal seams with the passage of time.

Northern hemisphere coals have higher rank coals due to the deep burial, rapidly subsiding geosynclines, intense tectonic stresses, pressures from thick overlying strata and the geothermal temperatures at the depths of burial (Falcon and Ham, 1988). This resulted in the formation of high quality metallurgical coals with high rank and vitrinite reflectance. South African coals accumulated on shallow shelves on continental platforms and have with a few exceptions not been subject to

deep burial, however some coalfields have been permeated by igneous intrusions (horizontal or vertical sills and dykes) and outpourings of lava on the ancient Karoo landscape which gave rise to the Drakensberg mountains (Falcon and Ham, 1988). The coals of Gondwana provinces have uneven increases in rank within localised areas due to varying sizes and types of intrusions (Falcon and Ham, 1988). South African anthracites are therefore the result of coals being subject to heat from igneous intrusions and out pouring of lava. The rank of these coals is generally low and less mature and therefore differs from the high rank counterparts of the northern hemisphere. Falcon and Ham (1988) noted that the SA coals differ from the European and other Laurasian coal in being variable between regions and seams and generally have high ash fusion temperatures, low sulphur, sodium, potassium, iron and chlorine contents. Falcon and Ham (1988) noted that Gondwana coals are also inertinite rich with lower volatile content. The bulk of northern hemisphere coals lie in the mid to low volatile bituminous range grading to anthracite while Gondwanaland coals range from sub bituminous to mid bituminous ranges with the exception of heat affected areas (Falcon and Ham, 1988). Coal petrography is utilised to determine the rank parameters and maceral composition of coals. Choudhury et al (2008) reported that the northern hemisphere coals have three fold classifications of macerals (recommended by ICCP and the International Standard Organization) and these include vitrinite, liptinite and inertinite but Gondwana coals have a four fold classification which includes semi-reactive macerals, namely, reactive semivitrinite or reactive semifusinite. Macerals can be divided into reactive/fusible and inert/infusible (Choudhury et al, 2008). Vitrinite, reactive semivitrinite/semifusinite and liptinite form reactive group macerals that fuse during carbonisation (Choudhury et al, 2008). The inertinite rich Gondwana coals have lower reactive maceral proportion than the northern hemisphere counterparts and do not necessarily yield very good coke (Choudhury et al, 2008). Crelling et al (1988) noted that the macerals and minerals in coal have physical and chemical properties which contribute to the behaviour of coal in different applications.

2.3.2 Reductant characterisation and the effect on reactivity

There is an extensive list of analysis that can be conducted to characterise a reductant for an operation. Sahajwalla et al (2004) evaluated the impact of reductant properties on its performance in the ferroalloy industry and indicated that optimum selection of the reductant was dependent on the characteristic of the reductant, product and process requirements as well as raw material availability and costs. Pinheiro (2009) indicated the impact of different parameters when the metallurgical coal is utilised as a reductant and as a fuel (Table 1).

Table 1 Reductant characteristics and implications on use (Pinheiro, 2009)

Parameter	Desired	Implication as a reductant	Implication as a fuel
Sizing	Specific to use	Burden resistivity and reactivity	Aesthetics and consistent burning
Moisture	As low as possible	Detrimental to power consumption	Detrimental to ignition
Volatiles	Variable	Detrimental to power consumption, increases porosity and reactivity, pollution increases	Enough required to allow for ignition. Pollution increases
Carbon	High	Highest possible, fundamental	High as possible for combustion
Ash	As low as possible	Detrimental to power consumption, slag disposal	Lowers the calorific value, ash disposal
Calorific value	As high as possible	Not important, but can assist in some applications	High, equivalent to heating value of the coal
Sulphur (S)	Low, <1% in EU	Inorganic S transfers to metal, detrimental	Combusts to form SO _x , severe pollutants
Phosphorous	Low	Transfers to metal in some processes, detrimental	Not significant
Rank	Variable	Relates to reactivity, lower for gas-solid reactivity, high for solid-liquid reactivity	Preferably Rr<5%. If rank is too high, it is difficult to ignite
Vitrinite	High	The ideal constituent to graphitise/crystallise resulting in increased reactivity	Lower ignition temperature than inertinite for most anthracites

This study involves the evaluation of the CO₂ reactivity of the reductant and its petrographic and chemical analysis. The analysis conducted included, chemical analysis, petrographic and reactivity tests.

Proximate, ultimate and ash analysis

The proximate analysis involves the evaluation of inherent moisture, volatile matter, ash and fixed carbon (by difference) in the coal. Beamish et al (1998) conducted an evaluation of the carbon dioxide reactivity of New Zealand coals and found that the volatile matter was not a reliable predictor of reactivity of sub bituminous and lignite coal chars. The proximate analysis is conducted according to standard procedures however different values for this analysis can be obtained if different procedures are used (Rosenqvist, 1974). Gibbins et al (1990) investigated the influence of heating rate on coals with carbon content of 70 to 90% (dry mineral matter free basis). The investigation indicated that secondary volatile matter char reactions could account for half of the differences between the proximate volatile matter yields and total volatile matter yields for heating rate of 5000K/s up to a temperature of 950°C. Ultimate analysis involves the determination of

elements present in the organic matter of coal viz; carbon, hydrogen, nitrogen, sulphur and oxygen. The ash composition of coal is determined by chemical analysis. Many researchers (Jordan (2009), Beamish et al (1998), Grigore et al (2006), Chan et al (1998)) have found that ash composition of a coal does affect the coal reactivity. Beamish et al (1998) found that calcium in New Zealand coal char was related to its reactivity. Calcium present as discrete minerals such as calcite tended to lower the reactivity however organically bound calcium enhanced reactivity in gasification reactions (Beamish et al, 1998). Hippo and Walker (1975) evaluated the reactivity coal chars in oxygen and carbon dioxide environments as well as the effect of acid washing and found that reactivity increased with increasing calcium content. Reactivity appeared to increase with increasing magnesium content however the increase in magnesium content above 1% appeared to have minimal effect on reactivity (Hippo and Walker, 1975). Jenkins et al (1973) also found that chars with high concentrations of magnesium and calcium were most reactive. Beamish et al (1998) evaluated the effect of other minerals and found the catalytic interaction to be complex but it was concluded that the distribution and content of minerals such as magnesium, iron, sodium and phosphorous played a role in the reactivity of the chars tested.

Petrographic analysis

Petrographic analysis is used to determine the maceral composition, microlithotypes, and reflectance of vitrinite as well as the ratio of reactive to inert macerals. There are three groups of macerals which include vitrinite (viscous coking-caking component), inertinite (generally unreactive) and exinite (main tar and hydrogen producer) (Falcon and Ham, 1988). Hurt et al (1986) evaluated the gasification reactivity of low chars from low rank coal lithotypes (from Penn State Coal Bank from the Alton Mine in Utah) in carbon dioxide atmosphere. It was found that vitrain char (containing 96% vitrinite by volume) was more reactive than the fusain sample (containing 92% inertinite by volume).

Falcon (2005) indicated that anthracitic vitrinites and some inertinites will react at similar rates at low temperature (temperature in the range of ambient and 1400°C) and in the gaseous environment. This process is limited by the rate of diffusion into the materials and their innermost surfaces (Falcon, 2005). Vitrinite molecules in anthracite will form two dimensional layers of graphitic lamellae with weak vertical links at temperatures above and including 1800°C whilst inertinite components form multidimensional disorientated aromatic structures with strong bonds in all directions (Falcon, 2005). Falcon (2005) reported that under these conditions the inertinite components will be consumed relatively easier than the vitrinite components at high temperatures in the gaseous phase. In the liquid phase, the vitrinite components are consumed faster due to the break down of the weak vertical bonds whereas the strong bonds (in all directions) of the inertinite components prove to be limiting (Falcon, 2005). Crelling et al (1988) indicated that the maceral and

microlithotype composition of a coal was related to reactivity and that for a given rank, a variation in the maceral composition of a coal could result in a deviation of up to 45% in the reactivity range linked with that coal rank (note these conclusions were made following the evaluation of reactivity tests conducted in an oxygen atmosphere).

The anthracite condition (measure of the degree of weathering and oxidation of the coal particles) also influences reactivity (Falcon, 2005). Falcon (2005) reported that in cases where the anthracite is weathered (i.e. the particles are fissured and cracked) and moisture is trapped on the fissure surfaces, deflagration and shattering of the particles may occur upon exposure to instant high temperatures. Fine particles of coal dust will possibly be generated and be carried in the gas stream and can expose the upper parts of the furnace or the smelter to higher temperatures which it may not be designed to handle (Falcon, 2005).

Various researchers (Beamish et al, (1998), Olivella et al, (2002)) have indicated that coal reactivity is influenced by the rank of the coal. Reactivity of low rank chars is higher than those from high rank coal. Crelling et al (1988) conducted reactivity tests on coal (sourced from seams in the Appalachian coal and Arkoma coal basins in USA respectively) in an oxygen atmosphere (5% volume O₂ in N₂) and also found that reactivity of the coal decreased with increasing coal rank. Beamish et al (1998) and Shaw et al (1997) also confirmed the same trend for reactivity of coals measured in a carbon dioxide atmosphere. Jenkins et al (1973) evaluated the reactivity of coals of varying rank in air at 500°C and found that reactivity increased with a decrease in rank. Falcon (2005) reported that anthracites lower in rank than a Meta anthracite with high internal porosity and active surfaces are required for effective reduction in gasification phase at temperatures between ambient and 1400°C. Higher vitrinite content (ranks in the Meta anthracite range) favours more efficient reactivity in the liquid slag phase reduction (Falcon, 2005). It must be noted that whilst many researchers have concluded that there is a relationship between coal rank and its reactivity, Jordan (2009) found in his investigation (which involved the evaluation of South African, Vietnamese and Russian anthracites) that no relationship between coal rank, maceral composition and reactivity could be established.

Reactivity tests

There are a number of reactivity tests which are utilised to determine the reactivity of the coal in a specific environment. Olivella et al (2002) defined reactivity as the rate at which coal reacts in an oxidising atmosphere following devolatilisation. The objective of the aforementioned investigation was to determine the rate of reduction of carbon dioxide to carbon monoxide in the gasifier. In terms of the present study the reactivity of anthracite in a carbon dioxide atmosphere will be investigated, therefore reactivity will be defined as the rate at which coal reacts in a carbon dioxide atmosphere.

Falcon et al (2004) indicated that reactivity was both a function of the inherent nature of the material and the composition of the gaseous environment but the effect of temperature was yet to be determined. Literature has indicated that reactivity tests have been conducted in different gas atmospheres and equipment on a variety of coals. Beamish et al (1998) indicated that a number of techniques could be utilised to determine coal char reactivity and these include the use of drop tube furnaces, fluidised bed reactions and thermogravimetry. Thermogravimetric tests have been found to be useful in the evaluation of factors such as particle size, sample weight, reactant gas, heating and reaction rates which effect reactivity (Beamish et al, 1998). Hurt et al (1991) used a thermogravimetric analyser to determine the relevance of microporous surface area in the gasification of chars from a sub bituminous coal.

Shaw et al (1997) agreed that coal reactivity could be consistently determined by thermogravimetry, however it was noted that a standard testing method had not been established. The results of an individual study could be evaluated meaningfully however comparisons could not be made between different researchers as thermogravimetric analysis was influenced by the equipment utilised and the experimental parameters (Shaw et al, 1997). Shaw et al (1997) summarised some of the different investigations published in literature that utilised thermogravimetric analyser to evaluate coal reactivity and this is indicated in Table 2.

Table 2 Reactivity studies using thermogravimetry adapted from Shaw et al (1997)

	Jenkins et al (1973)	Hippo & Walker (1975)	Crelling et al (1988)	Johns (1990)	Hurt (1991)	Shaw et al (1997)
Instrument	Fisher TGA	TGA	TGA ^a	Du Pont 1090	TGA ^a	Rheometric Scientific STA 1500
Particle size (µm)	< 425	<425	<75	na ^b	na ^b	<212
Sample weight (mg)	5-10 (char)	2-6 (char)	15 (coal)	na ^b	5-20 (char)	15.5 (coal)
heating rate (°C.min⁻¹)	10	10	99	25	na	50
Char preparation temperature	1000	1000	700	930	1200	900
Reactivity measurement (°C)	500	900	500	1050	900	900, 1100
Atmosphere	Air	CO ₂	5%O ₂ + 95% N ₂	CO ₂	CO ₂	Air & CO ₂
Origin of coal	USA Rank, mineral matter, pore structure, char temperature	USA Ca, Mg, particle size	USA & Australia Rank, maceral composition	na ^b Rank, methodology comparison	USA Mineral matter, untreated & washed coal	New Zealand Coal type & rank

a. Make and model not specified

b. Information not available

Experimental considerations

The conditions of the experiment i.e. time, temperature, reactant gas, particle size, sample weight and equipment geometry will affect the reactivity of the char/coal under investigation (Shaw et al, 1997). The temperature at which the char of the coals to be evaluated, was prepared in the investigation by Jenkins et al (1973) influenced the reactivity of the char and this was thought to be due to pore structure and the chemical nature of the char. Hippo and Walker (1975) found that reactivity increased with a decrease in sample particle size and concluded that this trend implied that reactivity was partly controlled by the diffusion resistance of the particles to the entry of carbon dioxide. In the evaluation of low rank coal lithotypes from Utah, Hurt et al (1986) found that particle size had no effect on reactivity thus indicating that intraparticle diffusion was not a limitation. Shaw et al (1997) found that reactivity of a sample increased with decreasing sample bed weight. This is supported by the findings of Hippo and Walker (1975) however Hurt et al (1986) found that sample bed size had no effect on the reaction rates of the low rank coal lithotypes from Utah that were investigated. Shaw et al (1997) also followed a specific process of heating the coal in a neutral atmosphere i.e. nitrogen for the formation of a char before introduction of a reactant gas. The effect of reactant gas on reactivity was also considered and Shaw et al (1997) found that since the reaction of coal and air is exothermic, the temperature of the furnace increased with highly reactive coals. The Boudouard reaction between coal and carbon dioxide is endothermic and there is very little effect on the furnace temperature (Shaw et al, 1997). Shaw et al (1997) chose CO₂ as the reactant gas as the researchers wanted to maintain an isothermal environment during the evaluation of highly reactive coals. CO₂ was utilised in the present study as the Boudouard reaction is reported to play a significant role in the ilmenite smelting mechanism.

Reactivity models

One of the models indicated in literature for the determination of reactivity of the coal include Equation 6 (Grigore et al, 2006):

$$\text{Equation 6 } R_{app} = \frac{1}{w} \left(\frac{dw}{dt} \right) \quad (6)$$

In Equation 6 R_{app} is the apparent reaction rate and w is the mass of sample (fixed carbon dry ash free basis) remaining at time t . This equation was utilised to determine the instantaneous reaction rate at the different levels of conversion. The units of R_{app} is g.g⁻¹.s⁻¹. Grigore et al (2006) used Equation 6 to determine the influence of mineral matter on the reactivity of coke and then utilised the Arrhenius equation (Equation 7) to determine activation energy by plotting the natural logarithm of the apparent reactivity against the inverse of reaction temperature (units Kelvin). The natural logarithm of the Arrhenius equation is indicated below:

$$\text{Equation 7 } \ln R_{app} = -\frac{E_a}{R''} \cdot \frac{1}{T} + \ln A \quad (7)$$

ln A is the constant and **E_a** is the activation energy in (J/mol), temperature (T) is in Kelvin. **R** is the universal gas constant (8.314 J.mol⁻¹.K⁻¹). Zhang et al (2006) utilised the shrinking core model (Equation 8) to determine reactivity where **x** is the fractional conversion of carbon reacted over time.

$$\text{Equation 8 } \frac{dx}{dt} = k(1-x)^{2/3} \text{ or } 1 - (1-x)^{1/3} = kt \quad (8)$$

Fractional conversion of fixed carbon (dry ash free basis) was evaluated by the Equation 9:

$$\text{Equation 9 } x(t) = \frac{C_0 - C(t)}{C(t)} \quad (9)$$

C₀ is the initial fixed carbon content of the anthracite and **C(t)** is the fixed carbon content at time **t**. The model assumes that the reaction occurs on the external surface of the particle and gradually moves inwards leaving a porous layer behind. From a plot of $1 - (1-x)^{1/3}$ against time one would be able to determine **k** (rate constant) which can then be utilised to determine the activation energy using the Arrhenius law in Equation 10:

$$\text{Equation 10 } k = k_0 e^{-E_a R/T} \quad (10)$$

The natural logarithm of the rate constant is plotted against inverse temperature and the activation energy can then be determined. This method was utilised by Atashi et al (2010), in the evaluation of the leaching kinetics of calcined magnesite in ammonium chloride solutions.

Zhang et al (2006) also mentioned a gasification reactivity index for the comparison of anthracite reactivity indicated in (Equation 11) where $\tau_{0.5}$ is the time required to reach 50% mass loss.

$$\text{Equation 11 } R = 0.5/\tau_{0.5} \quad (11)$$

Shaw et al (1997) and Olivella et al (2002) used Equation 12 for the evaluation of the reactivity where **dw/dt** is the maximum rate of fixed carbon loss and **W₀** is the initial weight of char on a dry ash free basis. **R** is the maximum reactivity and is expressed as mg.h⁻¹.mg⁻¹ or h⁻¹.

$$\text{Equation 12 } R = -W_0^{-1} \left(\frac{dw}{dt} \right) \quad (12)$$

The process used during the reactivity test by Shaw et al (1997) involved the heating of the coal to 110°C at a rate of 50°C/min in a nitrogen atmosphere. The sample was then held at this

temperature for 5 minutes and then heated to 900°C where it was held at this temperature for 10 minutes (so that volatiles were driven off). The reactant gas (CO₂) was then introduced at 900°C. Figure 3 indicates the results of a run at 900°C. Weight loss is plotted against time on the primary y axis. The secondary y axis indicates the plot of the first derivative of weight loss. In the nitrogen atmosphere, moisture is lost from the sample followed by volatile release. The maximum rate of fixed carbon loss is achieved in the CO₂ atmosphere.

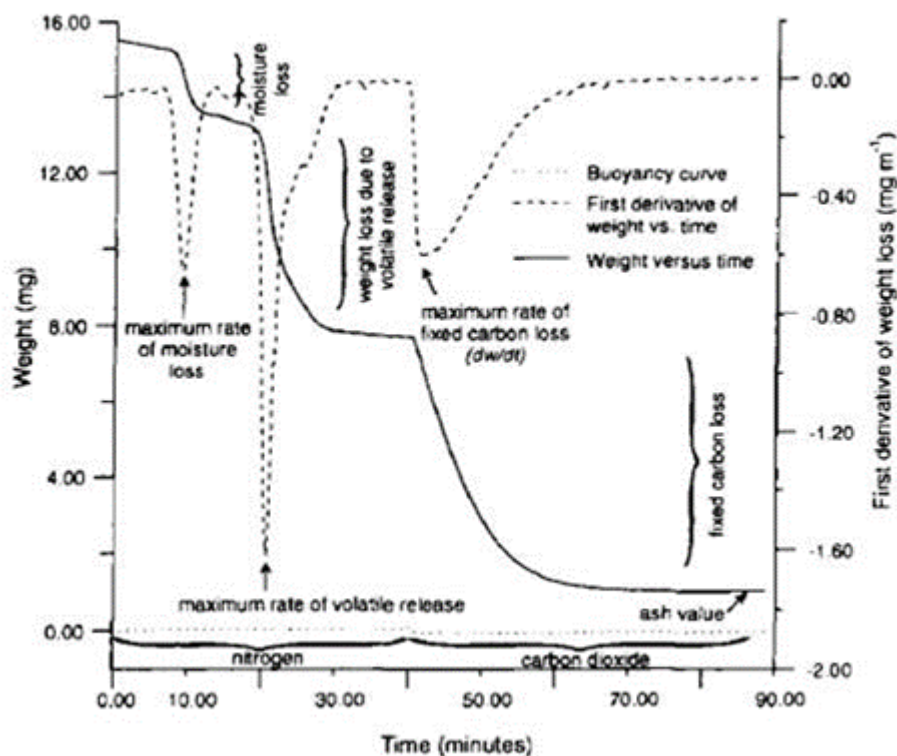


Figure 3 Characteristic of thermogravimetric reactivity analysis of New Zealand Coal in CO₂ at 900°C indicated in Shaw et al (1997)

Olivella et al (2002) followed a similar procedure to Shaw et al (1997) however the reactant gas was dry air. The results of one of the experiments are indicated in Figure 4. A similar trend of initial moisture loss, followed by volatile loss is indicated.

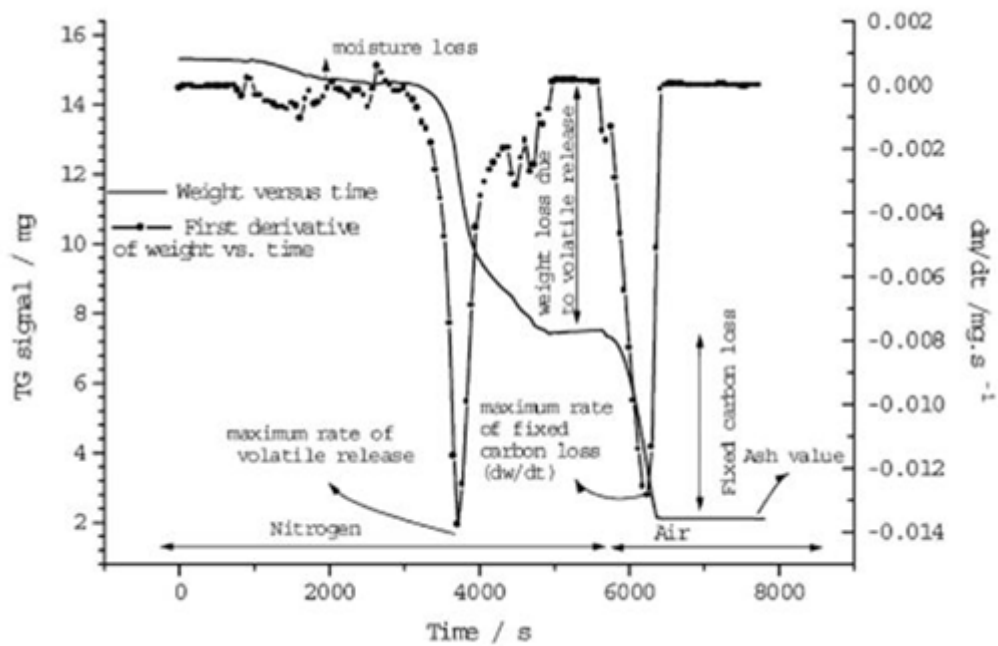


Figure 4 Characteristic of thermogravimetric reactivity of Mequinenza lignite in dry air at 900°C as indicated in Olivella et al (2002)

3 METHOD OF STUDY

3.1 Samples utilised

Four anthracite samples were sourced from South Africa, Vietnam and Russia. These coals were described as the following:

- South African Anthracite (SAA): southern hemisphere, High Rank B
- Vietnamese Anthracite (V): northern hemisphere, High Rank C
- Vietnamese Low Volatile Anthracite (VLV): northern hemisphere, High Rank A
- Russian anthracite (R): northern hemisphere, High Rank A

These samples were prepared in accordance with SABS/SANS 0135 Part II and ISO standards 13909 parts 3 and 4. Since the reductant feed to ilmenite furnace is in the size range of 5-8mm, the samples were crushed and prepared according to this size fraction. Petrographic analysis was conducted on the 5-8mm prepared size fraction.

3.2 Investigative methodology

3.2.1 Chemical analysis

Proximate and ultimate analysis of all samples was evaluated. The proximate analysis involves the evaluation of moisture in the analysis sample, volatile matter, ash and fixed carbon (by difference) in the coal by prescribed methods. Ultimate analysis entails the determination of elements present in the coal viz; carbon, hydrogen, nitrogen, sulphur and oxygen. The ash composition was determined by chemical analysis.

3.2.2 Petrographic analysis

Petrographic analysis of coal is determined by microscopic analyses/assessment of the coal under oil immersion via the use of a light reflecting microscope. The determination of the maceral composition of a coal comprises the quantification of the macerals (organic constituents) which are vitrinite, liptinite and inertinite. In bituminous coals semi reactive inertinite is also quantified (particularly in the case of inertinite dominant coals such as most South African coal). However, in high rank coals such as anthracites, liptinites are no longer identified/quantified microscopically and neither is the so called reactive inertinite. Another petrographic analytical technique is the measure of the vitrinite reflectance to quantify the rank of coal. Rank refers to the degree of maturity of a

coal. Reflectance measurements are also obtained using a photomultiplier to measure the light intensity emitted by the polished surface of vitrinite particles. Maximum and random reflectance measurements are possible and such techniques are standardised according to the ISO 7404-5 test method.

Given the microscopic analyses of coal, the assessment of the condition of each coal particle is also possible. It is common practice for a condition analysis to be done, to determine the degree of weathering and heat effects.

3.2.3 Reactivity analysis

Reactivity analysis was conducted by the evaluation of mass loss of the reductant in a carbon dioxide environment in a Thermogravimetric Analyser (TGA). The schematic of the furnace utilised is shown in Figure 5. The TGA utilised is lined with an Aluminium-Silica fibre board refractory lining and has a furnace tube size of 7.5cm in diameter and 90cm in length. The maximum design and operating temperature of the furnace is 1800°C and 1650°C respectively (Sooful, 2010). The furnace is open at the bottom and the sample is placed on the extended arm of a balance. The sample is raised and removed from the furnace manually by changing the level on which the balance rests. Gas enters through the top of the furnace and is vented to the atmosphere via the bottom of the furnace. Oxygen ingress is prevented by virtue of the flow rate of the desired gas input into the furnace (Sooful, 2010). Sooful (2010) has also indicated that chromium metal has been suspended in the furnace at 1500°C and no oxidation of the chromium metal pellet in an Argon atmosphere occurs which supports the claim that no ingress of oxygen occurs. Gas flow rate control is achieved via variable area flow controllers (Fischer Porter Rotameters). There are two temperature controllers (TC), one for the sample temperature and the other monitors furnace temperature. There are two types of thermocouples a B type (maximum operating temperature 2000°C) and a K type (maximum operating temperature of 1300°C). The thermocouple was varied according to the experimental test temperature. An Agilent bench link data logger was used to log data (Sooful, 2010).

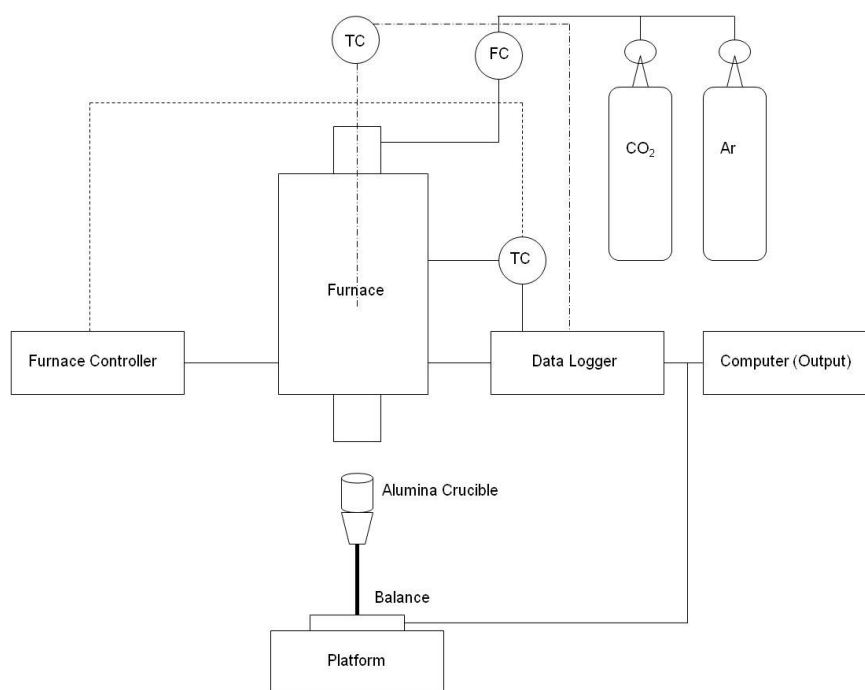


Figure 5 Thermogravimetric analyser furnace controllers and data output (adapted from Sooful, 2010)

4 EXPERIMENTAL PROCEDURE

4.1 Sample preparation

The samples were submitted to Witlab for preparation and they are identified in Table 3.

Table 3 Samples submitted for preparation

No.	Sample Identity	Top size (mm)	Mass (kg)	< 5mm %
1.	Vietnamese (V)	20	500	28.4
2.	Russian (R)	40	250	3.3
3.	Vietnamese Low Volatile (VLV)	19	500	20.5
4.	South African Anthracite (SAA)	25	500	75.4

Particle size analysis was conducted on each sample (appendix 9.1) to determine the mass fraction that was less than 5mm. A preparation flow diagram was then prepared to prevent the generation of additional fines as more than 70% of the SAA sample was already under 5mm. ISO 13909 Standard procedure was used to prepare the samples. Each sample was split into representative 20kg mass lots using a rotary splitter. One of the 20kg mass lots was then stage crushed using a jaw crusher to the desired 5-8mm size fraction which was subsequently split further into 5kg representative samples (procedure indicated in Figure 6).

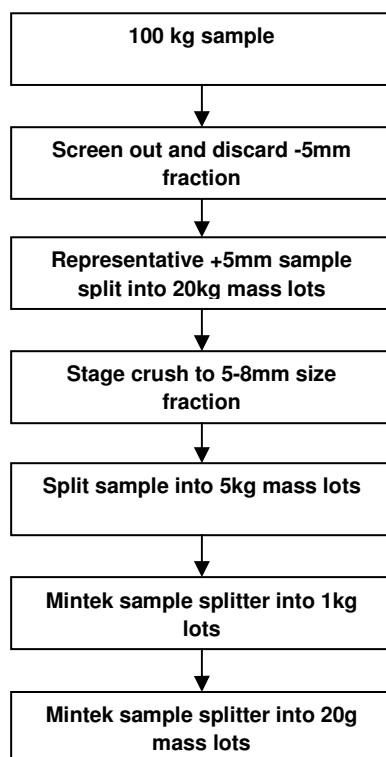


Figure 6 Sample preparation procedure

The 5kg samples were then submitted to Mintek for the Thermogravimetric Analysis (TGA). Mintek also followed a sample preparation route that was ISO accredited as the sample size that could be analysed in the TGA was 20g. The effect of sample mass on reactivity was not investigated as a fixed mass of 20g was processed by the Mintek TGA. The splitters used in the sample preparation are indicated in Figure 7.



Figure 7 First stage sample splitter



Figure 8 Second stage sample splitter

Each 20g sample was then placed in an alumina crucible. The Thermogravimetric Analyser (TGA) was heated up to the test temperature in an Argon (Ar) atmosphere (to ensure the reactor atmosphere was neutral). The rate of temperature increase utilised was 5°C/min. At 200°C the temperature was held for 10 minutes and then the temperature was ramped to the test temperature and held for 30 minutes before the carbon dioxide (reactant gas) is introduced. The Ar and CO₂ flow rate utilised in the tests for the current study (tests at 850°C and 1350°C) was 285sccm⁻¹ (standard cubic centimetres per minute) and 270sccm⁻¹ respectively. Results from the Jordan (2009) study were also evaluated. The Jordan (2009) study utilised the same samples and conducted tests at 1100°C and 1600°C, however the test conditions were not same, the sample masses varied between 20-48g and the CO₂ flow rate utilised was 150sccm⁻¹. In the Jordan (2009) study, the data was recorded from the time that CO₂ was introduced into the TGA and was run for 24 hours. Taking into account that different experimental procedures were followed, two repeat tests were conducted at 1100°C and 1600°C to determine the effect of change in experimental procedure. The result for both studies was determined from mass loss data recorded against time. The mass loss, time and temperature data was then used to determine the reactivity of each anthracite at the different temperatures. Apparent reactivity over the entire test period was evaluated using the model specified by Grigore et al (2006) in Equation 6. The apparent reactivity was then averaged over the time period that the anthracite was exposed to CO₂ whilst at the test temperature. The natural logarithm of the average apparent reactivity was then plotted against inverse temperature. In this manner the activation energy of each anthracite was determined.

Fractional conversion (x) of fixed carbon was evaluated by utilising Equation 9, which was then utilised to determine the rate constant in terms of the shrinking core model by plotting $1 - (1 - x)^{1/3}$ against time as specified in Equation 8. This was evaluated from the time CO_2 was introduced into the TGA until the time when the first anthracite indicated that the reaction had levelled off. The reaction rate constant evaluated from the gradient of the plot of $1 - (1 - x)^{1/3}$ against time was used to determine the activation energy of each anthracite. The activation energy calculated by these two methods was then compared.

5 RESULTS AND DISCUSSION

This chapter will outline the results obtained in this study. It will also make comparisons on the results obtained by Jordan (2009). The results obtained using the Mintek TGA at 850°C and 1350°C were plotted separately from the data evaluated from the Jordan (2009) study (which evaluated the 1100°C and 1600°C tests). The results were evaluated in this manner due to the difference in experimental procedure utilised by each study.

5.1 Chemical analysis of the different anthracites

The proximate, ultimate and ash composition analysis for the different anthracites are indicated in Table 4 to Table 6. An evaluation of the proximate and ultimate analysis of the four anthracites indicated that the moisture (air dried basis) varied between 1 and 3.6%. The volatile matter contents (air dried basis) ranged from 1.7 to 5.5%. The fixed carbon (dry basis) content of the samples varied between 85.3 and 94.6%. The sulphur content from the ultimate analysis indicates that all samples had a sulphur content of less than 1% with the SAA sample having the highest sulphur content of 0.9%. Table 4 also indicates that the ash content (dry basis) varied between 3.7 and 12.2% therefore the ash composition (Table 5) was recalculated as a percentage of the original sample mass (Table 6).

Table 4 Proximate and Ultimate analysis of the anthracites (5-8mm size fraction)

Proximate (air-dried)	V	R	VLV	SAA
% Inherent moisture content	1.00	3.60	1.70	2.80
% Ash content	6.10	3.50	12.00	8.50
% Volatile matter	5.50	1.70	2.40	4.70
% Fixed Carbon	87.40	91.20	83.90	84.00
Proximate (dry basis)				
% Ash Content	6.16	3.63	12.21	8.74
% Volatile matter	5.56	1.76	2.44	4.84
% Fixed carbon	88.28	94.61	85.35	86.42
Proximate (dry ash free basis)				
% Volatile	5.92	1.83	2.77	5.28
% Fixed carbon	94.02	98.04	96.99	94.45
Ultimate (dry-basis)				
% Carbon Content	88.20	92.80	84.70	85.20
% Hydrogen Content	3.06	1.30	1.13	2.40
% Nitrogen Content	1.20	0.87	0.63	1.79
% Oxygen Content	0.76	0.56	0.55	0.99
% Total Sulphur	0.59	0.82	0.79	0.88
% Ash content	6.20	3.70	12.20	8.70

Table 5 Ash composition analysis of anthracites (wt% on ash) (5-8mm size fraction)

Ash composition (% mass)	V	R	VLV	SAA
Al ₂ O ₃	30.49	20.74	26.51	29.95
CaO	1.31	6.58	0.66	1.55
Cr ₂ O ₃	0.07	1.06	0.06	0.11
Fe ₂ O ₃	7.80	19.89	12.46	13.74
K ₂ O	3.45	2.30	3.67	3.49
MgO	1.04	4.36	0.93	1.02
MnO	0.06	0.21	0.15	0.15
Na ₂ O	0.45	1.23	0.17	0.51
P ₂ O ₅	0.32	0.15	0.14	0.22
SiO ₂	53.56	34.71	53.30	46.56
TiO ₂	0.95	1.60	1.64	1.97
V ₂ O ₅	0.06	0.13	0.05	0.06
ZrO ₂	0.13	0.06	0.08	0.12
Ba	0.10	0.40	0.05	0.06
Sr	0.03	0.25	0.01	0.07
SO ₃	0.67	6.72	0.55	1.01

Table 6 Composition of oxides in coal (wt% in coal) (5-8mm size fraction)

Ash composition (% mass in coal)	V	R	VLV	SAA
Al ₂ O ₃	1.88	0.75	3.24	2.62
CaO	0.08	0.24	0.08	0.14
Cr ₂ O ₃	0.004	0.04	0.01	0.01
Fe ₂ O ₃	0.48	0.72	1.52	1.20
K ₂ O	0.21	0.08	0.45	0.31
MgO	0.06	0.16	0.11	0.09
MnO	0.004	0.01	0.02	0.01
Na ₂ O	0.03	0.04	0.02	0.04
P ₂ O ₅	0.02	0.01	0.02	0.02
SiO ₂	3.30	1.26	6.51	4.07
TiO ₂	0.06	0.06	0.20	0.17
V ₂ O ₅	0.004	0.005	0.01	0.01
ZrO ₂	0.01	0.002	0.01	0.01
Ba	0.01	0.01	0.01	0.01
Sr	0.002	0.01	0.001	0.01
SO ₃	0.04	0.24	0.07	0.09

5.2 Petrographic analysis of the different anthracites

Table 7 reports the petrographic analyses of the four anthracites. The coal type (petrographic composition), rank (maturity), grade (amount of impurities) and condition are assessed from these results.

Table 7 Petrographic analysis of the different anthracites (5-8mm size fraction)

	V	R	VLV	SAA
RANK (degree of maturity)	Anthracite	Meta-anthracite	Meta-anthracite	Anthracite
ISO 11760-2005 Classification of Coals	High Rank C	High Rank A	High Rank A	High Rank B
Mean random reflectance %	2.88	5.34	5.45	3.35
Vitrinite-class distribution	V 18 to V 44	V 33 to V 73	V 37 to V 75	V 20 to V 46
Standard deviation σ	0.340	0.785	0.752	0.552
PETROGRAPHIC COMPOSITION (vol. %)				
Maceral analysis, mineral matter basis				
Vitrinite content %	94	84	84	48
Total inertinite %	3	12	10	45
Heat altered / graphitized %	0	2	1	3
Visible minerals %	3	2	5	4
Other %	0	0	0	0
Maceral analysis - Total: 100%	100	100	100	100
Microolithotype analysis				
Vitrite %	89	79	76	35
Inertite %	1	6	5	36
Intermediates (vitrinertite) %	6	13	10	22
Visible minerals				
Carbominerite %	3	2	7	6
Minerite %	1	0	2	1
Microolithotype analysis - Total: 100%	100	100	100	100
Condition analysis				
"Fresh" coal particles %	84	76	80	82
Cracks and fissures %	15	21	17	15
Severely weathered %	1	0	1	1
Particles exhibiting oxidation rims %	0	0	0	0
Particles displaying low temperature devolatilization %	0	0	0	0
Heat altered %	0	3	2	2
Condition analysis - Total: 100%	100	100	100	100

5.2.1 Rank (Degree of maturity of a coal)

The mean random reflectance of vitrinite (R_r , %) is used as a measure of the rank or maturity of the coal samples. It is typically reported on a scale of 0-10 R_r % for South African coals (South African Coal Preparation Society, Coal Preparation (2002)). The mean reflectance of anthracites range

from 2-6% R_r (ISO11760 and consequently, SANS ISO 11760, International Classification of Coals). Within this range, anthracites can be grouped by the mean reflectance as indicated below:

- Semi-anthracite range from 2-3
- Anthracite range from 3-4
- Meta anthracite range from 4-6

R_r% above 6% indicates graphite. The mean reflectance of the samples analysed ranged from 2.88% to 5.45%. The anthracites were classified according to its rank and the sub categories for high rank coals are indicated in Table 8. SANS ISO (11760:2004) also defines anthracite as a high rank coal with R_r between 2-6% and a mean maximum reflectance less than 8% for a geographically unaltered coal.

Table 8 Sub categories for high rank coals: anthracites (SANS ISO 11760:2004)

Sub-category	Description
High rank C ^a (anthracite C)	$2,0 \% \leq \bar{R}_f < 3,0 \%$
High rank B ^b (anthracite B)	$3,0 \% \leq \bar{R}_f < 4,0 \%$
High rank A (anthracite A)	$4,0 \% \leq \bar{R}_f < 6,0 \%$ (or $\bar{R}_{v, \max} < 8,0 \%$)
^a $\bar{R}_f = 3,0 \%$ approximates the rank where the volatile matter yield has decreased to a level that results in a significant decrease in the ease of ignition and the bireflectance is beginning to increase strongly; see [1], [8], [11], [16]. ^b $\bar{R}_f = 4,0 \%$ approximates the rank where the development of bireflectance is beginning to accelerate due to the onset of a decrease in $\bar{R}_{v, \min}$ as $\bar{R}_{v, \max}$ continues to increase.	

The SAA anthracite with R_r 3.35% was classified as High Rank B anthracite (indicated in Table 8). The Vietnamese and the Vietnamese Low Volatile (VLV) were classified as an Anthracite, High Rank C and a Meta Anthracite, High Rank A respectively. The Russian anthracite was classified as Meta Anthracite, High Rank A. The age of these anthracites according to their location (van Krevelen (1993) and Taylor et al (1998)) is as follows:

- Russian: Carboniferous anthracite with age of 360 to 286 million years ago
- South African: Permian anthracites with age of 286 to 248 million years ago
- Vietnamese: Triassic anthracites 248 to 213 million years ago

The age of the anthracites and the conditions under which the anthracites were formed may contribute significantly to its behaviour during utilisation.

The relationship between the anthracites that were to be evaluated and the respective Mean Random Reflectance (%) and that of vitrinite and the total inertinite content was also evaluated. This can be seen in Figure 9 and Figure 10. It is quite evident that the SAA anthracite, Gondwana type coal, is not vitrinite rich compared to the other anthracites, typically North Atlantic (Russian) or formed in Laurasian-like conditions (the younger Vietnamese anthracites).

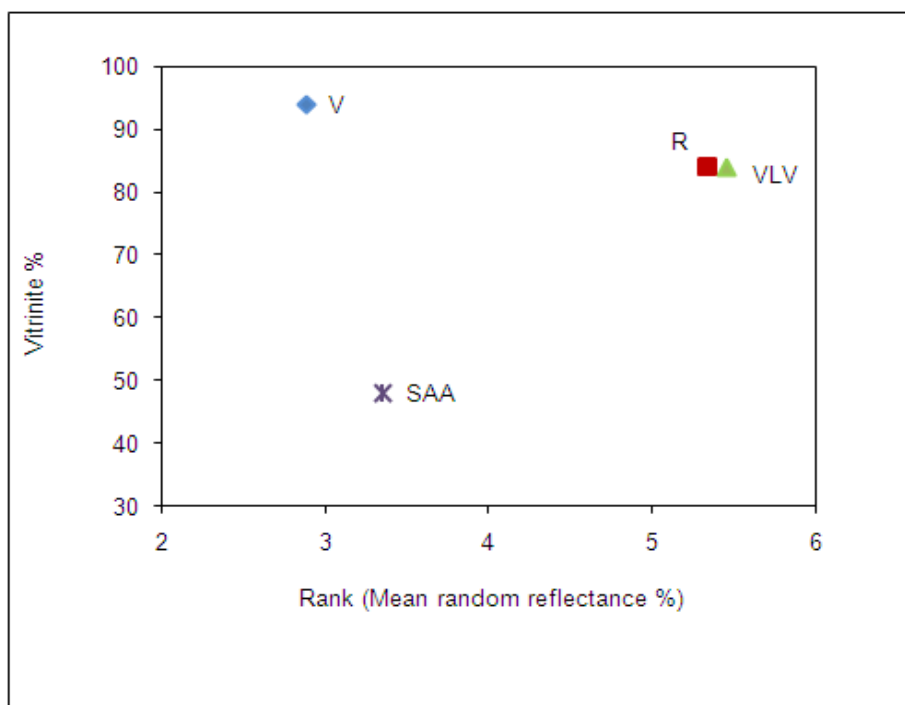


Figure 9 Vitrinite % versus Rank (Mean Random Reflectance %)

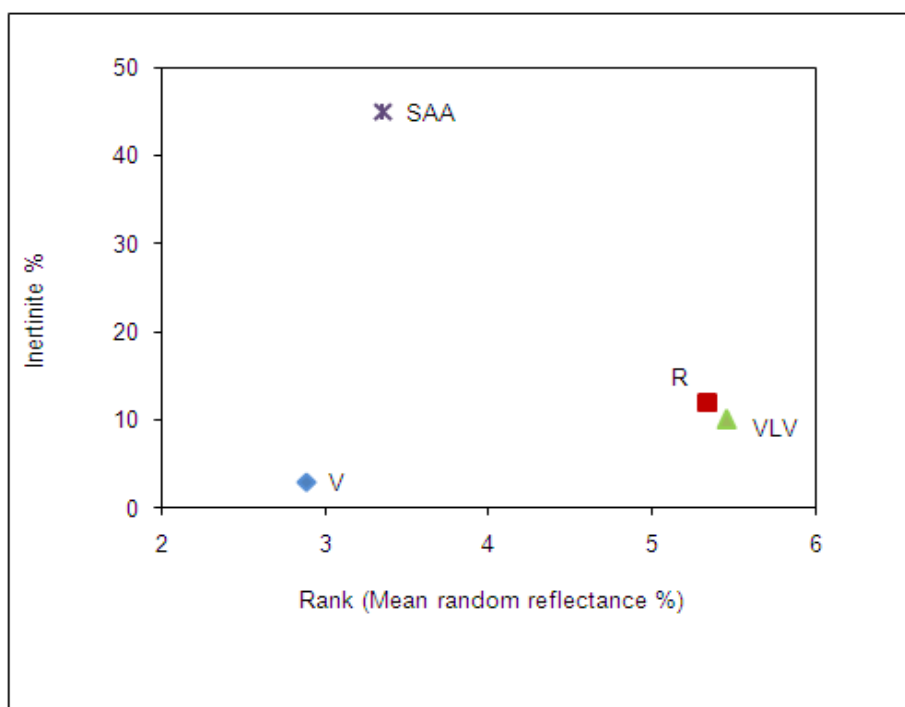


Figure 10 Total inertinite % versus Rank (Mean Random Reflectance %)

5.2.2 Grade

The content of microscopically visible minerals in all four samples is quite low. The carbominerite and minerite content varied from 2-7% and 0-2% respectively.

5.2.3 Condition

According to petrographic analytical report written by du Cann (2008), most of the coal particles of the samples analysed was “fresh” in nature. The amount of “fresh” coal particles ranged from 76 to 84%.

5.3 Comparison of mass loss and fractional conversion against time

A summary of the reactivity of each sample and the test inputs is indicated in Appendix 9.3 and the raw data (including the reactivity, fractional conversion and shrinking core model outputs) on an hourly basis is indicated in Appendix 9.4. Figure 11 to Figure 18 in the text below indicate the percentage mass loss and fractional conversion against time for the different anthracites. At 850°C (Figure 11) sample V has fastest rate of mass loss followed by VLV and then the SAA and the R anthracite, however one should note that the R and SAA anthracite seem to follow each other closely at this temperature. This trend is also indicated in the plot of fractional conversion against

time (Figure 12). Fractional conversion was calculated using Equation 9. In terms of the distinction between the northern hemisphere samples (V, R, VLV) it appears that at 850°C, the inertinite dominant SAA anthracite is comparable to the highest rank, vitrinite rich R sample in terms of rate of mass loss. Though R and VLV reported very similar organic composition and rank, the identified trend, lower reactivity corresponding to higher rank for the three vitrinite rich anthracites is expected, as is the lower reactivity for the SAA anthracite, given its inertinite predominance at the given rank level.

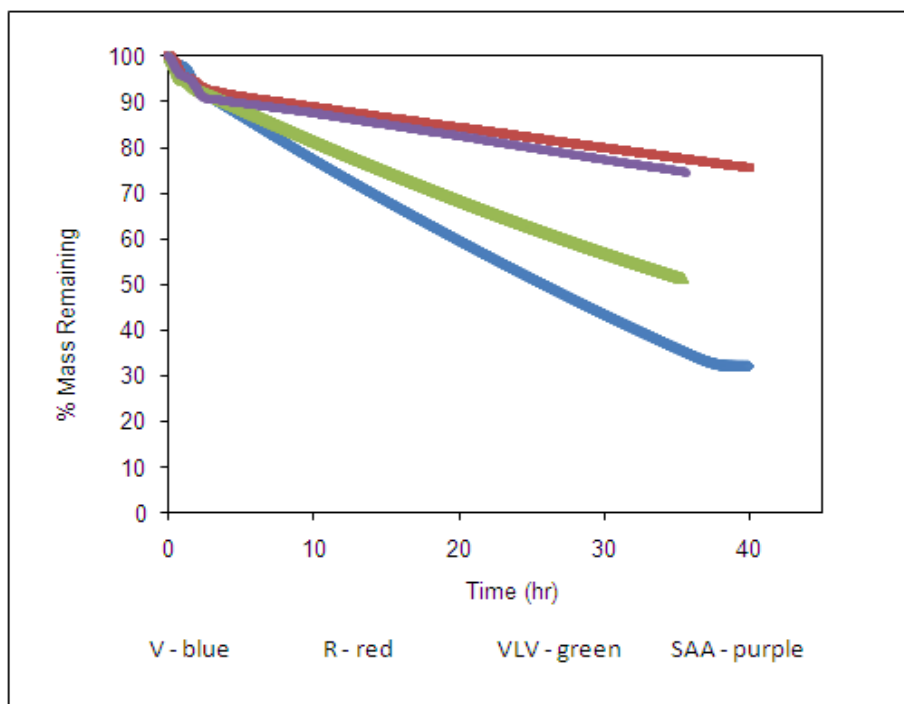


Figure 11 Comparison of mass loss against time at 850°C

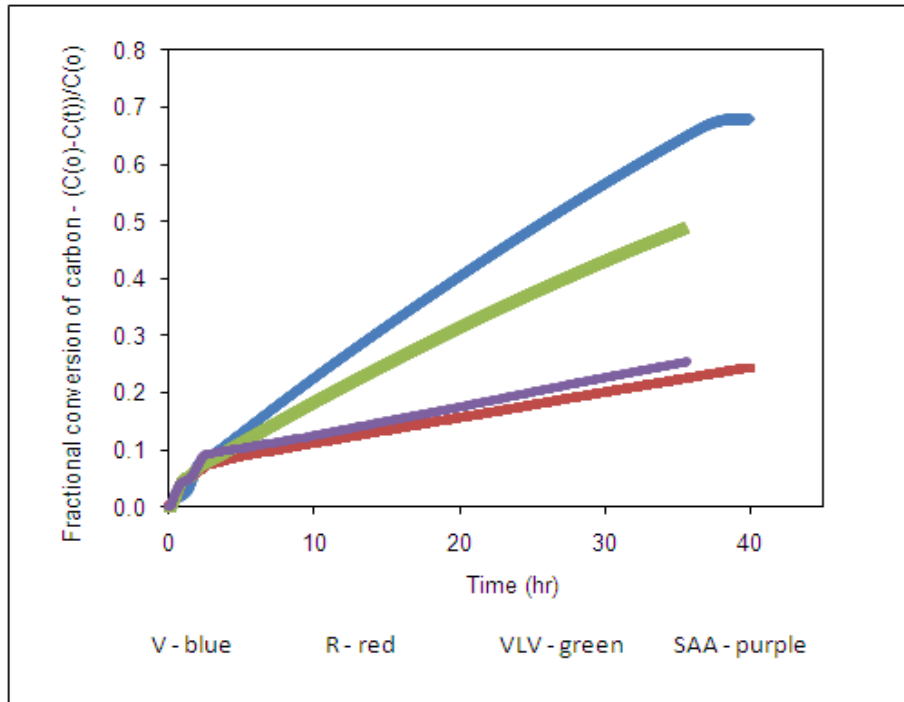


Figure 12 Fractional conversion of fixed carbon against time at 850°C

At 1100°C (Figure 13), sample R has the highest rate of mass loss followed by V and at this temperature the VLV and SAA anthracite have similar rate of mass loss. One should note that up to 15 hours the SAA, VLV and V sample rate of mass loss is very similar. The same order of anthracite conversion is seen in the fractional conversion plot in Figure 14.

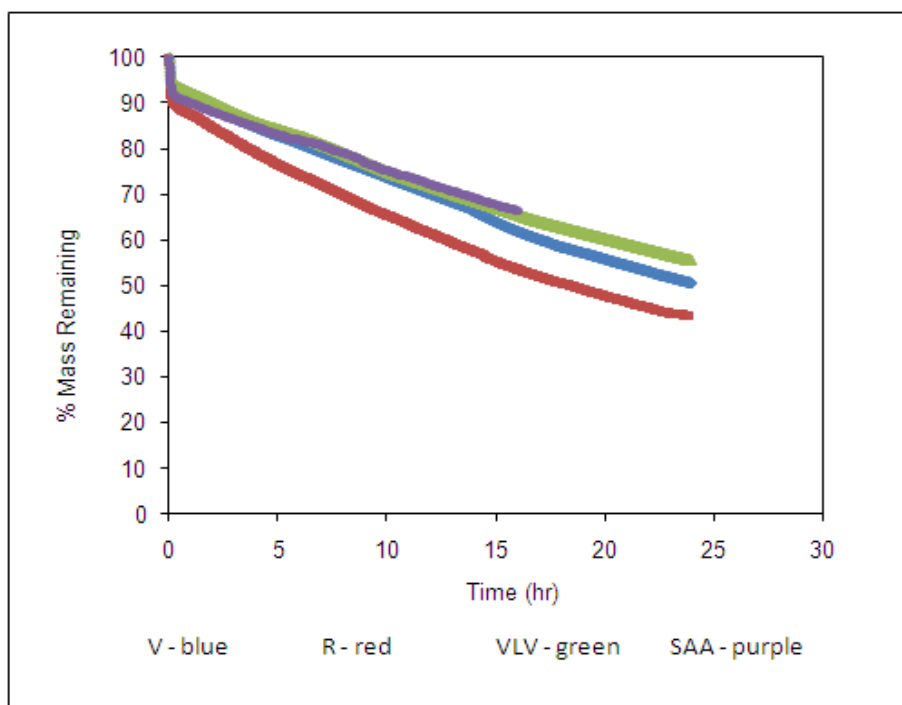


Figure 13 Comparison of mass loss against time at 1100°C

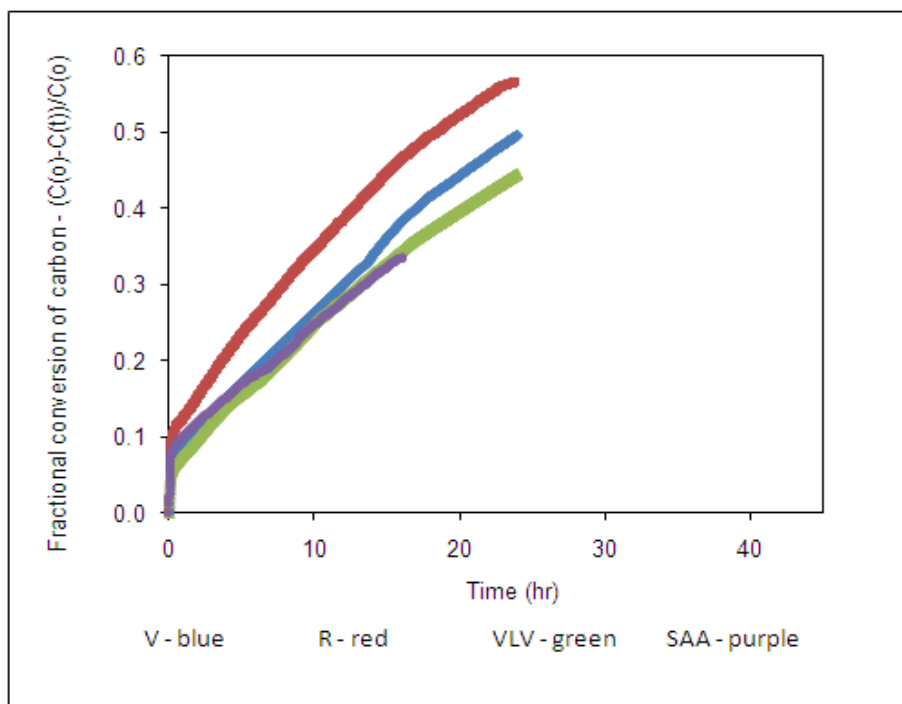


Figure 14 Fractional conversion of fixed carbon against time at 1100°C

Figure 15 indicates the mass loss against time at 1350°C. It appears that from start of the test till about 15 hours the rate of mass loss for all the anthracite samples was the same. From that point onwards, the V sample lags a little behind the other anthracites. At approximately 26 hours into the test the VLV sample becomes the slowest reacting and remains that way till the end of the test. The SAA anthracite also becomes slower reacting from about 29 hours onwards. Thus by the end of the reaction V and R sample have the same mass loss rate followed by the SAA and then the VLV. This figure indicates that at some temperatures the anthracites have more or less the same rate of mass loss rate but one sample can supersede the other samples if the test is left to continue. The fractional conversion graph, Figure 16, supports these findings.

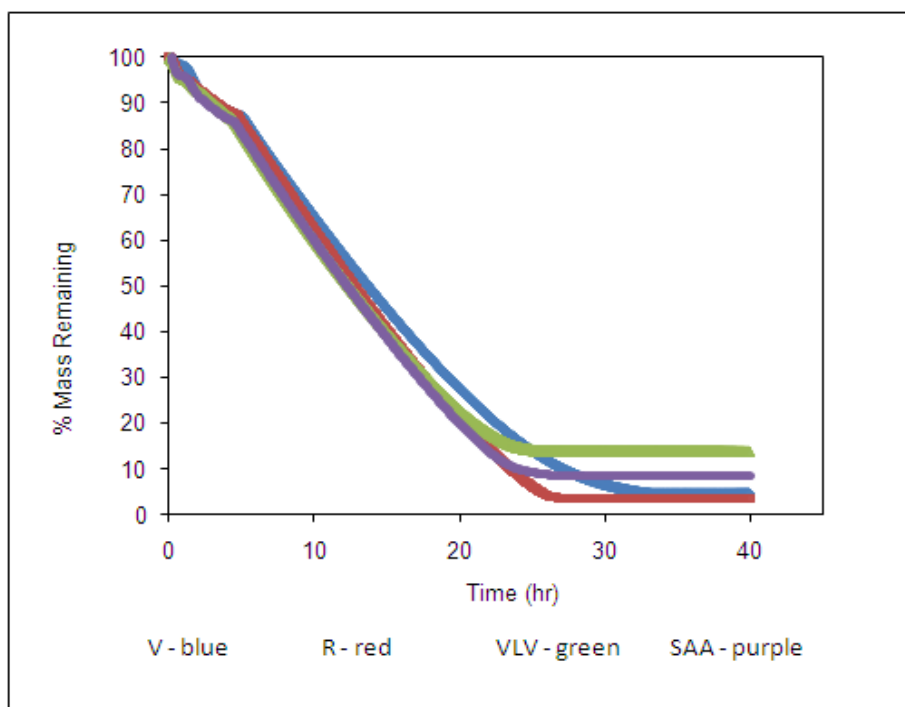


Figure 15 Comparison of mass loss against time at 1350°C

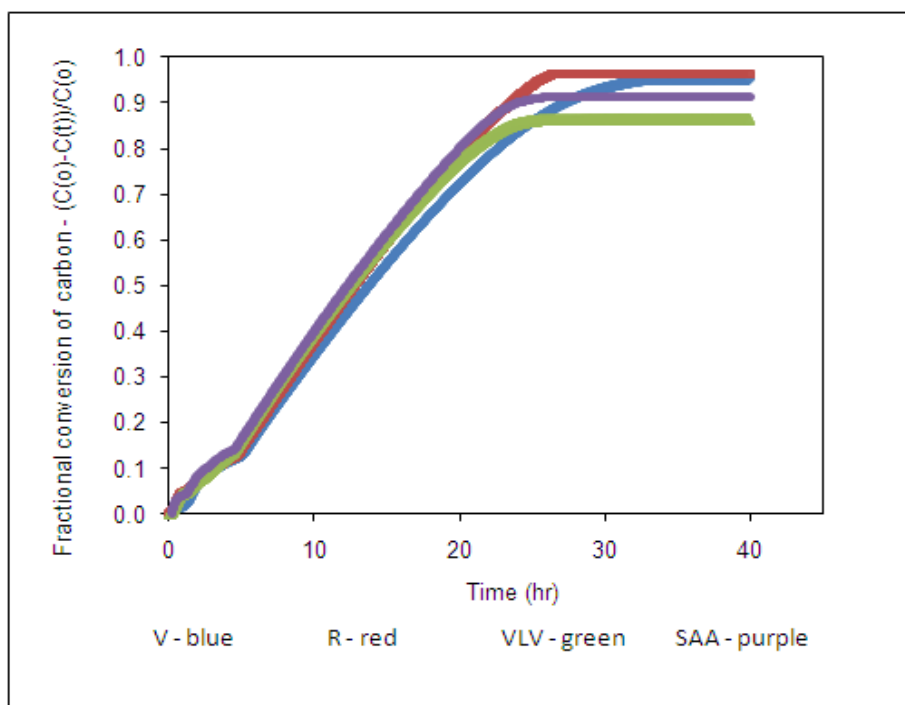


Figure 16 Fractional conversion of fixed carbon against time at 1350°C

Figure 17 indicates the mass loss curve at 1600°C where the rate of mass loss is fastest for the R anthracite followed by V, VLV and SAA. At this temperature SAA anthracite (inertinite dominant) mass loss is similar to that of the VLV sample (vitrinite rich, highest rank). The fractional conversion plot also supports this order.

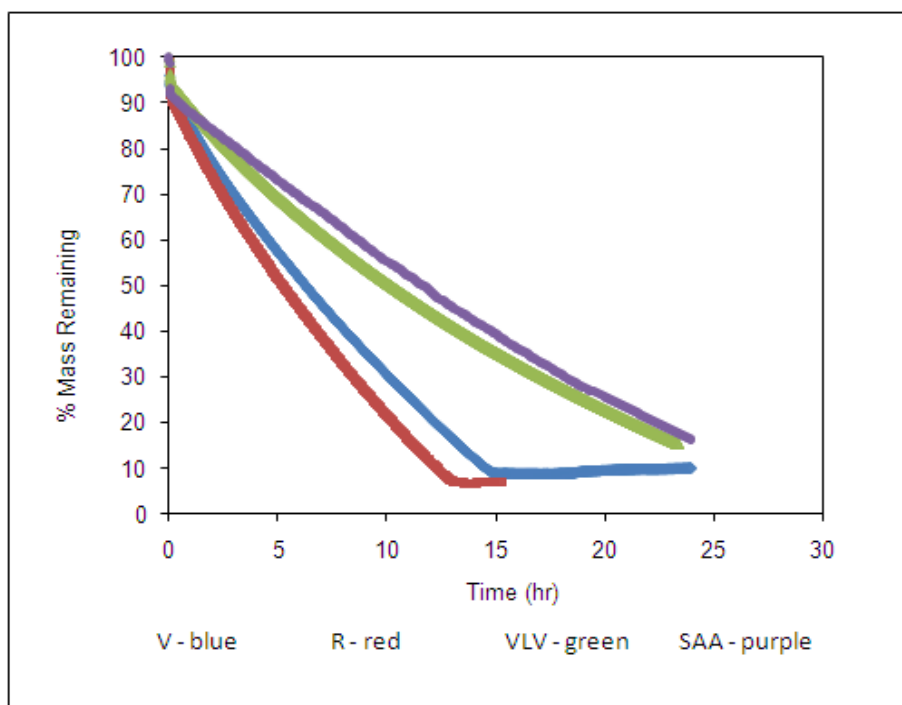


Figure 17 Comparison of mass loss against time at 1600°C

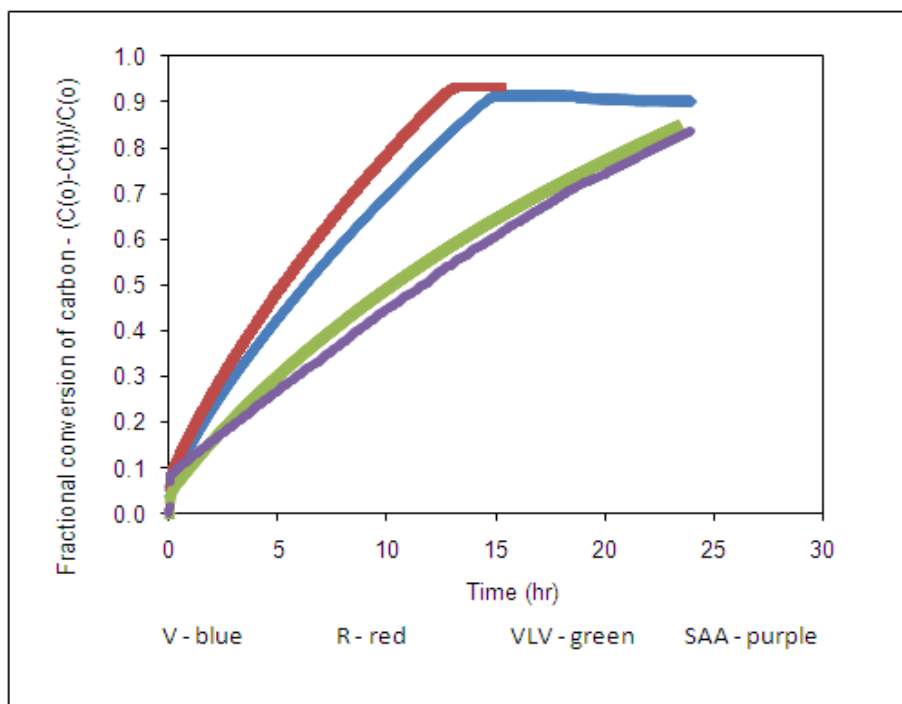


Figure 18 Fractional conversion of fixed carbon against time at 1600°C

5.3.1 Procedure comparison

This study involved the use of results obtained by Jordan (2009) (the same samples were assessed in Jordan (2009) and in the current study), where tests were conducted at 1100°C and 1600°C. Jordan (2009) conducted tests using a CO₂ flow rate of 150sccm⁻¹(standard cubic centimetres per minute). Mass loss data was recorded from the time the TGA reached reaction temperature (CO₂ was initiated) for 24 hours. Data was not recorded during the heat up and the circulation of Argon (Ar) gas. However, in the current study (which evaluated temperatures at 850°C and 1350°C); the TGA was heated up to the test temperature in an Ar atmosphere (to ensure the reactor atmosphere was neutral). The rate of temperature increase utilised was 5°C/min. At 200°C the temperature was held for 10 minutes and then the temperature was ramped to the test temperature and held for 30 minutes before the carbon dioxide (reactant gas) is introduced. The Ar and CO₂ flow rate utilised in the tests conducted at Mintek for this study (tests at 850°C and 1350°C) was 285sccm¹ (standard cubic centimetres per minute) and 270sccm⁻¹ respectively. Shaw et al (1997) reported that experimental procedure influences the results of the TGA test. Taking into account that different experimental procedures were followed, two repeat tests were conducted at 1100°C and 1600°C to determine the effect of change in experimental procedure. Figure 19 and Figure 20 report the repeat test conducted using the SAA and the R samples at 1100°C and 1600°C respectively. The current study test duration is much longer than that conducted by Jordan (2009), however in both cases the rate of mass loss differs distinctly. It is for this reason that the results obtained for the current study have been compared separately, in the sections that follow.

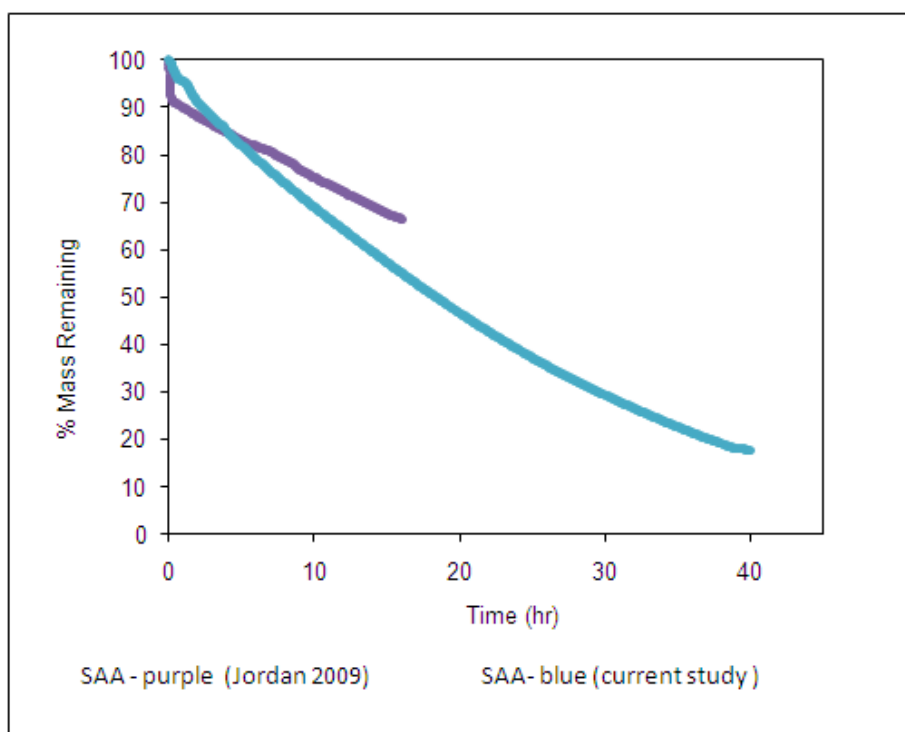


Figure 19 Mass loss comparison of test of SAA anthracite at 1100°C using current study method against the result obtained by Jordan (2009)

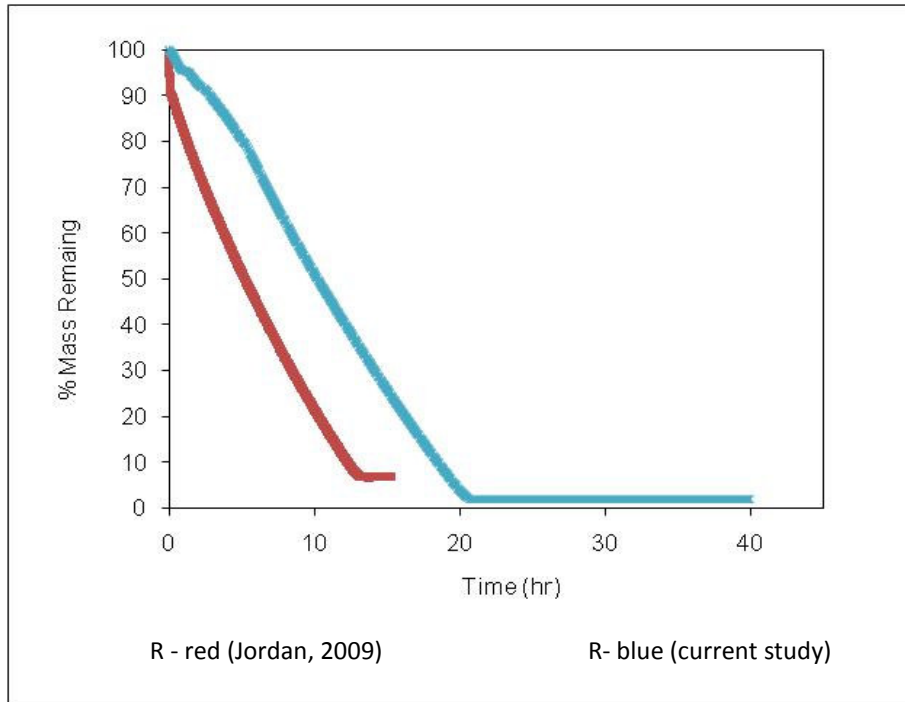


Figure 20 Mass loss comparison of test of R anthracite at 1600°C using current study method against the result obtained by Jordan (2009)

5.4 Comparison of the effect of fixed carbon, volatile matter, ash content and ash oxides on anthracite average apparent reactivity

Figure 21 indicates the trend of percentage fixed carbon (dry ash free basis, daf) against average apparent reactivity at 850°C and 1350°C. The different anthracites are represented by the different colours (V- blue, R - red, VLV - green, SAA - purple). The different temperatures are indicated by the different symbols. At 1350°C, there appears to be a decrease in average apparent reactivity ($R_{app, ave}$) with fixed carbon up to 97% fixed carbon (daf), thereafter $R_{app, ave}$ appears to increase with an increase in fixed carbon. This trend is not observed at 850°C. It seems as if, at low temperatures the effect of fixed carbon on the average apparent reactivity is not as prominent as it is at higher temperatures.

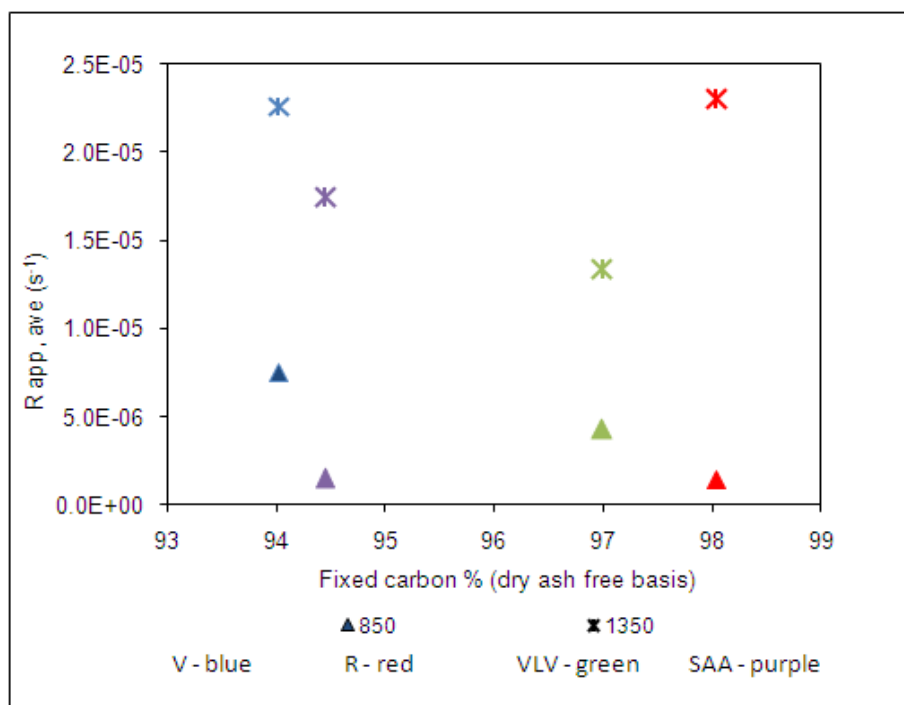


Figure 21 Comparison of fixed carbon against average apparent reactivity at 850°C and 1350°C

Figure 22 shows the plot of average apparent reactivity ($R_{app, ave}$) against fixed carbon (daf) for temperatures at 1100°C and 1600°C. At 1600°C, the $R_{app, ave}$ increases as fixed carbon increases, however at 1100°C, the fixed carbon has limited effect on the average apparent reactivity as indicated by the slight upward trend in the graph. It is tentative to suggest from Figure 21 and Figure 22 that the effect of fixed carbon on $R_{app, ave}$ below temperatures of 1100°C is somewhat limited.

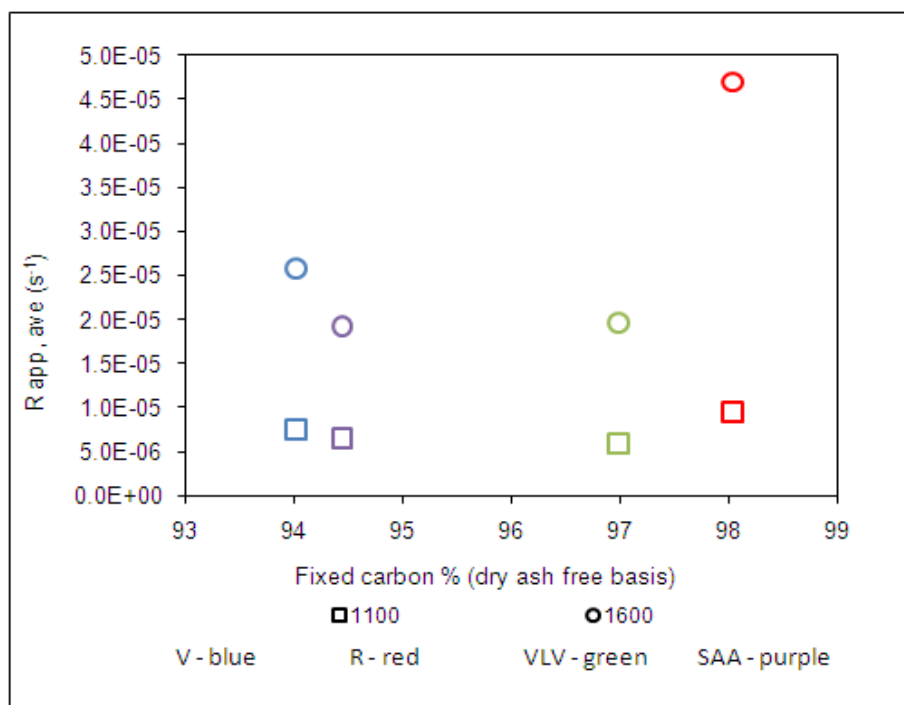


Figure 22 Comparison of fixed carbon against average apparent reactivity at 1100°C and 1600°C

From Figure 23 and Figure 24, it is clear that there is some relationship between the average apparent reactivity and percentage volatile matter (dry basis, db). At 1350°C and 1600°C, the average apparent reactivity decreases with increasing volatile matter content up to 2% and thereafter it appears to increase (this could have been confirmed had the investigation included samples with volatile matter content between 3 and 5%). At 850°C, this trend is not as prominent and at 1100°C, and there appears to be a slight downward trend.

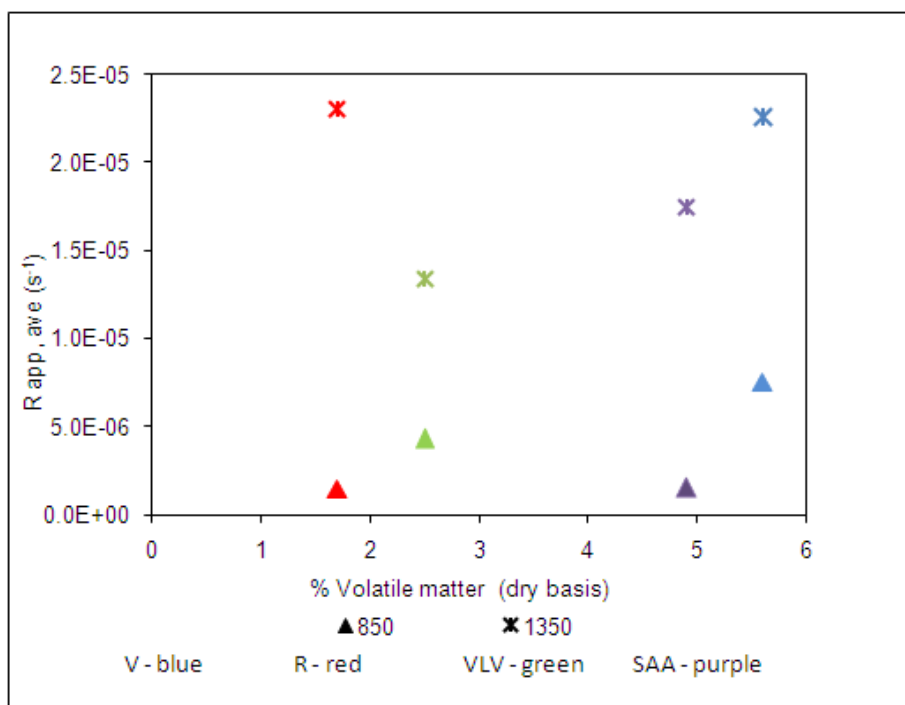


Figure 23 Comparison of percentage volatile matter content against average apparent reactivity 850°C and 1350°C

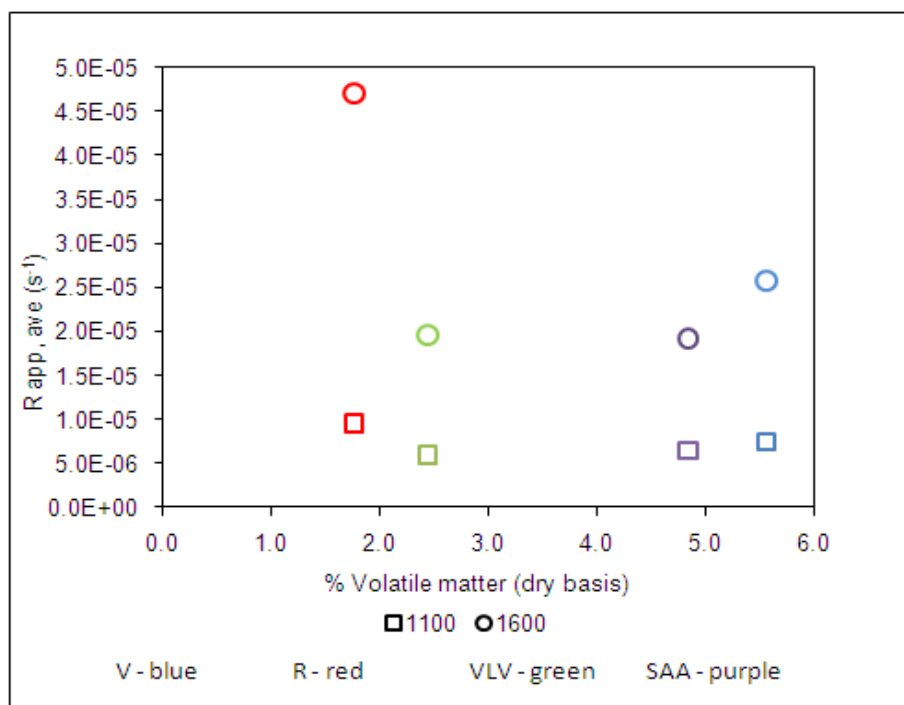


Figure 24 Comparison of percentage volatile matter content against average apparent reactivity at 1100°C and 1600°C

Figure 25 illustrates the plot of percentage ash content (dry basis, db) versus average apparent reactivity at 850°C and 1350°C. At 1350°C $R_{app, ave}$ decreases with an increase in ash content, however this is not apparent in the 850°C run which is most probably due to the fact that the temperature is too low to observe significant changes in characteristics of the anthracite. Figure 26 indicates the plot of percentage ash content (db) versus average apparent reactivity at 1100°C and 1600°C. The effect of ash content on $R_{app, ave}$ is prominent at 1600°C. As ash content increases, the $R_{app, ave}$ decreases at 1600°C up to 10% ash content, thereafter there is a possibility that it might increase with increasing ash content. However this can only be categorically evaluated if samples with higher ash content of similar composition are evaluated. It also appears from Figure 25 and Figure 26 that the relationship is temperature dependent i.e. as temperature increases above 1100°C, the effect of ash content on $R_{app, ave}$ becomes more prominent.

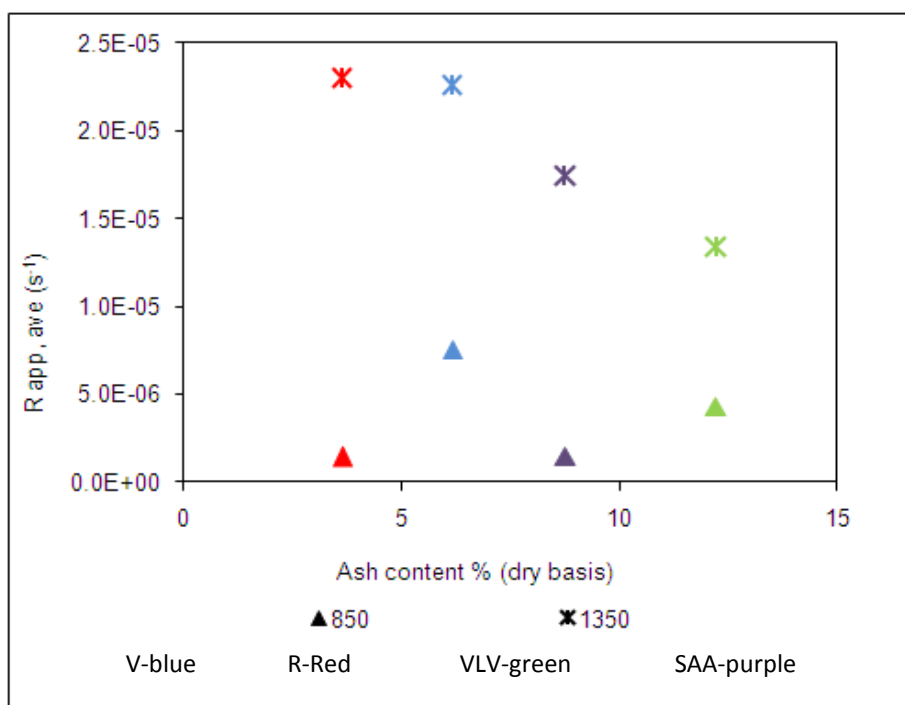


Figure 25 Comparison of ash content against average apparent reactivity at 850°C and 1350°C

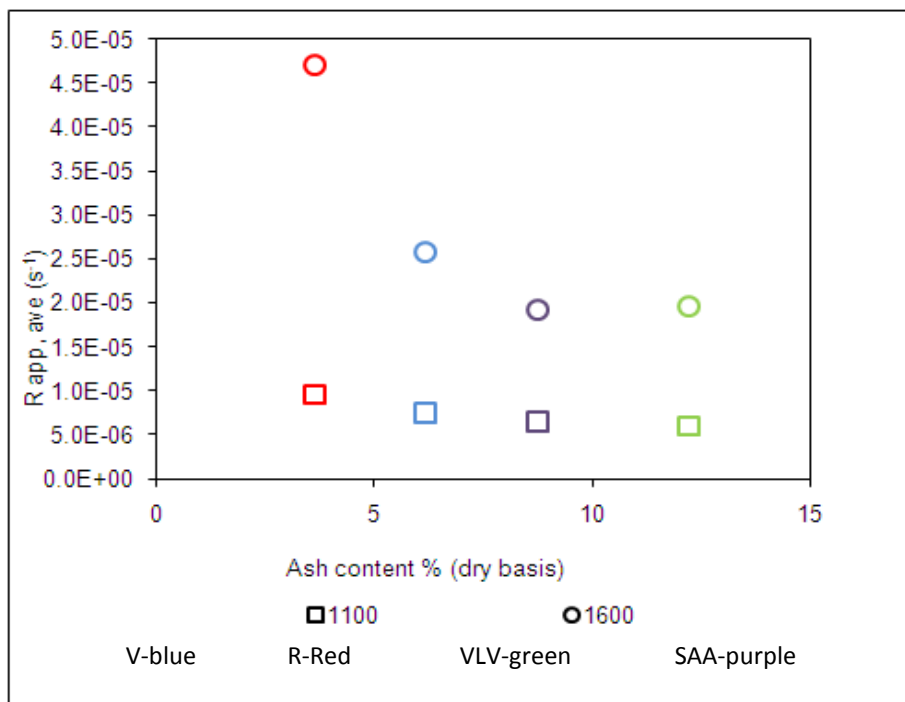


Figure 26 Comparison of ash content against average apparent reactivity at 1100°C and 1600°C

The effect of the different ash constituents on the average apparent reactivity was also evaluated. It has been reported in literature that calcium oxide (CaO) and magnesium oxide (MgO) may have a catalytic effect and increase reactivity. In addition the CaO and MgO content in anthracite is monitored in an ilmenite operation as these elements report as impurities to the product adversely affecting downstream processing. From Figure 27, it can be seen that CaO does have some impact on the reactivity at 1350°C, however this is not evident at 850°C. At 1350°C the V and R sample have similar reactivity, but the CaO content of these samples is different. This seems to indicate that at 1350°C, CaO content cannot be used as a measure of the average apparent reactivity. At 1600°C there appears to be an increase in reactivity with increasing CaO content (Figure 28), but at the lower temperature i.e. 1100°C, there is a marginal effect of CaO on reactivity. It appears that the catalytic effect of CaO might only be evident at temperatures above 1100°C. Between the R and VLV anthracites (identical rank and organic composition), higher CaO content favours higher reactivity at temperature above 850°C. On the other hand the SAA has slightly higher CaO content than the V anthracite and the average apparent reactivity of this sample is adversely affected at all temperatures except at 1100°C where the average apparent reactivity of these samples is similar.

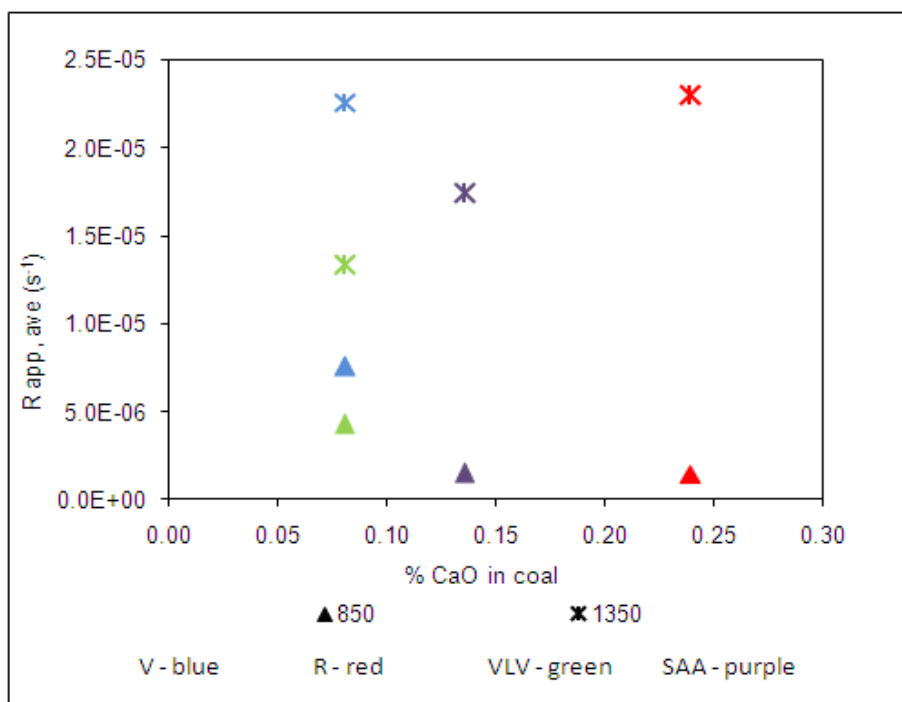


Figure 27 Comparison of calcium oxide (CaO) against average apparent reactivity at 850°C and 1350°C

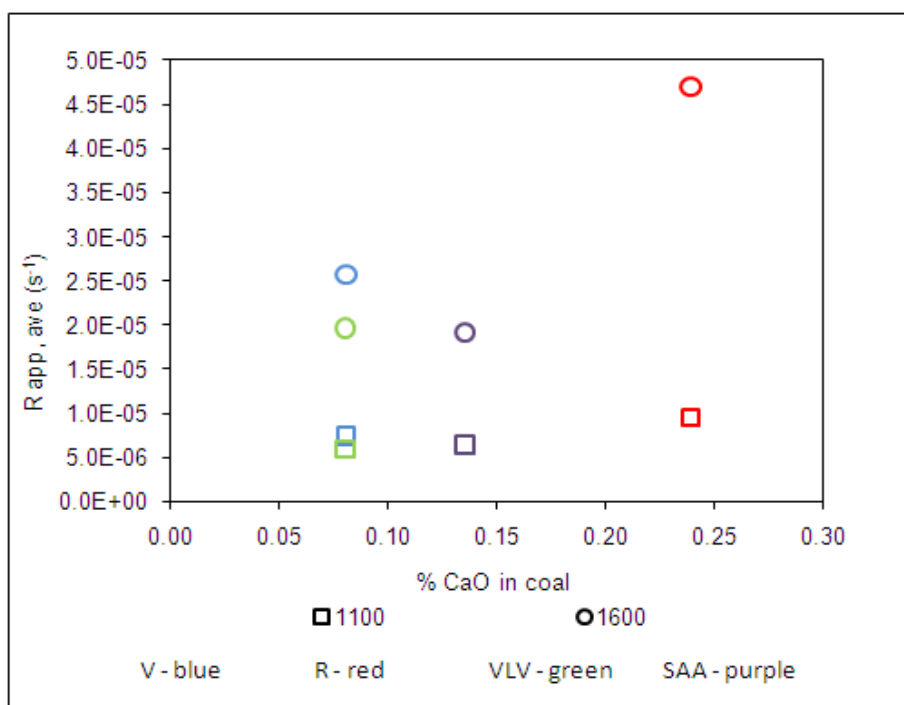


Figure 28 Comparison of percentage calcium oxide (CaO) against average apparent reactivity at 1100°C and 1600°C

Figure 29 plots the relationship between MgO content versus average apparent reactivity at 850°C and 1350°C. The effect of MgO content at 1350°C is not very clear, $R_{app, ave}$ appears to be decreasing up to 0.11% MgO. At 1350°C, the V and R anthracite have the same reactivity despite the different MgO content in both samples. This implies that at this temperature there is little or no effect of MgO content on the V and R samples. In Figure 30, an increase in $R_{app, ave}$ at 1600°C with increasing MgO content is noted, however it has limited effect at 1100°C.

The V anthracite and SAA anthracite have similar rank and seem to indicate a decrease in reactivity with increase in MgO content (notwithstanding the fact that the SAA anthracite has about half the vitrinite content as the V anthracite). When the R and VLV anthracite (identical rank and organic composition) are compared one notes that the R sample has significantly higher MgO content as opposed to the VLV sample and at all temperatures, the R anthracite reported higher reactivity. Though the MgO content cannot be used as a measure of reactivity in isolation, when compared between anthracites with identical rank and petrographic composition, it is possible that higher MgO content favours reactivity but at lower anthracitic ranks (High Rank B and C), increase in MgO content may result in a decrease in reactivity.

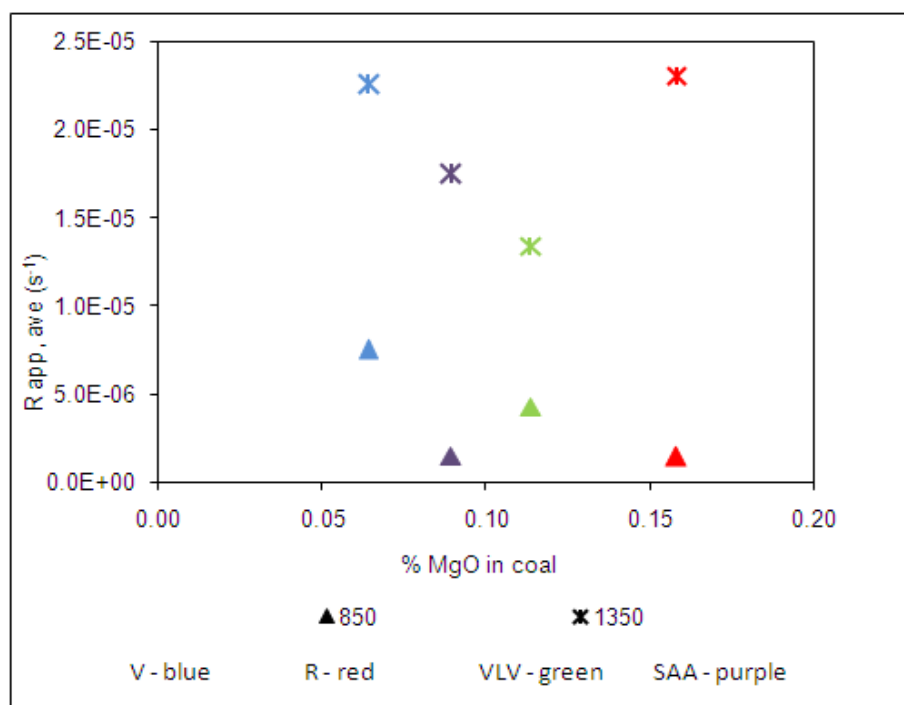


Figure 29 Comparison of percentage magnesium oxide (MgO) against average apparent reactivity at 850°C and 1350°C

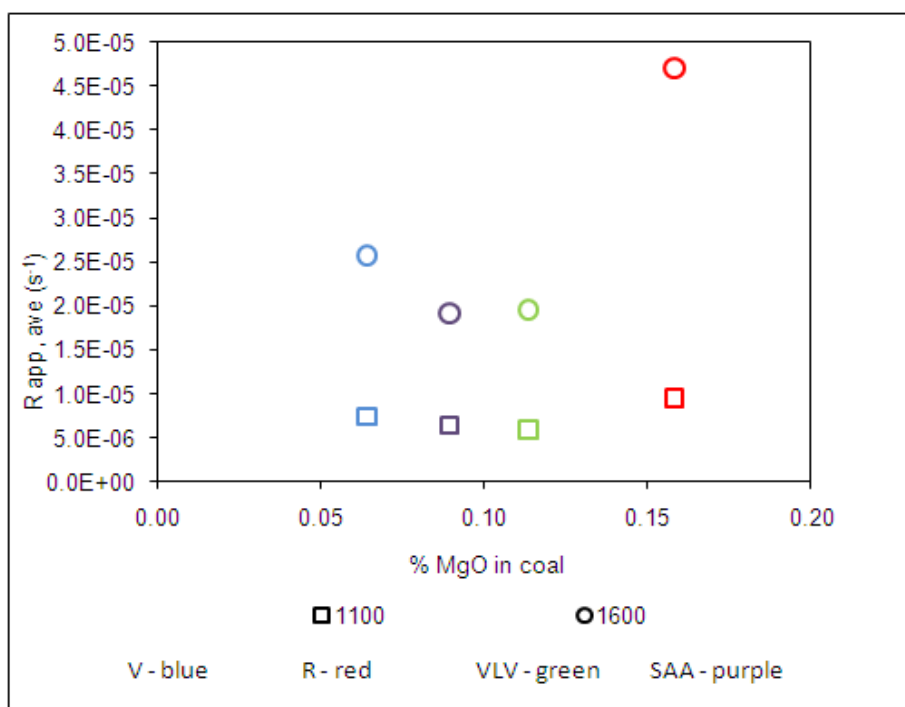


Figure 30 Comparison of percentage magnesium oxide against average apparent reactivity at 1100°C and 1600°C

Percentage silica oxide (SiO₂) content was also plotted against average apparent reactivity and like the MgO and CaO plots, the effect of SiO₂ is also influenced at temperature (Figure 31 and Figure 32). At temperatures above 850°C, the average apparent reactivity decreases with an increase in SiO₂ content.

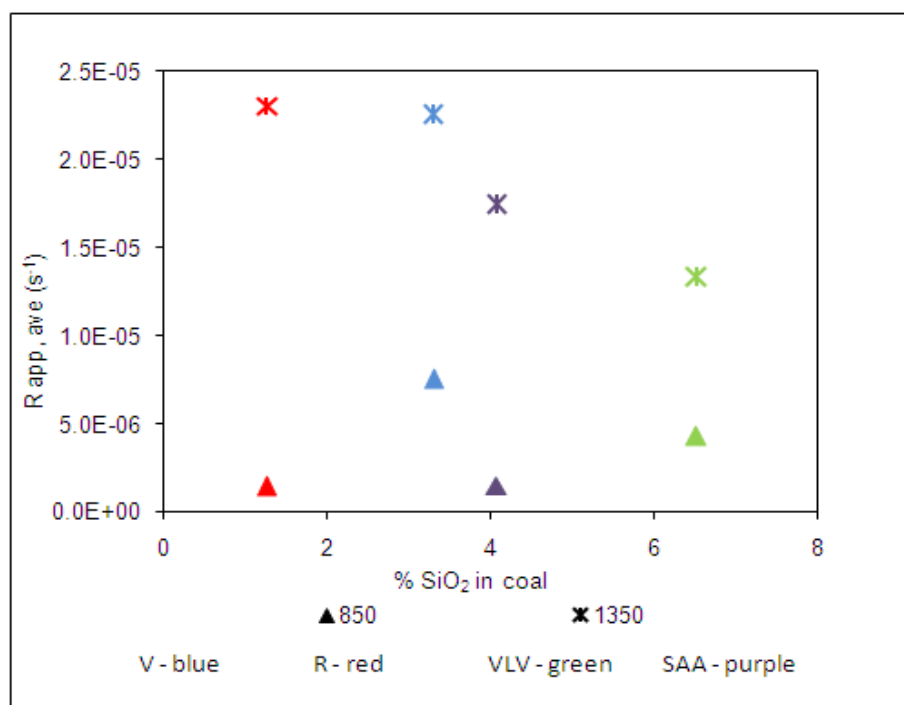


Figure 31 Comparison of percentage silica oxide against average apparent reactivity 850°C and 1350°C

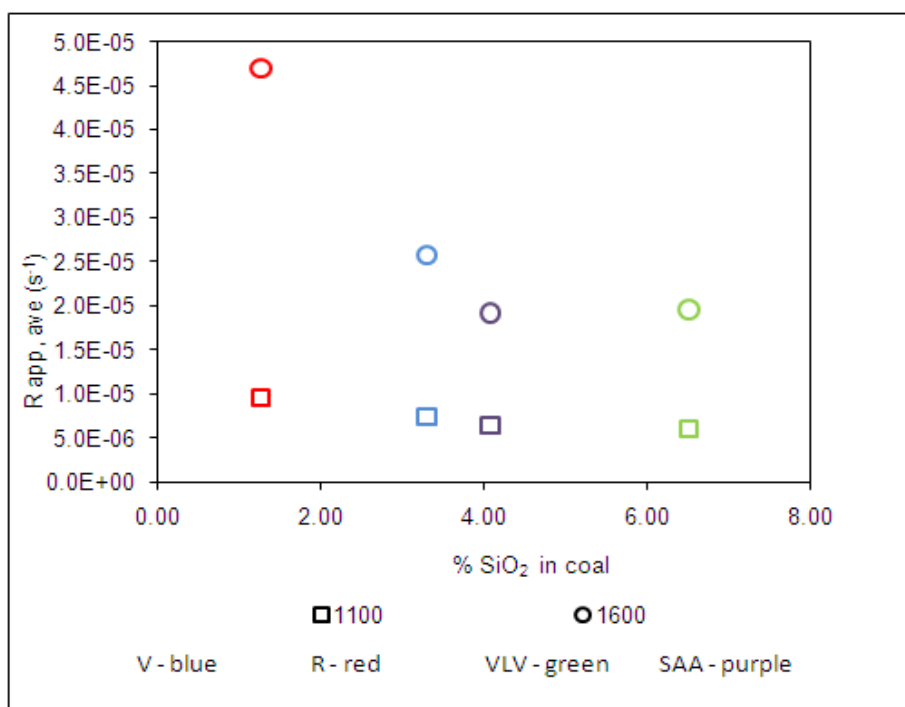


Figure 32 Comparison of percentage silica oxide (SiO₂) against average apparent reactivity 1100°C and 1600°C

5.5 Comparison of rank, vitrinite, volatile matter (dry basis) and inertinite on anthracite average apparent reactivity

Whilst most researchers found that reactivity decreased with increase in rank, Jordan (2009) did not find a relationship between rank and anthracite reactivity. This trend was not prominent in the current investigation. The reason might lie with the nature of the anthracites utilised in this investigation, only one southern hemisphere anthracite (SAA), with Gondwana characteristics (i.e. inertinite dominant, formed in stable platforms, Permian in age) was compared to three northern hemisphere anthracites (V, VLV and R), two of which are Mesozoic in age, vitrinite rich (V and VLV) and the other north Atlantic, vitrinite rich of Carboniferous age (R). There is limited if any, effect of rank on reactivity at 1100°C which seems to be consistent with findings on other parameters. At 850°C (Figure 33), there appears to be a downward trend, decrease in $R_{app, ave}$ with increase in rank. The shortcoming of the tests conducted in the current investigation is that anthracites with a complete data set of rank in between 2.5% to 6% was not available. Two samples had a mean reflectance of rank of 2.88% and 3.35% respectively whilst the remaining two samples had a mean reflectance of rank of 5.34% and 5.45% respectively. Samples with mean reflectance between 3.5% and 4.5% would have assisted in providing a more conclusive observation of the relationship

between rank and the average apparent reactivity. When comparing the effect of rank on the average apparent reactivity, at all temperatures for the SAA and V samples, as the rank decreases between these two samples average apparent reactivity increases (at 1100°C this is not as prominent). In the case of the two meta anthracites of identical rank and petrographic composition, the R and VLV samples indicate a similar trend when compared separately from the SAA and V samples if one considers the marginal difference in rank. The R sample has slightly lower rank than the VLV sample and has higher average apparent reactivity at all temperatures. When comparing all four anthracites, the trend of increasing rank and the decreasing $R_{app, ave}$ is noted with the exception that the R anthracite (Carboniferous age) always reports higher than expected reactivity.

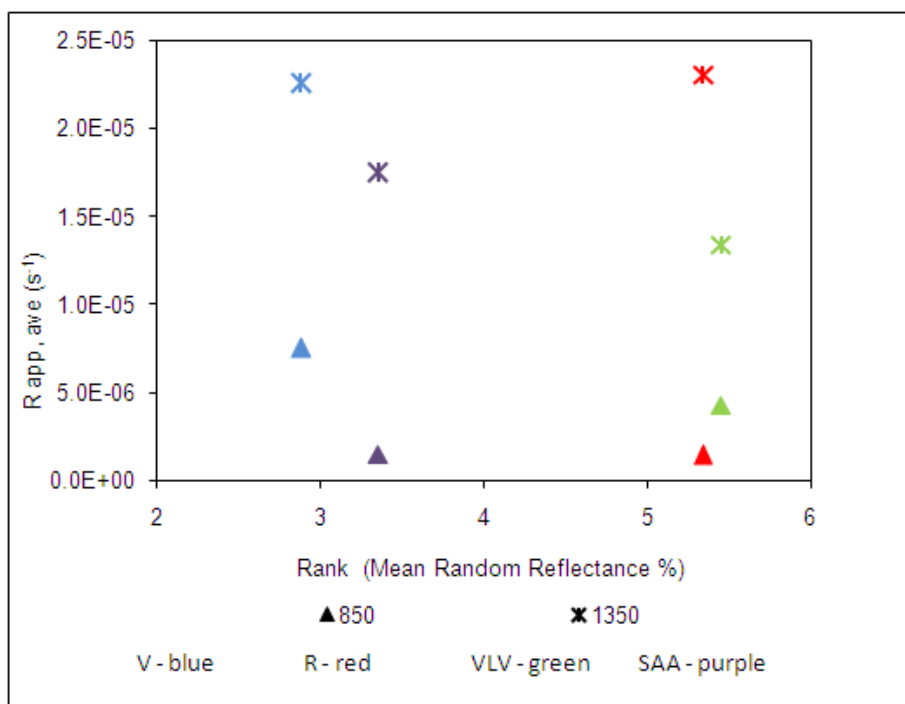


Figure 33 Comparison of rank against average apparent reactivity at 850°C and 1350°C

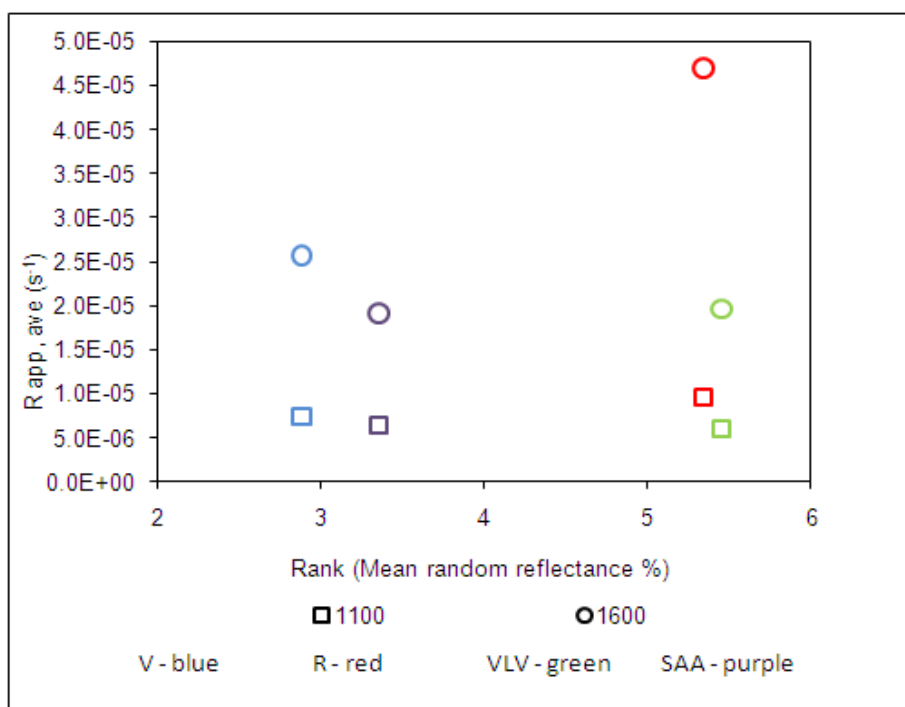


Figure 34 Comparison of rank against average apparent reactivity at 1100°C and 1600°C

Figure 35 and Figure 36 plots a comparison of vitrinite content against average apparent reactivity. Unsurprisingly there is limited trending visible from these plots given that rank also plays a role. However at temperatures above 850°C, the R sample, again the exception, reported the highest reactivity, despite the fact that the VLV sample has the same vitrinite content. At 850°C (Figure 35), there appears to be an increase in average apparent reactivity with increasing vitrinite content. At 1100°C and 1600°C, the SAA anthracite has similar reactivity as the northern hemisphere V and VLV anthracites despite having much lower vitrinite content (48%). As previously mentioned the SAA and V anthracites (High Rank B and C respectively) are similar and the R and VLV (High Rank A, meta anthracites) are similar. At temperatures above 850°C for the R and VLV anthracites, the higher vitrinite content favours higher average apparent reactivity. At 850°C and 1350°C, the V anthracite has higher $R_{app, ave}$ than the SAA but at 1100°C and 1600°C, the $R_{app, ave}$ of the SAA anthracite is similar to the V anthracite. The V anthracite has a slightly higher reactivity at these temperatures. It is possible that at high ranks, the effect of vitrinite content on reactivity is positive, but at low rank the effect is not as dominant as lower vitrinite content can be compensated by the presence of reactive inertinite at low rank (however it is yet not possible to quantify “reactive” inertinite in anthracites, as it is in bituminous coals, and for that reason the presence of reactive inertinite in anthracites is only presumed but not proven).

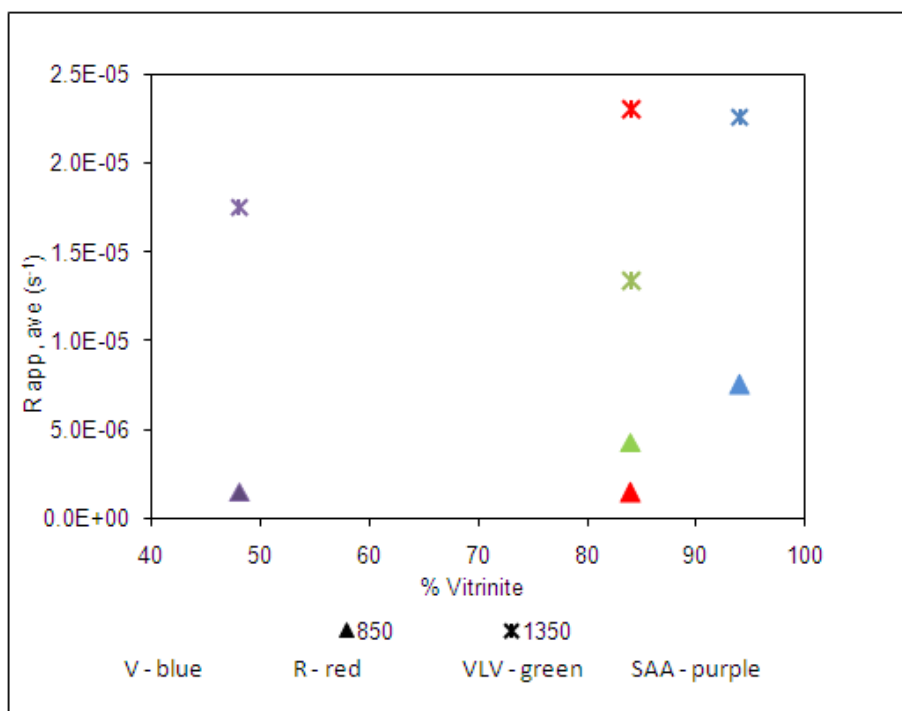


Figure 35 Comparison of vitrinite against average apparent reactivity at 850°C and 1350°C

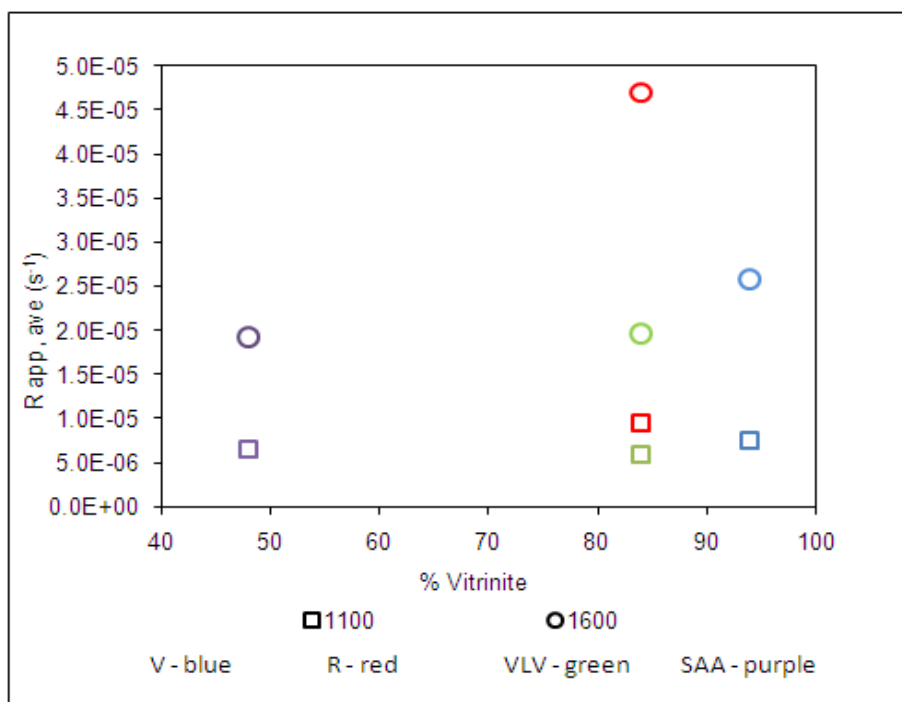


Figure 36 Comparison of vitrinite against average apparent reactivity at 1100°C and 1600°C

Limited trending can be observed when evaluating the plot of inertinite content versus $R_{app, ave}$ (Figure 37 and Figure 38). It is essentially the reciprocal of the vitrinite versus reactivity discussed above. It should be noted that at 1100°C and 1600°C, the R anthracite has the highest reactivity despite having the highest inertinite content from the northern hemisphere anthracites (albeit all of 12%). This is not observed at 850°C. It is tentative to suggest that at temperatures above 850°C, the R anthracite may have 'reactive' inertinite (not yet determined for anthracites as it is for bituminous coals) which contributes to its average apparent reactivity or perhaps the fact that it is the only anthracite (Carboniferous) that would have been formed through normal geological process, unlike either the Permian Gondwana SAA anthracite or the two Mesozoic anthracites (V and VLV) which are known to have been influenced by additional temperature effects and geological factors that would have accelerated their path to achieving the anthracite rank in a much shorter time than the Carboniferous anthracite.

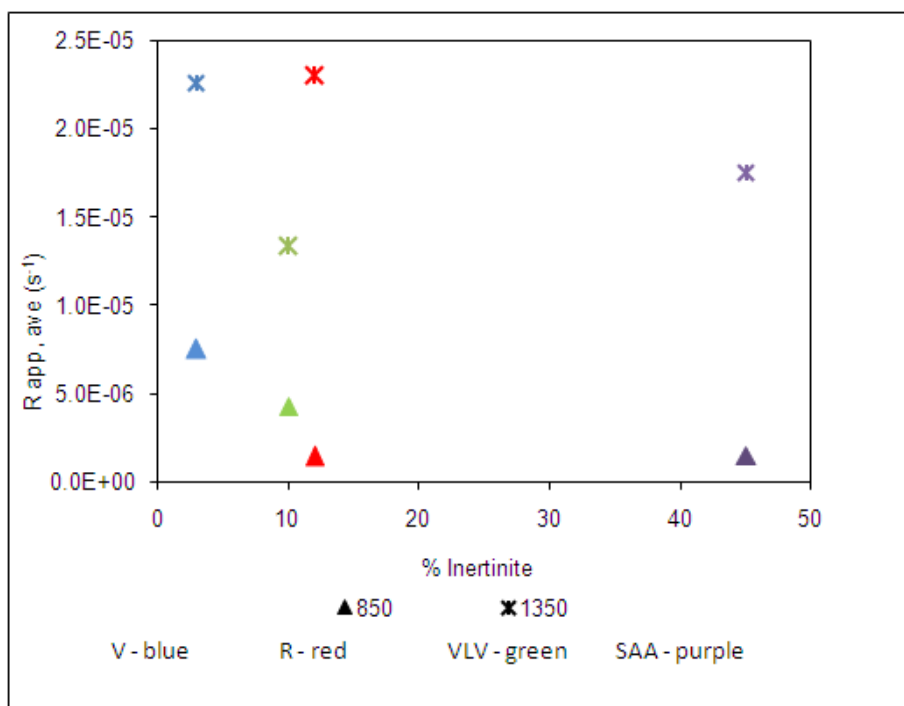


Figure 37 Comparison of inertinite content against average apparent reactivity at 850°C and 1350°C

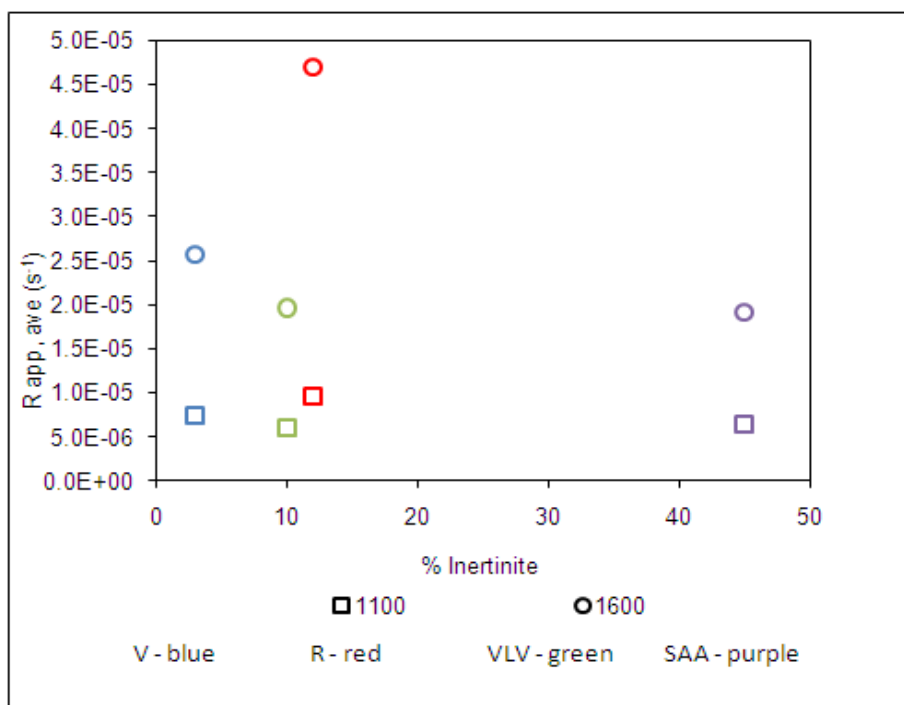


Figure 38 Comparison of inertinite content against average apparent reactivity at 1100°C and 1600°C

5.6 Comparison of the effect of temperature on anthracite average apparent reactivity

The reactivity of the four anthracites was evaluated at 850°C, 1100°C, 1350°C and 1600°C. Figure 39 indicates a plot of temperature versus average apparent reactivity. The black markers indicate results obtained from Jordan (2009) and the red markers are the results obtained in the current study. It is evident that average apparent reactivity ($R_{app, ave}$) increases with temperature for all anthracites. Figure 39 also indicates that the V, VLV and SAA anthracites have similar reactivity at 850°C and 1100°C. At 1350°C and 1600°C the difference in the reactivity of the anthracites becomes more prominent. The R anthracite reported the highest reactivity at 1600°C. This plot also includes the repeat tests conducted at 1100°C and 1600°C using experimental test procedure of the current study and this is indicated by the red markers at 1100°C and 1600°C. It is noted that the reactivity decreased with the change in experimental procedure for the R sample at 1600°C, however reactivity increased at 1100°C for the SAA anthracite with the change in experimental procedure. This implies that higher CO_2 (repeat test at 1100°C was run with CO_2 content 270sccm⁻¹ whilst Jordan (2009) used 150sccm⁻¹) flow rate during the test at 1100°C favoured the reactivity of the SAA anthracite but this was not the case for the R sample at 1600°C, in which case the

reactivity decreased. Shaw et al (1997) discussed the fact that changes in experimental procedure affect the outcome of the TGA result and this was corroborated in the current study.

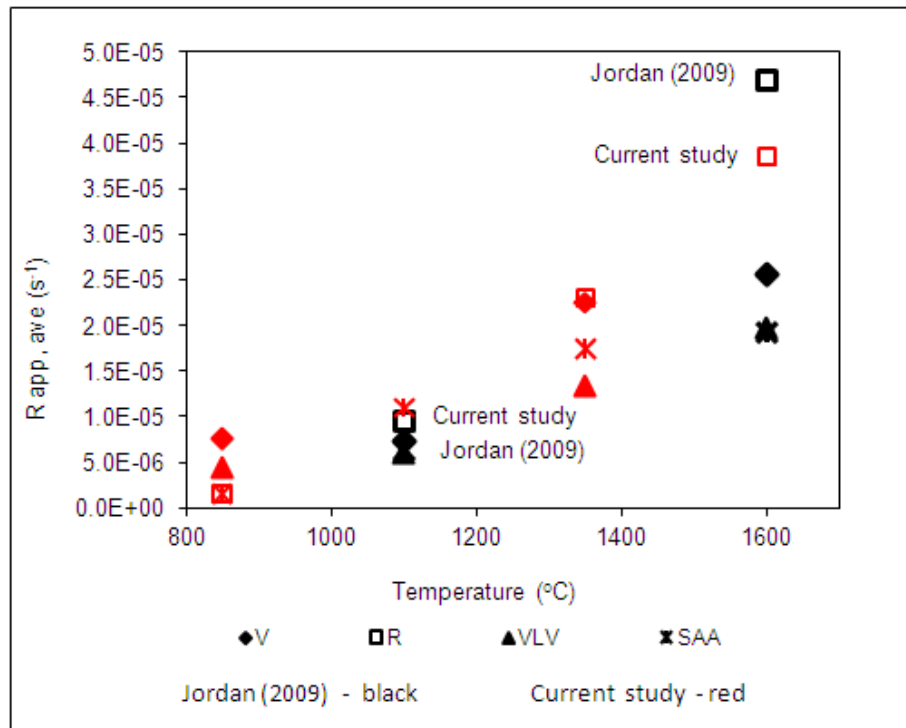


Figure 39 Plot of average apparent reactivity against temperature

5.7 Evaluation of shrinking core model and activation energy

The shrinking core model was also evaluated and plotted against time. Figure 40 to Figure 43 indicate the plot of $1 - (1 - x)^{1/3}$ against time for the entire test period. This includes temperature ramp up using Ar gas in the case of Figure 40 and Figure 42. The graphs are linear for the period after heat up and the introduction of CO₂. In the case of the 1100°C and 1600°C, temperature ramp up data was not available in the Jordan study (2009). At 850°C, 1350°C and 1600°C, some of the anthracites reached a state where no further reaction was taking place and therefore the trend levelled off. For the purpose of determining the rate constant **k** in Equation 8, the period when no further reaction occurred and the period during heat up was removed from the data set and replotted in Figure 44 to Figure 47.

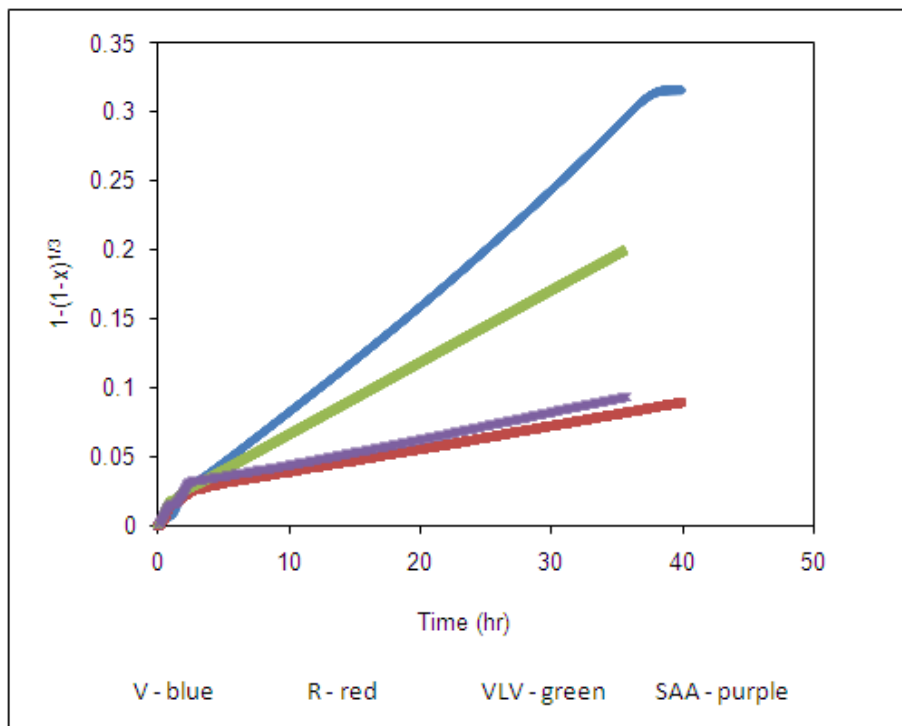


Figure 40 Plot of shrinking core model against time at 850°C

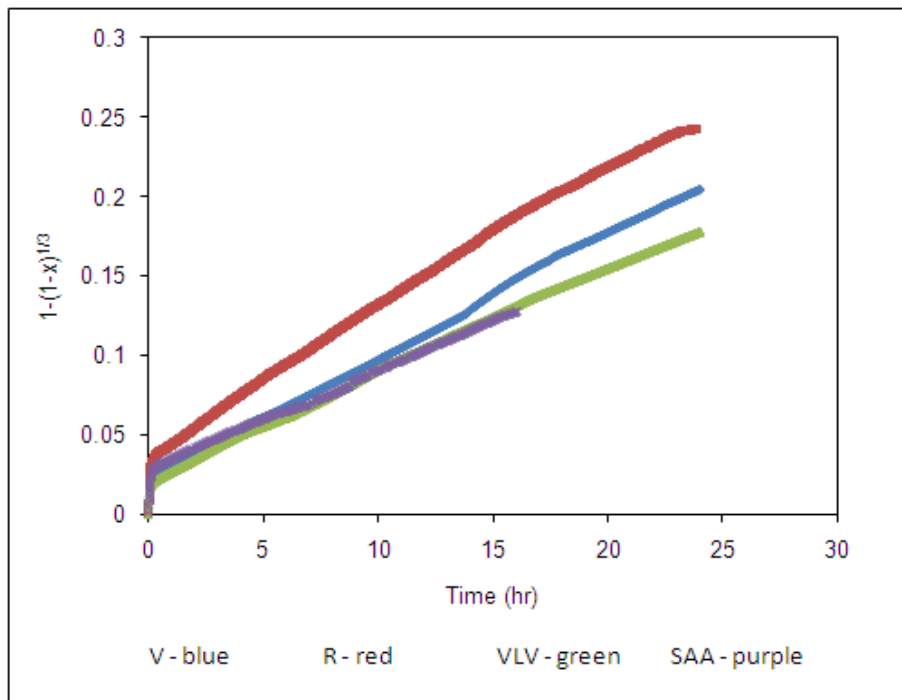


Figure 41 Plot of shrinking core model against time at 1100°C

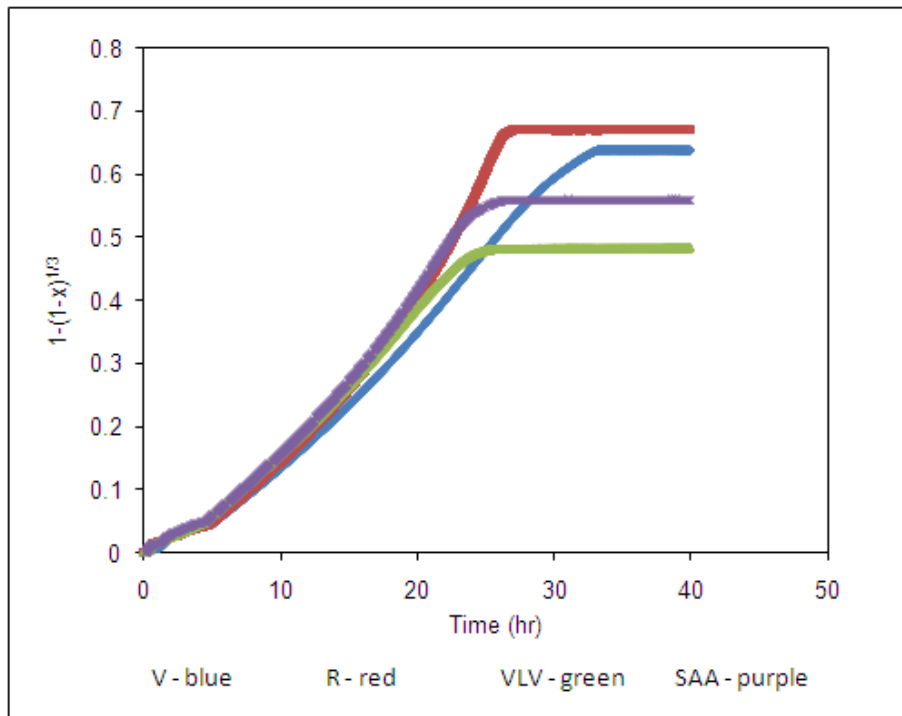


Figure 42 Plot of shrinking core model against time at 1350°C

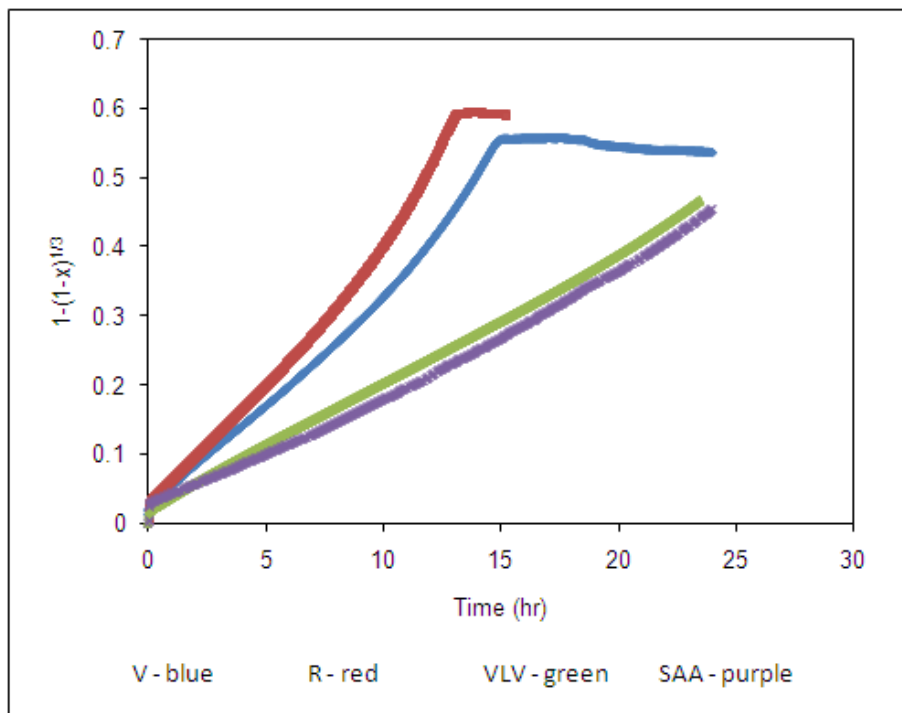


Figure 43 Plot of shrinking core model against time at 1600°C

Figure 44 to Figure 47 indicate that the linear nature of the graphs has an above 98% fit to the data. The slope of each of these graphs was then plotted for the individual anthracites against inverse temperature to determine activation energy which is shown in Figure 48.

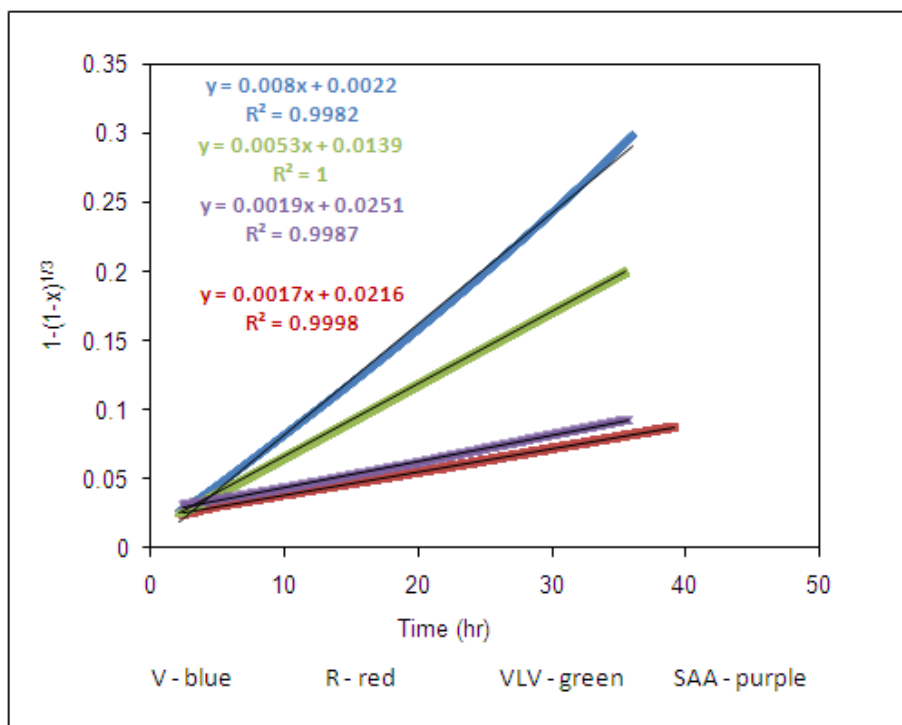


Figure 44 Plot of $1-(1-x)^{1/3}$ against time at 850°C to determine reaction constant of each anthracite

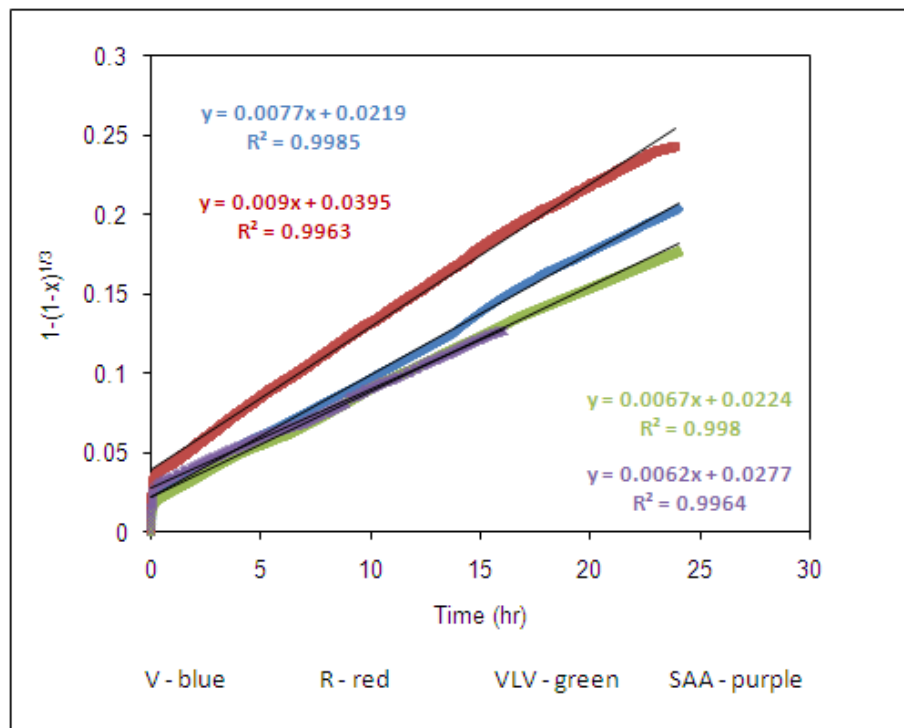


Figure 45 Plot of $1-(1-x)^{1/3}$ against time at 1100°C to determine reaction constant of each anthracite

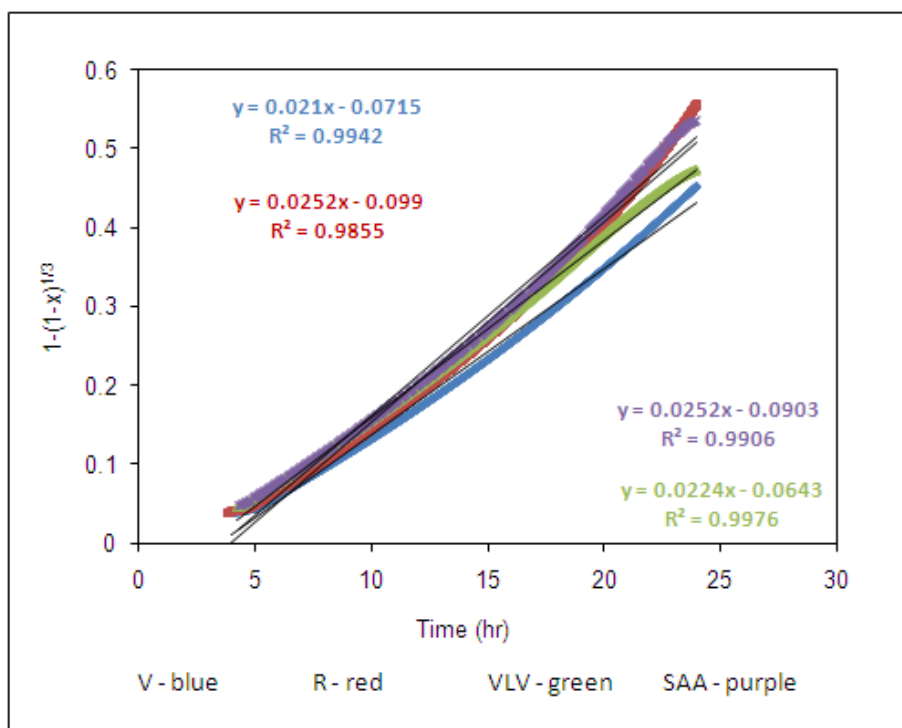


Figure 46 Plot of $1-(1-x)^{1/3}$ against time at 1350°C to determine reaction constant of each anthracite

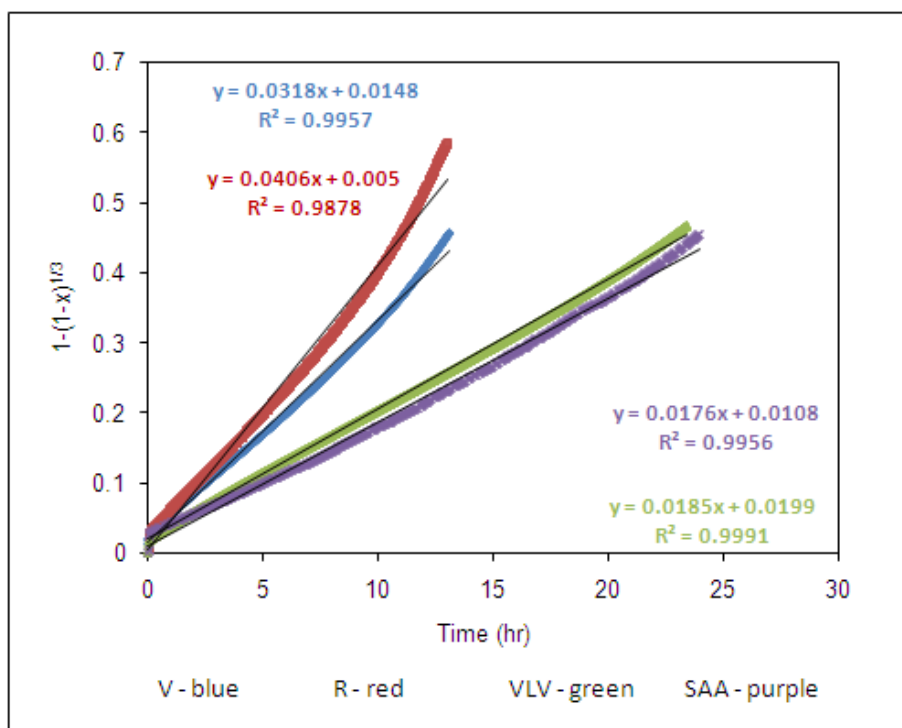


Figure 47 Plot of $1-(1-x)^{1/3}$ against time at 1600°C to determine reaction constant of each anthracite

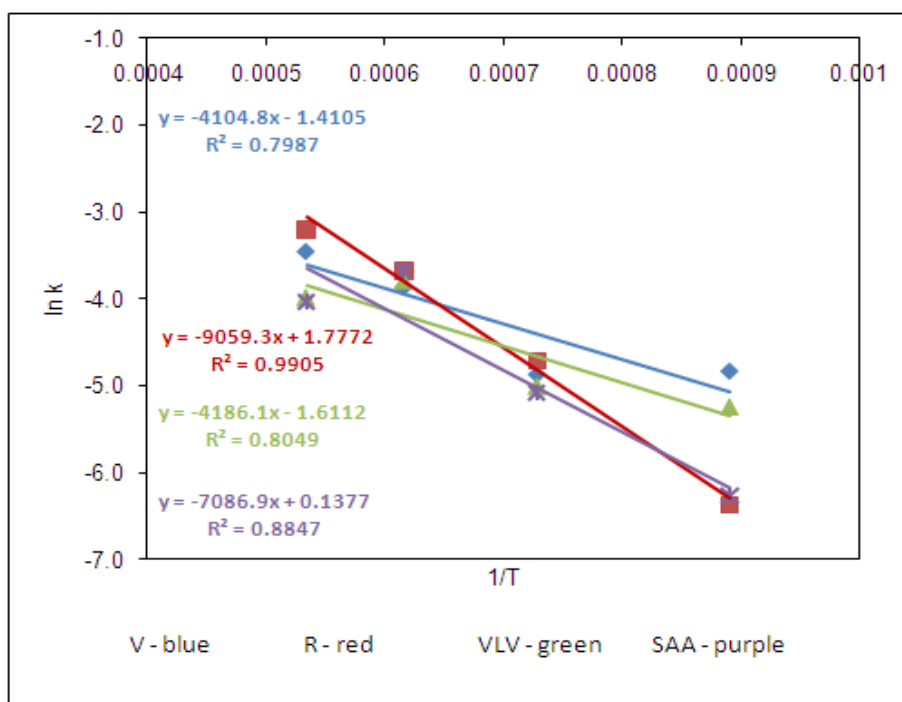


Figure 48 Natural logarithm of rate constant against inverse temperature (Kelvin)

Activation energy was also calculated by plotting the natural logarithm of the average of the apparent reactivity ($R_{app, ave}$) specified by Grigore et al (2006) against the inverse of temperature (kelvin). Figure 49 indicates a plot the $R_{app, ave}$ against inverse temperature. The slope of the graphs was used to calculate activation energy.

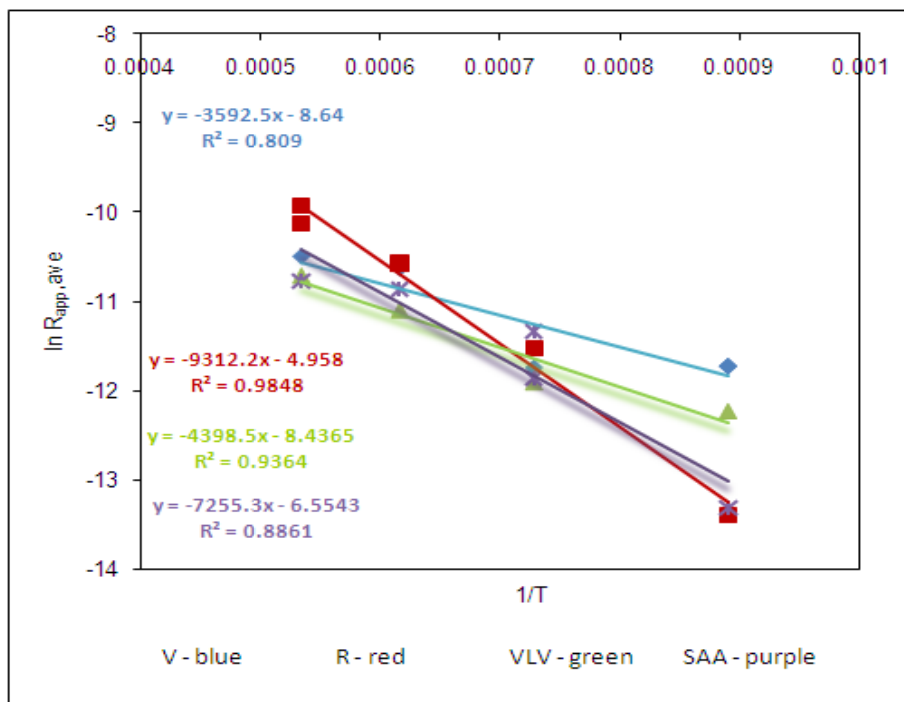


Figure 49 Natural logarithm of $R_{app, ave}$ against inverse temperature

Table 9 indicates the results of the activation energy (E_a) determined using the $R_{app, ave}$ and the rate constant (k). The percentage difference in the result obtained by the two methods varied from 2.4 to 5.2% which indicated that the models support each other. The anthracites are listed in ascending order with highest activation energy listed at the end. The R anthracite had the highest activation energy of 75-77 kJ/mol with the lowest being that of the V anthracite at 32-34 kJ/mol. The activation energy indicates amount of energy required for the reaction to occur and has been utilised in this study to differentiate between the different samples tested. Given the identical rank and petrographic composition shown by R and VLV, these were expected to report identical activation energies which was not the case. The younger meta-anthracite, VLV, reported a lower activation energy than the R sample of older age. On the other hand, the VLV and V samples are similar in age, however the VLV a meta-anthracite (High Rank A) reported higher activation energy than the meso-anthracite V (High Rank C). The inertinite-dominant Gondwana anthracite SAA (High Rank B) reported lower activation energy than R but higher than the VLV and V, which confirms the effect of inertinite in increasing activation energy.

Table 9 Comparison between the activation energy calculated using the shrinking core model rate constant (k) and the average apparent reactivity ($R_{app, ave}$)

Anthracite	Ea (rate constant - k)	Ea ($R_{app,ave}$)	% Difference
	kJ/mol	kJ/mol	
V	34.13	32.36	5.2
VLV	34.80	36.57	5.1
SAA	58.92	60.32	2.4
R	75.32	77.14	2.4

6 CONCLUSIONS

This chapter outlines the results obtained from the investigation which attempted to correlate the characteristics of the anthracite samples with its CO₂ reactivity as obtained by the TGA tests.

- It is clear from the plots of mass loss against time for all four anthracites for the different temperatures, that temperature influences the rate of mass loss. The rate of mass loss increases as temperature increases.
- In terms of average apparent reactivity, the most reactive anthracite at 850°C was V (High Rank C , vitrinite rich), followed by VLV (High Rank A, vitrinite rich) and the SAA (Gondwana, inertinite dominant, High Rank B) and R (High Rank A, Carboniferous, vitrinite rich) anthracites were similar. At 1350°C and 1600°C, the order of reactivity was R followed by V, VLV and SAA being the least reactive, however the SAA and VLV samples had similar average apparent reactivity and mass loss rates. At 1100°C, the average apparent reactivity of all samples were similar. The northern hemisphere anthracite (Carboniferous and Mesozoic age) were more reactive than the southern hemisphere sample (SAA), however the SAA sample had average apparent reactivity that was comparable to the northern hemisphere samples under specific conditions.
- The plots of fractional fixed carbon conversion correlate well with the mass loss against time graphs in terms of the order of reactive anthracites at all temperatures.
- The TGA test is influenced by the experimental method and therefore changes in experimental procedure will result in different outcomes.
- Increasing fixed carbon content appears to positively influence reactivity at temperatures above 1100°C, as at 850°C this trend does not hold and at 1100°C it has no effect on average apparent reactivity of the samples tested.
- The effect of temperature on ash content and specific mineral content appears to be complex. It was found that average apparent reactivity decreased with increasing ash content for temperatures above 1100°C but this was not apparent at 850°C.
- Literature has indicated that some minerals can have a catalytic effect on reactivity. Samples with similar rank such as the R (5.34%) and VLV (5.45%) anthracite showed an increase in average apparent reactivity with increasing MgO and CaO content at temperatures above 1100°C. With the SAA rank at 3.35% and the V anthracite rank at 2.88%, both anthracites reported similar MgO content however at 850°C and 1350°C the V anthracite had higher average apparent reactivity than the SAA sample. It follows that lower rank and increased MgO content may favour reactivity under certain conditions. In terms of the effect of CaO content, average apparent reactivity appears to decrease with increasing CaO content for the SAA and V samples at all temperatures. In terms of SiO₂, average

apparent reactivity increased with decreasing SiO₂ content at temperatures above 850°C. Despite the trending that was achieved by plotting the mineral matter content against average apparent reactivity, it was also noted that samples with similar reactivity had different CaO, MgO or SiO₂ content. It follows that mineral matter content on its own is not a direct indicator of reactivity.

- The effect of petrographic characteristics was evaluated. The distinct relationship between rank by reflectance of vitrinite and the average apparent reactivity (i.e. decreasing reactivity with increasing rank) was not clearly evident in this investigation. A shortcoming of this investigation was that it did not include samples that would have covered a wider range of rank. In addition three of the samples were from the northern hemisphere (two High Rank A (meta-anthracites) samples and one High Rank C) and only one southern hemisphere sample (High rank B) was evaluated. The influence of the formation of these anthracites, one meta anthracite of Carboniferous age (R), two of much younger Mesozoic (V and VLV) and the Gondwana Permian anthracite (SAA) is unknown, but clearly geological factors have left imprints in the anthracites that may have influenced the way in which they will ultimately perform. Taking this shortcoming into account, one could note that when the SAA (rank 3.35%) and V (rank 2.88%) samples are compared, the average apparent reactivity increases with decrease in rank at all temperatures (with exception of 1100°C where it is not as prominent). The same trend holds at all temperatures for the R (rank 5.34%) and VLV (rank 5.45%) even though the difference is within permissible analytical tolerance.
- In terms of the effect of vitrinite content on the average apparent reactivity, there appeared to be a positive trend (increased reactivity with increased vitrinite content). At all temperatures, except 1100°C, there is a general increase in average apparent reactivity with increased vitrinite content. At 1100°C all samples had similar reactivity. A comparison between the R and VLV anthracite (High Rank A meta-anthracites), indicated that higher vitrinite content favoured increased reactivity. The SAA and VLV indicated a similar trend (at 850°C and 1350°C) however at 1100°C and 1600°C, the V anthracite had slightly higher average apparent reactivity than the SAA anthracites. Therefore it is possible that at high ranks, the effect of vitrinite content on reactivity is positive, but at low rank the effect is not as dominant as lower vitrinite content may be compensated by some inertinites behaving like vitrinites (i.e. the concept of reactive inertinites are identified in bituminous coals but it has yet to be quantified or identified in high rank coals such as anthracites). These plots also indicated that the SAA anthracite (southern hemisphere anthracite or Permian age) performed just as well as some of the northern hemisphere anthracites. The southern hemisphere anthracite also had significantly higher inertinite content (45%) and had similar

reactivity as the northern hemisphere (V and VLV) anthracite at 1100°C and 1600°C. At 850°C it performed similar to the R anthracite.

- Interestingly at 1100°C and 1600°C, the R anthracite has the highest reactivity despite having the highest inertinite content from the northern hemisphere anthracites (albeit all of 12%). This is not observed at 850°C. It is tentative to suggest that at temperatures above 850°C, the R anthracite may have reactive inertinite which contributes to its average apparent reactivity or perhaps the average apparent reactivity is influenced by the fact that the R sample is the only anthracite (Carboniferous) that would have been formed through normal geological process, unlike either the Permian Gondwana SAA anthracite or the two Mesozoic anthracites (V and VLV) which are known to have been influenced by additional temperature effects and geological factors that would have accelerated their path to achieving the anthracite rank in a much shorter time than the Carboniferous anthracite.
- Activation energy was determined using the shrinking core model rate constant and that of the average apparent reactivity (specified by Grigore et al, 2006). The percentage difference in the activation energy derived from the two methods varied between 2.4 to 5.2%. The R sample had the highest activation energy and the V sample had the lowest however this is not a measure of the reactivity of the anthracite as it only indicates the amount of energy required by each anthracite for a reaction to occur. The younger meta-anthracite, VLV, reported a lower activation energy than the R sample of older age. On the other hand, the VLV and V samples are similar in age, however the VLV a meta-anthracite (High Rank A) reported higher activation energy than the meso-anthracite V (High Rank C). The inertinite-dominant Gondwana anthracite SAA (High Rank B) reported lower activation energy than R but higher than the VLV and V, which confirms the effect of inertinite in increasing activation energy.
- Despite the findings of the order of CO₂ reactivity of the anthracites evaluated in this study, it is apparent from discussion with personnel that the smelter performance is influenced by operational and design conditions which also impact on how a reductant will perform under those conditions and thus influence the suitability of a reductant in the operation.

7 RECOMMENDATIONS

This chapter covers the recommendations for further research taking into account the limitations of this investigation. These recommendations are as follows:

- The current investigation only included anthracites and majority of the coal characteristics for three of the four samples were in more or less the same range with just one sample as an outlier. Therefore a wider range of coal samples (i.e. bituminous, sub bituminous, anthracites) and graphites should be included in the investigation.
- Another point to be investigated is the petrographic analysis of the residual sample remaining after a reactivity test. Petrographic analysis of the residual sample was not included in this investigation due to insufficient material. However a number of repeat tests could be conducted to accumulate sufficient sample for evaluation. Such work would provide the answer to which macerals are consumed and at what rate. In addition, assessing the impact of particle size, ash content and distribution of minerals on reactivity would be added.
- A limitation to the current investigation was that maximum operating temperature reached by the Mintek equipment used (i.e. 1600°C only). Temperatures above this maximum, approximating the maximum reached in a ilmenite furnace (ca 2500°C, when graphitisation of anthracites is known to begin or to occur) should be evaluated to determine the effect of molecular re-ordering of the anthracite matrix on the reactivity of the anthracites. Since the rate of mass loss is extremely slow at 850°C, tests at or below 850°C are essentially useless and therefore not required.
- Finally, any future investigation into the performance of reductants in an ilmenite smelting furnace should include the correlation of TGA tests at high temperatures with actual tests in an operating furnace if at all physically possible.

8 REFERENCES

Atashi H, Fazlollahi F, Tehrani.rad S (2010). Leaching kinetics of calcined magnesite in ammonium chloride solutions. Australian Journal of Basic and Applied Sciences. 4(12). 5956-5962

Beamish B.B, Shaw K.J, Rodgers J.N (1998). Thermogravimetric determination of the carbon dioxide reactivity of char from some New Zealand coals and its association with the inorganic geochemistry of the parent coal. Fuel Processing technology. 53. 243-253

Chan M.L, Jones J.M, Pourkashanian M, Williams A, 1998. The oxidative reactivity of coal chars in relation to their structure. Fuel. 78. 1539-1552

Choudhury N, Mohanty D, Boral P, Kumar S, Hazra S.K (2008). Microscopic evaluation of coal and coke for metallurgical usage. Current Science. 94. 1. 74-81

Crelling J.C, Skorupska N.M, Marsh H (1988). Reactivity of coal macerals and lithotypes. Fuel. 67. 781-785

du Cann, V (2008). Test Report: A petrographic investigation of five anthracites: ZAC, Vietnam, Vietnam low volatile, Russian, Russian low volatile. Petrographics SA

Falcon R, Ham A.J (1988). The characteristics of Southern African coals. Journal of the South African Institute of Mining and Metallurgy. Vol. 88. Issue 5. 145-161

Falcon R, du Cann V, Comins D, Erasmus R, den Hoed P, Luckos A (2004). The characterization of carbon reductants in the metallurgical industry – a case study. Tenth International Ferroalloys Congress. INFACONX. 363-381

Falcon R (2005). Exxaro Internal report on assessment of five anthracites samples supplied by Namakwa Sands and a comparison of five foreign anthracites and two previously analysed Vietnamese anthracites

Gibbins J.R, Khogali K, Kandiyoti R (1990). Relationship between results from conventional proximate analyses and pyrolysis yields under rapid heating conditions. Fuel processing technology. 24. 3-9

Gous M (2006). An overview of the Namakwa Sands Ilmenite smelting operations. South African Pyrometallurgy 2006 International Conference. 189-201

Grigore M, Sakurovs R, French D, Sahajwalla V (2006). Influence of mineral matter on coke reactivity with carbon dioxide. ISIJ International. 46. 4. 503-512

Hippo E, Walker P.L (1975). Reactivity of heat-treated coals in carbon dioxide at 900°C. Fuel. 54. 245-248

Hurt R.H, Longwell J.P, Sarofim A.F (1986). Gasification reactivity of chars from low rank coal lithotypes. Fuel. 65. 451-452

Hurt R.H, Sarofim A.F, Longwell J.P (1991). The role of microporous surface area in the gasification of chars from a sub bituminous coal. Fuel. 70. 1079-1082

ISO 7404-5. Methods for petrographic analysis of coals

ISO 13909. Hard coal and coke, Mechanical sampling

Jenkins R.G, Nandi S.P, Walker P.L (1973). Reactivity of heat-treated coals in air at 500°C. Fuel. 52. 288-293

Jordan P (2009). Evaluation of reductants for ilmenite smelting. Exxaro Resources internal report

Kotze H, Bessinger D, Beukes J (2006). Ilmenite smelting at Ticom SA. Journal of the South African Institute of Mining and Metallurgy. 106. 165-170

Olivella M.A, Heras F.X.C de las, (2002). Study of the reactivities of chars from sulphur rich Spanish coals. Thermochemica Acta. 385. 171-175

Pinheiro H.J. S de B (2006). Springlake Anthracite characterization and potential industrial utilization. PhD thesis. Departamento de Geologia. Faculdade de Ciencias. Universidade do Porto. Portugal

Pistorius P.C (2008). Ilmenite smelting: the basics. Journal of South African Institute of Mining and Metallurgy. 108. 35-43

Rosenqvist T (1974). Principles of extractive Metallurgy. McGraw-Hill Kogakusha Ltd. 225

Rughubir N (2011). Personal Communication

Sahajwalla V, Dubikova M, Khanna R (2004). Reductant characterization and selection: implications for ferroalloys processing. Proceedings 10th International Ferroalloys Congress (INFACON X). 351-362

Shaw K.J, Beamish B.B, Rodgers K.A (1997). Thermogravimetric analytical procedures for determining reactivities of chars from New Zealand coals. Thermochemica Acta. 302. 181-187

Sooful N, (2010). Mintek TGA analysis internal test report

South African Coal Processing Society. Coal Preparation (2002). 4th Edition. England T, Hand P.E, Michael D.C, Falcon L.M, Yell A.D

South African National Standard. SANS 0135.

South African National Standard Classification of Coals. SANS 11760:200X. 1st Edition. ISO 11760:2005. 1st Edition

Taylor G.H, Teichmuller M, Davis A, Diessel CF, Littke R, Robert P (1998). Organic Petrology. Gebruder Borntraeger.704

van Krevelen D.W (1993), Coal Typology, Physics, Chemistry, Constitution. Elsevier Science Publishers.1979

Zhang L, Huang J, Fang Y, Wang Y (2006). Gasification reactivity and kinetics of chinese anthracite chars with steam and CO₂. Energy and Fuels. 20. 1201-1210

9 APPENDICES

9.1 Anthracite size analysis

Table 10 Vietnamese (V) size analysis

Sample ID:	V		
Initial mass (g)	14988		
Size	Mass (g)	Mass (%)	% Passing
25.0	0.0	0.0	100.0
20.0	149.5	1.0	100.0
19.0	135.1	0.9	99.0
16.0	821.5	5.7	98.0
12.5	2588.8	17.8	92.4
10.0	2408.4	16.6	74.5
9.5	658.4	4.5	57.9
8.0	1184.1	8.2	53.4
6.3	1363.7	9.4	45.3
5.0	1085.1	7.5	35.9
4.0	626.5	4.3	28.4
3.4	9.2	0.1	24.1
2.0	1305.1	9.0	24.0
1.0	852.2	5.9	15.0
0.0	1326.3	9.1	0.0
Totals	14513.9	100.0	
Loss	474.1	0.0	

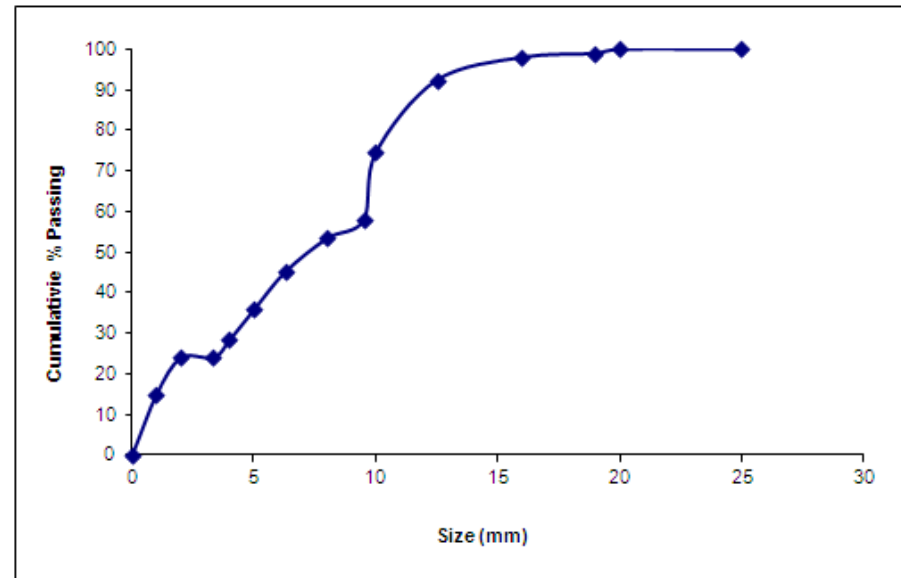


Table 11 Russian (R) size analysis

Sample ID:	R		
Initial mass (g)	5329		
Size	Mass (g)	Mass (%)	% Passing
41.0	0.00	0.0	100.0
40.0	97.70	1.8	100.0
37.5	54.20	1.0	98.2
31.5	133.20	2.5	97.1
26.5	592.50	11.2	94.6
25.0	115.30	2.2	83.5
20.0	1008.80	19.0	81.3
16.0	1348.30	25.4	62.3
12.5	1150.10	21.7	36.9
10.0	368.20	6.9	15.2
9.5	52.40	1.0	8.3
8.0	96.30	1.8	7.3
6.3	76.60	1.4	5.5
5.0	38.90	0.7	4.0
4.0	29.80	0.6	3.3
3.4	14.20	0.3	2.8
2.0	28.50	0.5	2.5
1.0	17.00	0.3	1.9
0.0	86.40	1.6	0.0
Totals	5308.40	100.0	
Loss	20.60	0.39%	

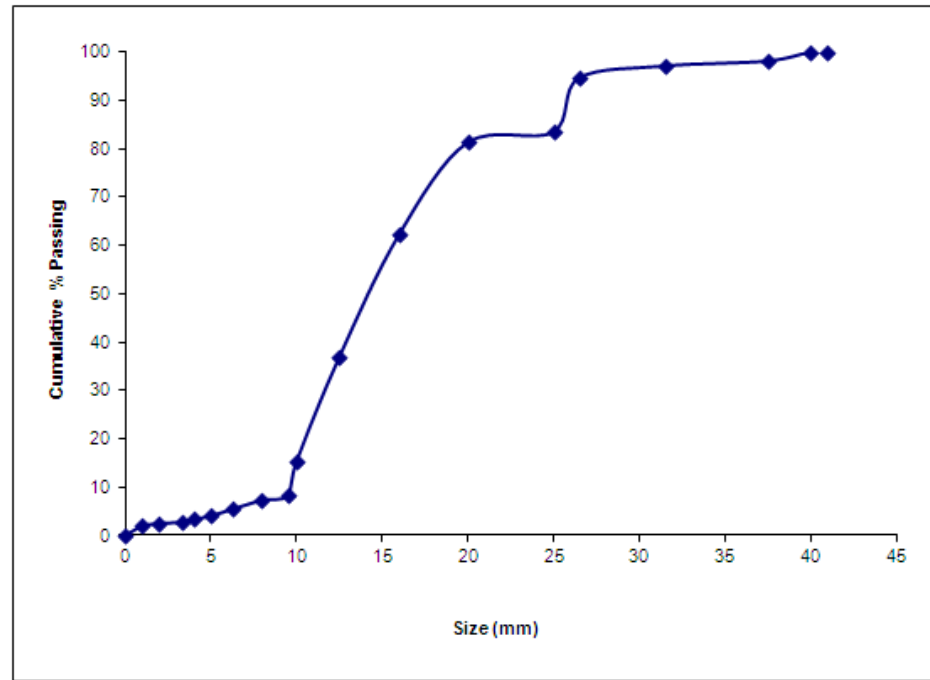


Table 12 Vietnamese Low Volatile (VLV) size analysis

Sample ID:	VLV		
Initial mass (g)	14694		
Size	Mass (g)	Mass (%)	% Passing
19.0	19.5	0.1	100.0
16.0	7.0	0.0	99.9
12.5	481.8	3.4	99.8
10.0	2662.8	18.8	96.4
9.5	949.7	6.7	77.6
8.0	2478.3	17.5	70.9
6.3	2901.1	20.5	53.4
5.0	1754.4	12.4	32.9
4.0	660.9	4.7	20.5
3.4	4.2	0.0	15.8
2.0	836.4	5.9	15.8
1.0	398.1	2.8	9.9
0.0	1002.9	7.1	0.0
Totals	14157.1	100.0	
Loss	536.9	0.0	

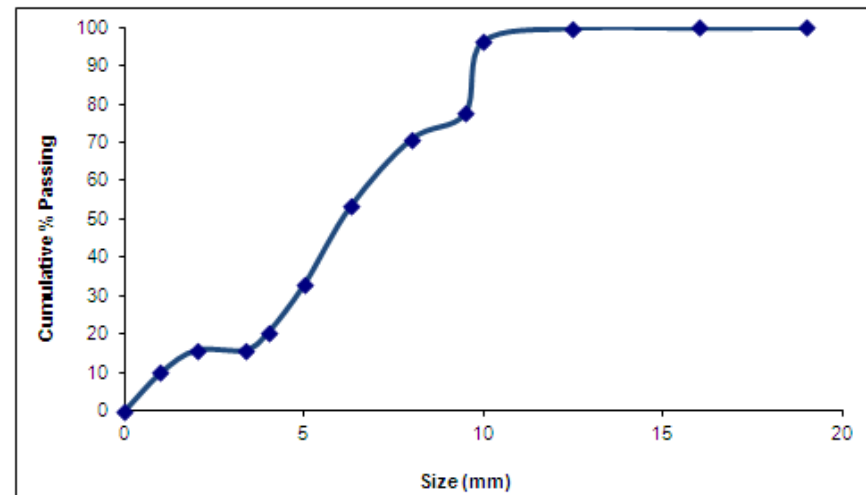
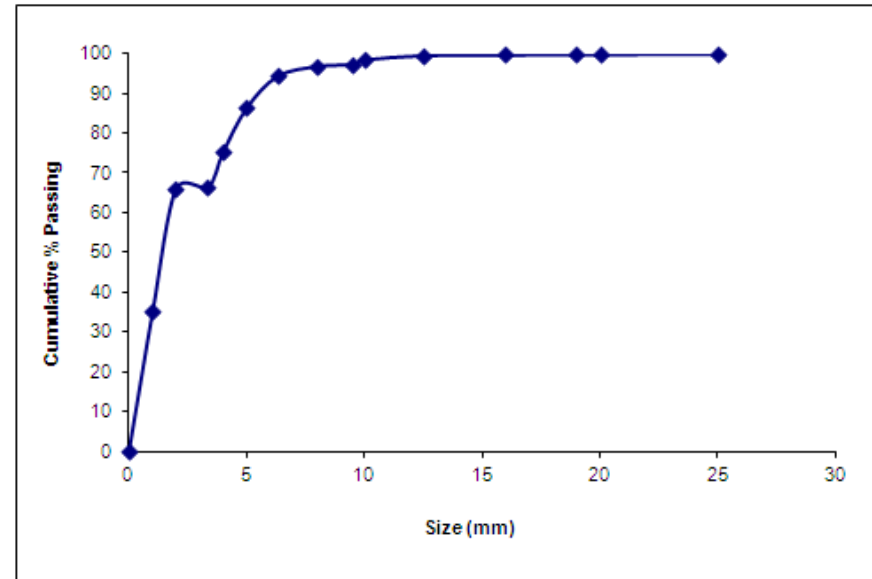


Table 13 South African Anthracite (SAA) size analysis

Sample ID:	SAA		
Initial mass	16653.6		
Size	Mass (g)	Mass (%)	% Passing
25.0	23.2	0.1	100.0
20.0	9.1	0.1	99.9
19.0	8.1	0.0	99.8
16.0	27.6	0.2	99.8
12.5	175.2	1.1	99.6
10.0	191.0	1.2	98.5
9.5	67.4	0.4	97.3
8.0	412.7	2.5	96.9
6.3	1295.7	7.9	94.4
5.0	1804.5	11.1	86.5
4.0	1462.2	9.0	75.4
3.4	46.6	0.3	66.5
2.0	5069.9	31.0	66.2
1.0	4029.1	24.7	35.1
0.0	1706.4	10.5	0.0
Totals	16328.7	100.0	
Loss	324.90	1.95%	



9.2 Reflectance histograms

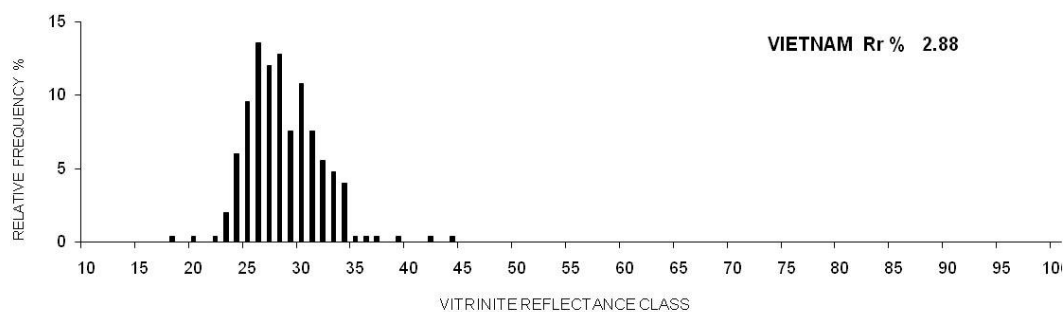


Figure 50 Reflectance histogram for Vietnamese anthracite

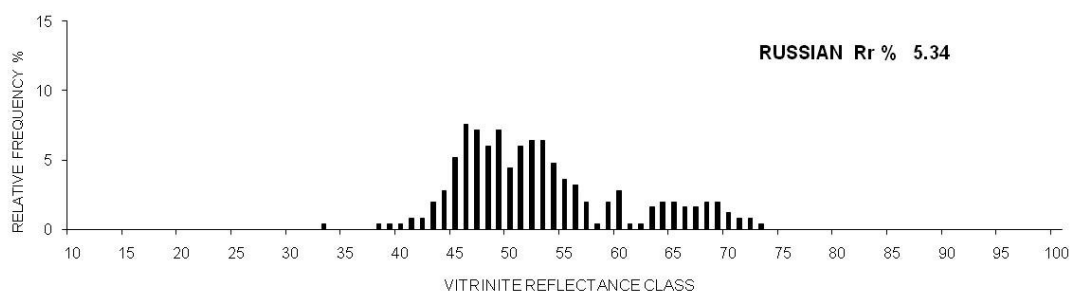


Figure 51 Reflectance histogram for Russian anthracite

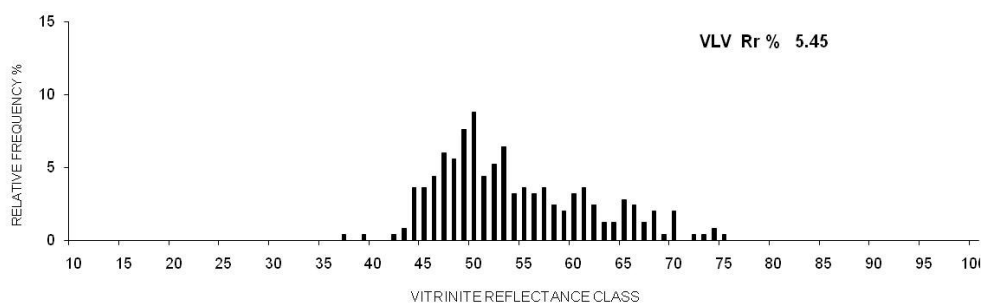


Figure 52 Reflectance histogram for VLV

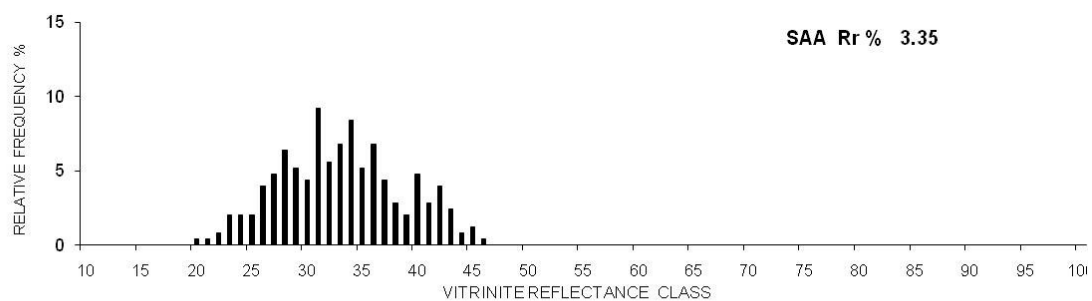


Figure 53 Reflectance histogram for South African Anthracite

9.3 Summary of reactivity results

Table 14 Summary of reactivity results

V					
Temperature	°C	850	1100	1350	1600
Crucible	g	44.14	40.48	42.37	43.65
Crucible + sample	g	64.47	62.88	62.70	67.04
Sample	g	20.33	22.40	20.33	23.39
Fixed carbon mass (dry ash free)	g	19.11	21.06	19.11	21.99
Reactivity (average)	s ⁻¹	7.55E-06	7.43E-06	2.26E-05	2.57E-05

R						
Temperature	°C	850	1100	1350	1600	1600 repeat
Crucible	g	43.37	40.10	43.59	45.43	44.93
Crucible + sample	g	63.48	66.78	64.28	66.00	64.31
Sample	g	20.11	26.68	20.69	20.57	19.38
Fixed carbon mass (dry ash free)	g	19.75	26.21	20.32	20.21	19.04
Reactivity (average)	s ⁻¹	1.46E-06	9.54E-06	2.30E-05	4.70E-05	3.86E-05

VLV					
Temperature	°C	850	1100	1350	1600
Crucible	g	44.19	40.79	44.60	67.89
Crucible + sample	g	64.53	70.74	64.94	116.00
Sample	g	20.34	29.95	20.34	48.11
Fixed carbon mass (dry ash free)	g	19.76	29.10	19.76	46.74
Reactivity (average)	s ⁻¹	4.32E-06	5.96E-06	1.34E-05	1.96E-05

SAA						
Temperature	°C	850	1100	1350	1600	1100 repeat
Crucible	g	44.02	73.05	42.91	73.18	44.95
Crucible + sample	g	64.51	108.50	63.36	105.70	65.13
Sample	g	20.49	35.45	20.45	32.52	20.18
Fixed carbon mass (dry ash free)	g	19.39	33.55	19.35	30.77	19.10
Reactivity (average)	s ⁻¹	1.92E-05	6.43E-06	1.75E-05	1.92E-05	1.10E-05

9.4 Raw data

The raw data was converted from a second to an hourly basis for the purpose of the ease of viewing in this document.

9.4.1 Raw data on an hourly basis at 850°C

Table 15 Raw data for V at 850°C

V at 850°C						
Time	Mass	Sample Temp	W (Fixed carbon dry ash free)	Rapp,ave	x	$1-(1-x)^{1/3}$
hr	%	°C	g	s ⁻¹		
0	100.00	0.00	19.11	-1.57E-05	0.000	0.000
1	97.79	501.97	18.69	-1.60E-05	0.022	0.007
2	92.37	800.70	17.66	0.00E+00	0.076	0.026
3	90.80	850.29	17.36	-1.72E-05	0.092	0.032
4	88.83	850.19	16.98	0.00E+00	0.112	0.039
5	86.91	850.27	16.61	0.00E+00	0.131	0.046
6	84.95	850.12	16.24	0.00E+00	0.151	0.053
7	82.98	850.46	15.86	0.00E+00	0.170	0.060
8	81.11	850.14	15.50	-1.93E-05	0.189	0.067
9	79.19	850.36	15.14	0.00E+00	0.208	0.075
10	77.30	850.14	14.77	-4.05E-06	0.227	0.082
11	75.45	850.43	14.42	-8.29E-06	0.246	0.090
12	73.62	850.31	14.07	-8.49E-06	0.264	0.097
13	71.82	850.32	13.73	-8.72E-06	0.282	0.104
14	70.03	850.22	13.39	-8.94E-06	0.300	0.112
15	68.26	850.20	13.05	-1.37E-05	0.317	0.120
16	66.49	850.32	12.71	-4.70E-06	0.335	0.127
17	64.75	850.37	12.38	-9.66E-06	0.353	0.135
18	63.02	850.29	12.05	-9.92E-06	0.370	0.143
19	61.31	850.21	11.72	-1.02E-05	0.387	0.150
20	59.60	850.35	11.39	-1.05E-05	0.404	0.158
21	57.90	850.30	11.07	0.00E+00	0.421	0.167
22	56.24	850.24	10.75	-5.56E-06	0.438	0.175
23	54.57	850.16	10.43	-5.73E-06	0.454	0.183
24	52.92	850.21	10.11	-5.91E-06	0.471	0.191
25	51.30	850.21	9.81	-6.10E-06	0.487	0.199
26	49.69	850.37	9.50	-1.26E-05	0.503	0.208
27	48.09	850.20	9.19	-6.50E-06	0.519	0.217
28	46.50	850.25	8.89	-6.72E-06	0.535	0.225
29	44.95	850.22	8.59	-6.95E-06	0.551	0.234
30	43.42	850.31	8.30	-1.44E-05	0.566	0.243
31	41.88	850.17	8.00	0.00E+00	0.581	0.252
32	40.38	850.16	7.72	-7.74E-06	0.596	0.261
33	38.89	850.16	7.43	-1.61E-05	0.611	0.270
34	37.42	850.38	7.15	-1.67E-05	0.626	0.279
35	35.98	850.29	6.88	-8.69E-06	0.640	0.289
36	34.54	850.29	6.60	-9.05E-06	0.655	0.298
37	33.21	591.51	6.35	-9.41E-06	0.668	0.307
38	32.34	465.92	6.18	0.00E+00	0.677	0.314
39	32.08	382.93	6.13	-9.74E-06	0.679	0.315
40	32.06	323.19	6.13	0.00E+00	0.679	0.316

Table 16 Raw data for R at 850°C

R at 850°C						
Time	Mass	Sample Temp	W (Fixed carbon dry ash free)	Rapp,ave	x	$1-(1-x)^{1/3}$
hr	%	°C	g	s ⁻¹		
0	100.00	0.00	19.75	0.00E+00	0.000	0.000
1	95.43	444.29	18.85	0.00E+00	0.046	0.015
2	93.64	743.53	18.50	0.00E+00	0.064	0.022
3	92.44	850.29	18.26	0.00E+00	0.076	0.026
4	91.70	850.23	18.12	0.00E+00	0.083	0.028
5	91.15	850.30	18.01	0.00E+00	0.088	0.030
6	90.70	850.36	17.92	0.00E+00	0.093	0.032
7	90.25	850.20	17.83	0.00E+00	0.098	0.034
8	89.81	850.08	17.74	-1.79E-05	0.102	0.035
9	89.31	849.86	17.64	0.00E+00	0.107	0.037
10	88.86	850.24	17.55	0.00E+00	0.111	0.039
11	88.41	850.17	17.47	0.00E+00	0.116	0.040
12	87.97	850.25	17.38	0.00E+00	0.120	0.042
13	87.52	850.03	17.29	0.00E+00	0.125	0.043
14	87.07	850.32	17.20	0.00E+00	0.129	0.045
15	86.62	850.25	17.11	0.00E+00	0.134	0.047
16	86.18	850.16	17.02	0.00E+00	0.138	0.048
17	85.73	850.26	16.94	0.00E+00	0.143	0.050
18	85.28	850.22	16.85	0.00E+00	0.147	0.052
19	84.83	850.38	16.76	0.00E+00	0.152	0.053
20	84.39	850.34	16.67	0.00E+00	0.156	0.055
21	83.99	850.23	16.59	0.00E+00	0.160	0.056
22	83.54	850.30	16.50	0.00E+00	0.165	0.058
23	83.09	850.26	16.41	0.00E+00	0.169	0.060
24	82.63	850.11	16.32	-3.89E-06	0.174	0.062
25	82.17	850.11	16.23	-3.91E-06	0.178	0.063
26	81.72	850.17	16.14	-3.93E-06	0.183	0.065
27	81.25	850.32	16.05	0.00E+00	0.188	0.067
28	80.81	850.25	15.96	0.00E+00	0.192	0.069
29	80.37	850.30	15.88	0.00E+00	0.196	0.070
30	79.92	850.25	15.79	4.02E-06	0.201	0.072
31	79.49	850.49	15.70	0.00E+00	0.205	0.074
32	79.05	850.28	15.62	0.00E+00	0.210	0.075
33	78.62	850.20	15.53	0.00E+00	0.214	0.077
34	78.17	850.28	15.44	4.11E-06	0.218	0.079
35	77.76	850.24	15.36	-4.13E-06	0.222	0.080
36	77.31	850.27	15.27	0.00E+00	0.227	0.082
37	76.89	850.32	15.19	-4.17E-06	0.231	0.084
38	76.46	850.38	15.10	-8.40E-06	0.235	0.086
39	76.01	850.23	15.02	0.00E+00	0.240	0.087

Table 17 Raw data for VLV at 850°C

VLV at 850°C						
Time	Mass	Sample Temp	W (Fixed carbon dry ash free)	Rapp,ave	x	1-(1-x) ^{1/3}
hr	%	°C	g	s ⁻¹		
0	99.95	0.00	19.75	0.00E+00	0.001	0.000
1	94.89	516.65	18.75	0.00E+00	0.051	0.017
2	92.62	816.69	18.30	-1.27E-05	0.074	0.025
3	91.25	850.22	18.03	0.00E+00	0.087	0.030
4	89.87	850.26	17.76	0.00E+00	0.101	0.035
5	88.45	850.26	17.48	0.00E+00	0.116	0.040
6	87.02	850.16	17.19	-1.69E-05	0.130	0.045
7	85.59	850.27	16.91	0.00E+00	0.144	0.051
8	84.17	850.25	16.63	0.00E+00	0.158	0.056
9	82.79	850.16	16.36	-1.77E-05	0.172	0.061
10	81.36	850.18	16.08	0.00E+00	0.186	0.066
11	80.04	850.09	15.82	-1.83E-05	0.200	0.072
12	78.66	850.24	15.54	0.00E+00	0.213	0.077
13	77.35	850.19	15.28	-3.80E-06	0.227	0.082
14	76.03	850.27	15.02	-3.86E-06	0.240	0.087
15	74.73	850.31	14.77	-3.93E-06	0.253	0.093
16	73.43	850.35	14.51	-4.00E-06	0.266	0.098
17	72.16	850.30	14.26	0.00E+00	0.278	0.103
18	70.90	850.21	14.01	-8.28E-06	0.291	0.108
19	69.63	850.22	13.76	-4.21E-06	0.304	0.114
20	68.40	850.27	13.52	-4.29E-06	0.316	0.119
21	67.17	850.29	13.27	-4.37E-06	0.328	0.124
22	65.95	850.29	13.03	0.00E+00	0.341	0.130
23	64.77	850.22	12.80	-4.53E-06	0.352	0.135
24	63.60	850.23	12.57	-9.23E-06	0.364	0.140
25	62.44	850.22	12.34	-4.70E-06	0.376	0.145
26	61.30	850.23	12.11	-4.79E-06	0.387	0.151
27	60.18	850.18	11.89	4.88E-06	0.398	0.156
28	59.06	850.18	11.67	-4.97E-06	0.409	0.161
29	57.95	850.25	11.45	-5.07E-06	0.421	0.166
30	56.86	850.25	11.23	0.00E+00	0.431	0.172
31	55.80	850.22	11.03	-5.26E-06	0.442	0.177
32	54.75	850.36	10.82	-5.36E-06	0.453	0.182
33	53.71	850.38	10.61	-5.47E-06	0.463	0.187
34	52.69	850.35	10.41	-5.57E-06	0.473	0.192
35	51.68	850.31	10.21	-5.68E-06	0.483	0.198
35.5	51.20	850.92	10.12	6.88E-06	0.488	0.200

Table 18 Raw data for SAA at 850°C

SAA at 850°C						
Time	Mass	Sample Temp	W (Fixed carbon dry ash free)	Rapp,ave	x	$1-(1-x)^{1/3}$
hr	%	°C	g	s ⁻¹		
0	100.00	0.00	19.39	0.00E+00	0.000	0.000
1	95.66	441.80	18.55	0.00E+00	0.043	0.015
2	92.63	742.95	17.96	-1.65E-05	0.074	0.025
3	90.63	850.00	17.57	0.00E+00	0.094	0.032
4	90.14	850.30	17.48	0.00E+00	0.099	0.034
5	89.75	850.20	17.40	0.00E+00	0.103	0.035
6	89.31	850.32	17.32	0.00E+00	0.107	0.037
7	88.87	850.27	17.23	0.00E+00	0.111	0.039
8	88.43	850.25	17.15	0.00E+00	0.116	0.040
9	87.99	850.08	17.06	0.00E+00	0.120	0.042
10	87.51	850.23	16.97	0.00E+00	0.125	0.043
11	87.02	850.37	16.87	0.00E+00	0.130	0.045
12	86.53	850.38	16.78	0.00E+00	0.135	0.047
13	85.99	850.25	16.67	0.00E+00	0.140	0.049
14	85.50	850.27	16.58	0.00E+00	0.145	0.051
15	85.02	850.21	16.48	0.00E+00	0.150	0.053
16	84.48	850.38	16.38	0.00E+00	0.155	0.055
17	83.99	850.32	16.29	0.00E+00	0.160	0.056
18	83.50	850.28	16.19	0.00E+00	0.165	0.058
19	83.02	850.29	16.10	0.00E+00	0.170	0.060
20	82.53	850.19	16.00	0.00E+00	0.175	0.062
21	81.99	850.19	15.90	0.00E+00	0.180	0.064
22	81.50	850.14	15.80	0.00E+00	0.185	0.066
23	80.97	850.12	15.70	0.00E+00	0.190	0.068
24	80.43	850.23	15.59	0.00E+00	0.196	0.070
25	79.94	850.17	15.50	0.00E+00	0.201	0.072
26	79.40	850.25	15.40	0.00E+00	0.206	0.074
27	78.92	850.08	15.30	0.00E+00	0.211	0.076
28	78.38	850.22	15.20	0.00E+00	0.216	0.078
29	77.87	850.21	15.10	0.00E+00	0.221	0.080
30	77.37	850.23	15.00	-3.95E-06	0.226	0.082
31	76.87	850.44	14.90	-3.97E-06	0.231	0.084
32	76.37	849.84	14.81	-4.00E-06	0.236	0.086
33	75.89	850.35	14.71	0.00E+00	0.241	0.088
34	75.42	850.49	14.62	0.00E+00	0.246	0.090
35	74.93	850.35	14.53	0.00E+00	0.251	0.092
36	74.58	850.92	14.46	7.10E-06	0.254	0.093

9.4.2 Raw data on an hourly basis at 1100°C

Table 19 Raw data for V at 1100°C

V at 1100°C						
Time	Mass	Sample Temp	W (Fixed carbon dry ash free)	Rapp,ave	x	$1-(1-x)^{1/3}$
hr	%	°C	g	s ⁻¹		
0	99.96	1088.82	21.05	-1.29E-04	0.000	0.000
1	91.07	1092.88	19.18	0.00E+00	0.089	0.031
2	88.79	1094.47	18.70	-1.41E-05	0.112	0.039
3	86.61	1093.12	18.24	0.00E+00	0.134	0.047
4	84.64	1093.44	17.83	-1.48E-05	0.154	0.054
5	82.77	1092.75	17.43	0.00E+00	0.172	0.061
6	80.98	1092.94	17.06	0.00E+00	0.190	0.068
7	79.11	1092.82	16.66	-1.98E-05	0.209	0.075
8	77.23	1093.67	16.27	-1.62E-05	0.228	0.083
9	75.40	1092.41	15.88	0.00E+00	0.246	0.090
10	73.57	1092.59	15.50	-1.70E-05	0.264	0.097
11	71.74	1092.84	15.11	0.00E+00	0.283	0.105
12	69.96	1092.97	14.74	-2.23E-05	0.300	0.112
13	68.17	1092.86	14.36	-2.29E-05	0.318	0.120
14	66.12	1094.02	13.93	0.00E+00	0.339	0.129
15	63.79	1092.64	13.44	-1.96E-05	0.362	0.139
16	61.74	1093.36	13.00	-2.03E-05	0.383	0.148
17	59.96	1093.04	12.63	0.00E+00	0.400	0.157
18	58.30	1093.88	12.28	0.00E+00	0.417	0.165
19	56.92	1094.45	11.99	2.20E-05	0.431	0.171
20	55.62	1094.05	11.72	0.00E+00	0.444	0.178
21	54.29	1093.11	11.43	0.00E+00	0.457	0.184
22	52.95	1093.03	11.15	0.00E+00	0.471	0.191
23	51.61	1092.66	10.87	0.00E+00	0.484	0.198
24	50.36	1093.14	10.61	1.09E-05	0.496	0.204

Table 20 Raw data for R at 1100°C

R at 1100°C						
Time	Mass	Sample Temp	W (Fixed carbon dry ash free)	R _{app,ave}	x	1-(1-x) ^{1/3}
hr	%	°C	g	s ⁻¹		
0	99.93	1090.20	26.19	-2.80E-04	0.001	0.000
1	87.44	1093.26	22.92	-1.10E-05	0.126	0.044
2	84.63	1092.62	22.18	-1.14E-05	0.154	0.054
3	81.86	1093.48	21.45	-1.57E-05	0.181	0.065
4	79.09	1093.43	20.73	0.00E+00	0.209	0.075
5	76.54	1093.03	20.06	-1.68E-05	0.235	0.085
6	74.25	1092.66	19.46	-1.73E-05	0.258	0.094
7	72.11	1094.01	18.90	-1.34E-05	0.279	0.103
8	69.72	1093.50	18.27	0.00E+00	0.303	0.113
9	67.47	1093.01	17.68	0.00E+00	0.325	0.123
10	65.40	1092.34	17.14	0.00E+00	0.346	0.132
11	63.38	1094.31	16.61	0.00E+00	0.366	0.141
12	61.43	1094.57	16.10	-2.09E-05	0.386	0.150
13	59.37	1096.08	15.56	0.00E+00	0.406	0.160
14	57.50	1093.39	15.07	-2.23E-05	0.425	0.168
15	55.32	1093.26	14.50	0.00E+00	0.447	0.179
16	53.56	1093.08	14.04	-2.40E-05	0.464	0.188
17	51.91	1092.36	13.61	0.00E+00	0.481	0.196
18	50.49	1093.12	13.23	0.00E+00	0.495	0.204
19	49.14	1094.60	12.88	0.00E+00	0.509	0.211
20	47.68	1093.53	12.50	0.00E+00	0.523	0.219
21	46.44	1093.88	12.17	0.00E+00	0.536	0.226
22	45.13	1094.76	11.83	0.00E+00	0.549	0.233
23	43.89	1093.96	11.50	0.00E+00	0.561	0.240
24	43.44	748.43	11.39	1.12E-05	0.566	0.243

Table 21 Raw data for VLV at 1100°C

VLV at 1100°C						
Time	Mass	Sample Temp	W (Fixed carbon dry ash free)	Rapp,ave	x	$1-(1-x)^{1/3}$
hr	%	°C	mg	s ⁻¹		
0	99.97	1088.35	29.09	-3.93E-04	0.000	0.000
1	92.19	1093.41	26.82	-1.27E-05	0.078	0.027
2	90.02	1093.10	26.19	0.00E+00	0.100	0.034
3	87.78	1093.18	25.54	0.00E+00	0.122	0.043
4	85.74	1092.88	24.95	-1.03E-05	0.143	0.050
5	84.24	1093.74	24.51	0.00E+00	0.158	0.056
6	82.77	1093.42	24.08	0.00E+00	0.172	0.061
7	80.97	1093.01	23.56	-1.45E-05	0.190	0.068
8	79.07	1093.06	23.01	-1.48E-05	0.209	0.075
9	77.06	1093.18	22.42	0.00E+00	0.229	0.083
10	75.03	1093.38	21.83	-1.56E-05	0.250	0.091
11	73.42	1093.43	21.36	-1.20E-05	0.266	0.098
12	71.85	1093.01	20.91	-1.22E-05	0.282	0.104
13	70.22	1093.62	20.43	0.00E+00	0.298	0.111
14	68.65	1093.33	19.98	0.00E+00	0.314	0.118
15	67.15	1094.27	19.54	0.00E+00	0.329	0.124
16	65.61	1093.56	19.09	-1.34E-05	0.344	0.131
17	64.07	1094.21	18.64	0.00E+00	0.359	0.138
18	62.80	1094.26	18.27	0.00E+00	0.372	0.144
19	61.60	1093.14	17.92	0.00E+00	0.384	0.149
20	60.33	1094.07	17.55	0.00E+00	0.397	0.155
21	59.13	1094.19	17.21	0.00E+00	0.409	0.161
22	57.90	1093.41	16.85	0.00E+00	0.421	0.167
23	56.73	1093.55	16.51	-2.06E-05	0.433	0.172
24	55.59	1094.56	16.18	1.02E-05	0.444	0.178

Table 22 Raw data for SAA at 1100°C

SAA at 1100°C						
Time	Mass	Sample Temp	W (Fixed carbon dry ash free)	Rapp,ave	x	$1-(1-x)^{1/3}$
hr	%	°C	mg	s ⁻¹		
0	99.89	1085.86	33.51	-2.93E-04	0.001	0.000
1	89.96	1095.44	30.18	0.00E+00	0.100	0.035
2	88.07	1095.70	29.55	0.00E+00	0.119	0.041
3	86.35	1095.54	28.97	-1.06E-05	0.137	0.048
4	84.74	1094.68	28.43	0.00E+00	0.153	0.054
5	83.07	1094.73	27.87	0.00E+00	0.169	0.060
6	81.86	1094.56	27.46	-1.86E-05	0.181	0.065
7	80.71	1094.88	27.08	-1.13E-05	0.193	0.069
8	79.01	1094.32	26.51	0.00E+00	0.210	0.076
9	76.90	1094.52	25.80	-1.19E-05	0.231	0.084
10	75.26	1096.00	25.25	-1.21E-05	0.247	0.090
11	73.82	1095.92	24.76	0.00E+00	0.262	0.096
12	72.24	1093.40	24.23	-1.26E-05	0.278	0.103
13	70.72	1095.08	23.72	-1.29E-05	0.293	0.109
14	69.17	1095.76	23.20	0.00E+00	0.308	0.116
15	67.73	1095.55	22.72	0.00E+00	0.323	0.122
16	66.52	1095.80	22.32	-1.37E-05	0.335	0.127

Table 23 Raw data for SAA repeat test at 1100°C

SAA repeat test at 1100°C						
Time	Mass	Sample Temp	W (Fixed carbon dry ash free)	Rapp,ave	x	$1-(1-x)^{1/3}$
hr	%	°C	g	s ⁻¹		
0	100.00	0.00	19.10	0.00E+00	0.000	0.000
1	95.49	499.88	18.23	0.00E+00	0.045	0.015
2	90.88	797.14	17.35	0.00E+00	0.091	0.031
3	87.91	1095.10	16.79	0.00E+00	0.121	0.042
4	85.03	1099.71	16.24	0.00E+00	0.150	0.053
5	81.96	1099.76	15.65	0.00E+00	0.180	0.064
6	79.19	1099.82	15.12	0.00E+00	0.208	0.075
7	76.51	1099.76	14.61	0.00E+00	0.235	0.085
8	73.96	1099.87	14.12	-1.24E-05	0.260	0.096
9	71.44	1099.84	13.64	-1.28E-05	0.286	0.106
10	68.99	1099.82	13.17	-8.81E-06	0.310	0.116
11	66.59	1099.83	12.72	-1.37E-05	0.334	0.127
12	64.22	1099.87	12.26	-9.48E-06	0.358	0.137
13	61.91	1099.88	11.82	-1.97E-05	0.381	0.148
14	59.60	1099.81	11.38	0.00E+00	0.404	0.158
15	57.35	1099.81	10.95	-1.06E-05	0.427	0.169
16	55.12	1099.80	10.53	-5.52E-06	0.449	0.180
17	52.93	1099.87	10.11	-5.75E-06	0.471	0.191
18	50.80	1099.88	9.70	-1.20E-05	0.492	0.202
19	48.70	1099.86	9.30	-6.24E-06	0.513	0.213
20	46.65	1099.90	8.91	-6.52E-06	0.534	0.224
21	44.67	1099.75	8.53	-1.36E-05	0.553	0.236
22	42.72	1099.80	8.16	-1.42E-05	0.573	0.247
24	39.03	1099.84	7.45	-7.80E-06	0.610	0.269
25	37.26	1099.82	7.11	-1.63E-05	0.627	0.280
26	35.53	1099.83	6.78	-1.71E-05	0.645	0.292
27	33.90	1099.95	6.47	-1.80E-05	0.661	0.303
28	32.34	1099.78	6.18	-1.88E-05	0.677	0.314
29	30.85	1099.68	5.89	-1.97E-05	0.692	0.324
30	29.38	1099.83	5.61	-1.04E-05	0.706	0.335
31	27.95	1099.85	5.34	-1.09E-05	0.721	0.346
32	26.58	1099.81	5.08	-2.29E-05	0.734	0.357
33	25.23	1099.76	4.82	-2.41E-05	0.748	0.368
34	23.91	1100.05	4.57	0.00E+00	0.761	0.379
35	22.63	1099.85	4.32	-1.35E-05	0.774	0.391
36	21.41	1099.81	4.09	0.00E+00	0.786	0.402
37	20.24	1095.87	3.86	-1.50E-05	0.798	0.413
38	19.16	797.31	3.66	-1.59E-05	0.808	0.424
39	18.11	607.09	3.46	0.00E+00	0.819	0.434
40	17.86	0.57	3.41	6.34E-06	0.821	0.437

9.4.3 Raw data on an hourly basis at 1350°C

Table 24 Raw data for V at 1350°C

V at 1350°C						
Time	Mass	Sample Temp	W (Fixed carbon dry ash free)	Rapp,ave	x	1-(1-x) ^{1/3}
hr	%	°C	g	s ⁻¹		
0	100.34	0.00	19.18	-1.25E-05	-0.003	-0.001
1	98.13	502.25	18.76	0.00E+00	0.019	0.006
2	93.01	799.90	17.78	-1.68E-05	0.070	0.024
3	90.75	1089.28	17.34	-1.72E-05	0.093	0.032
4	88.64	1348.86	16.94	-1.76E-05	0.114	0.039
5	87.16	1348.83	16.66	0.00E+00	0.128	0.045
6	82.65	1349.02	15.80	-1.51E-05	0.174	0.062
7	78.11	1349.01	14.93	-1.60E-05	0.219	0.079
8	73.74	1348.97	14.09	-2.12E-05	0.263	0.097
9	69.42	1348.92	13.27	-1.35E-05	0.306	0.115
10	65.19	1349.08	12.46	-1.92E-05	0.348	0.133
11	61.02	1348.95	11.66	-2.05E-05	0.390	0.152
12	56.92	1348.90	10.88	-2.20E-05	0.431	0.171
13	52.89	1349.02	10.11	-1.77E-05	0.471	0.191
14	48.97	1349.01	9.36	-1.92E-05	0.510	0.212
15	45.13	1348.95	8.63	-1.39E-05	0.549	0.233
16	41.41	1348.94	7.91	-2.26E-05	0.586	0.255
17	37.80	1349.06	7.22	-3.31E-05	0.622	0.277
18	34.31	1348.99	6.56	-2.73E-05	0.657	0.300
19	30.93	1348.92	5.91	-2.02E-05	0.691	0.324
20	27.70	1349.01	5.29	-1.13E-05	0.723	0.348
21	24.63	1349.00	4.71	-5.08E-05	0.754	0.373
22	21.71	1349.02	4.15	-2.88E-05	0.783	0.399
23	18.97	1348.98	3.63	-6.59E-05	0.810	0.425
24	16.44	1348.94	3.14	-1.90E-05	0.836	0.452
25	14.16	1348.93	2.71	-6.62E-05	0.858	0.479
26	12.15	1348.92	2.32	-7.72E-05	0.879	0.505
27	10.39	1348.90	1.99	-9.02E-05	0.896	0.530
28	8.90	1348.97	1.70	-3.52E-05	0.911	0.554
29	7.68	1348.98	1.47	0.00E+00	0.923	0.575
30	6.72	1348.86	1.28	-4.65E-05	0.933	0.593
31	5.95	1348.98	1.14	0.00E+00	0.941	0.610
32	5.30	1349.00	1.01	-5.91E-05	0.947	0.624
33	4.82	1349.13	0.92	-6.49E-05	0.952	0.636
34	4.72	1348.96	0.90	0.00E+00	0.953	0.639
35	4.72	1348.99	0.90	0.00E+00	0.953	0.639
36	4.70	1349.01	0.90	1.33E-04	0.953	0.639
37	4.71	1349.02	0.90	6.64E-05	0.953	0.639
38	4.72	1290.35	0.90	0.00E+00	0.953	0.639
39	4.73	992.22	0.90	-6.61E-05	0.953	0.638
40	4.74	741.40	0.91	6.52E-06	0.953	0.638

Table 25 Raw data for R at 1350°C

R at 1350°C						
Time	Mass	Sample Temp	W (Fixed carbon dry ash free)	Rapp,ave	x	$1-(1-x)^{1/3}$
hr	%	°C	g	s ⁻¹		
0	100.00	0.00	20.32	0.00E+00	0.000	0.000
1	95.26	499.44	19.36	0.00E+00	0.047	0.016
2	92.80	799.09	18.86	0.00E+00	0.072	0.025
3	90.53	1096.49	18.40	0.00E+00	0.095	0.033
4	88.40	1348.91	17.97	0.00E+00	0.116	0.040
5	85.84	1349.15	17.45	-1.75E-05	0.142	0.050
6	81.10	1349.18	16.48	-1.85E-05	0.189	0.067
7	76.42	1349.13	15.53	-1.57E-05	0.236	0.086
8	71.70	1349.08	14.57	-2.51E-05	0.283	0.105
9	67.04	1349.07	13.63	-2.24E-05	0.330	0.125
10	62.43	1349.13	12.69	-1.44E-05	0.376	0.145
11	57.84	1349.08	11.76	-2.08E-05	0.422	0.167
12	53.38	1349.11	10.85	-2.25E-05	0.466	0.189
13	48.99	1349.09	9.96	-1.84E-05	0.510	0.212
14	44.68	1349.15	9.08	-2.69E-05	0.553	0.236
15	40.48	1349.09	8.23	-2.97E-05	0.595	0.260
16	36.31	1349.08	7.38	-8.26E-06	0.637	0.287
17	32.33	1349.03	6.57	-2.78E-05	0.677	0.314
18	28.47	1349.07	5.79	-4.21E-05	0.715	0.342
19	24.73	1349.06	5.03	-7.27E-05	0.753	0.372
20	21.18	1349.06	4.30	-4.25E-05	0.788	0.404
21	17.80	1349.09	3.62	-5.05E-05	0.822	0.437
22	14.56	1349.11	2.96	-8.23E-05	0.854	0.474
23	11.52	1349.05	2.34	-7.82E-05	0.885	0.513
24	8.73	1349.07	1.77	-3.44E-05	0.913	0.556
25	6.18	1349.01	1.26	-1.46E-04	0.938	0.605
26	4.26	1349.15	0.87	-1.41E-04	0.957	0.651
27	3.60	1348.93	0.73	-8.34E-05	0.964	0.670
28	3.59	1348.98	0.73	0.00E+00	0.964	0.670
29	3.58	1349.05	0.73	8.39E-05	0.964	0.670
30	3.59	1349.12	0.73	1.67E-04	0.964	0.670
31	3.60	1349.07	0.73	8.34E-05	0.964	0.670
32	3.62	1349.24	0.74	-2.49E-04	0.964	0.669
33	3.60	1349.07	0.73	-8.35E-05	0.964	0.670
34	3.60	1349.12	0.73	0.00E+00	0.964	0.670
35	3.59	1349.14	0.73	8.37E-05	0.964	0.670
36	3.59	1349.02	0.73	-8.35E-05	0.964	0.670
37	3.58	1348.98	0.73	0.00E+00	0.964	0.670
38	3.59	1349.18	0.73	-1.67E-04	0.964	0.670
39	3.58	1194.69	0.73	-8.37E-05	0.964	0.670
40	3.57	900.34	0.73	6.24E-06	0.964	0.671

Table 26 Raw data for VLV at 1350°C

VLV at 1350°C						
Time	Mass	Sample Temp	W (Fixed carbon dry ash free)	Rapp,ave	x	$1-(1-x)^{1/3}$
hr	%	°C	g	s ⁻¹		
0	100.00	0.00	19.76	-1.47E-05	0.000	0.000
1	95.43	498.82	18.86	-1.54E-05	0.046	0.015
2	92.58	799.03	18.29	0.00E+00	0.074	0.025
3	90.07	1097.74	17.80	0.00E+00	0.099	0.034
4	87.32	1349.44	17.25	0.00E+00	0.127	0.044
5	83.48	1349.10	16.50	-1.76E-05	0.165	0.058
6	78.56	1349.04	15.52	-1.87E-05	0.214	0.077
7	73.75	1349.18	14.57	-1.59E-05	0.263	0.097
8	69.03	1349.01	13.64	-2.13E-05	0.310	0.116
9	64.50	1349.08	12.75	-2.28E-05	0.355	0.136
10	60.08	1349.20	11.87	-9.77E-06	0.399	0.156
11	55.77	1349.20	11.02	-1.58E-05	0.442	0.177
12	51.61	1349.19	10.20	-2.28E-05	0.484	0.198
13	47.57	1349.14	9.40	-2.47E-05	0.524	0.219
14	43.58	1349.20	8.61	-1.35E-05	0.564	0.242
15	39.79	1349.27	7.86	-2.95E-05	0.602	0.264
16	36.06	1349.11	7.13	-2.44E-05	0.639	0.288
17	32.51	1349.11	6.42	-4.51E-05	0.675	0.312
18	29.07	1349.21	5.74	-5.05E-05	0.709	0.338
19	25.72	1349.13	5.08	-1.14E-05	0.743	0.364
20	22.73	1349.11	4.49	-2.58E-05	0.773	0.390
21	20.10	1349.25	3.97	-1.46E-05	0.799	0.414
22	17.83	1349.10	3.52	-6.59E-05	0.822	0.437
23	15.95	1349.14	3.15	-3.67E-05	0.841	0.458
24	14.69	1349.16	2.90	-2.00E-05	0.853	0.472
25	14.06	1349.14	2.78	0.00E+00	0.859	0.480
26	13.87	1349.10	2.74	-2.12E-05	0.861	0.482
27	13.86	1349.10	2.74	-2.12E-05	0.861	0.482
28	13.84	1349.08	2.73	-2.12E-05	0.862	0.483
29	13.82	1349.19	2.73	0.00E+00	0.862	0.483
30	13.82	1349.02	2.73	0.00E+00	0.862	0.483
31	13.79	1349.02	2.72	4.26E-05	0.862	0.483
32	13.81	1349.10	2.73	-2.13E-05	0.862	0.483
33	13.81	1348.97	2.73	0.00E+00	0.862	0.483
34	13.79	1349.18	2.72	2.13E-05	0.862	0.483
35	13.80	1349.05	2.73	2.13E-05	0.862	0.483
36	13.80	1349.11	2.73	-2.13E-05	0.862	0.483
37	13.79	1349.03	2.72	2.12E-05	0.862	0.483
38	13.77	1258.09	2.72	2.13E-05	0.862	0.484
39	13.71	957.50	2.71	2.14E-05	0.863	0.484
40	13.68	718.43	2.70	6.10E-06	0.863	0.485

Table 27 Raw data for SAA at 1350°C

SAA at 1350°C						
Time	Mass	Sample Temp	W (Fixed carbon dry ash free)	Rapp,ave	x	$1-(1-x)^{1/3}$
hr	%	°C	g	s ⁻¹		
0	100.88	0.00	19.52	0.00E+00	-0.009	-0.003
1	95.89	499.98	18.56	-1.59E-05	0.041	0.014
2	91.59	797.75	17.72	-1.66E-05	0.084	0.029
3	88.85	1096.10	17.19	0.00E+00	0.112	0.039
4	86.65	1348.85	16.77	-1.76E-05	0.134	0.047
5	83.51	1348.95	16.16	-1.83E-05	0.165	0.058
6	78.70	1348.99	15.23	-1.55E-05	0.213	0.077
7	73.90	1348.93	14.30	-1.65E-05	0.261	0.096
8	69.17	1349.16	13.39	-1.76E-05	0.308	0.116
9	64.52	1349.15	12.49	-1.42E-05	0.355	0.136
10	59.97	1349.16	11.61	-2.03E-05	0.400	0.157
11	55.53	1349.21	10.75	-2.19E-05	0.445	0.178
12	51.17	1349.01	9.90	-2.38E-05	0.488	0.200
13	46.90	1349.09	9.08	-1.30E-05	0.531	0.223
14	42.74	1349.01	8.27	-2.85E-05	0.573	0.247
15	38.65	1349.06	7.48	-3.15E-05	0.614	0.272
16	34.66	1349.01	6.71	-1.76E-05	0.653	0.298
17	30.78	1349.07	5.96	-9.89E-06	0.692	0.325
18	27.04	1349.07	5.23	-3.38E-05	0.730	0.353
19	23.40	1349.02	4.53	-1.30E-05	0.766	0.384
20	19.96	1349.09	3.86	-4.57E-05	0.800	0.416
21	16.74	1349.12	3.24	-3.63E-05	0.833	0.449
22	13.88	1349.10	2.69	-4.39E-05	0.861	0.482
23	11.50	1349.07	2.23	-2.65E-05	0.885	0.514
24	9.98	1349.15	1.93	-3.05E-05	0.900	0.536
25	9.21	1348.72	1.78	-3.30E-05	0.908	0.548
26	8.73	1349.06	1.69	-6.97E-05	0.913	0.556
27	8.56	1349.12	1.66	0.00E+00	0.914	0.559
28	8.56	1349.05	1.66	3.55E-05	0.914	0.559
29	8.55	1349.19	1.65	3.56E-05	0.915	0.559
30	8.55	1349.18	1.65	7.13E-05	0.915	0.559
31	8.55	1349.08	1.65	0.00E+00	0.915	0.559
32	8.57	1349.07	1.66	0.00E+00	0.914	0.559
33	8.57	1349.14	1.66	0.00E+00	0.914	0.559
34	8.57	1349.06	1.66	-3.56E-05	0.914	0.559
35	8.56	1349.06	1.66	0.00E+00	0.914	0.559
36	8.55	1349.14	1.65	0.00E+00	0.915	0.559
37	8.54	1349.04	1.65	0.00E+00	0.915	0.560
38	8.54	1297.32	1.65	0.00E+00	0.915	0.560
39	8.53	999.30	1.65	0.00E+00	0.915	0.560
40	8.53	740.93	1.65	6.34E-06	0.915	0.560

9.4.4 Raw data at 1600°C

Table 28 Raw data for V at 1600°C

V at 1600°C						
Time	Mass	Sample Temp	W (Fixed carbon dry ash free)	Rapp,ave	x	$1-(1-x)^{1/3}$
hr	%	°C	g	s ⁻¹		
0	96.11	1592.80	21.14	-4.60E-04	0.039	0.013
1	84.65	1605.50	18.62	-1.48E-05	0.154	0.054
2	76.74	1605.64	16.88	-1.63E-05	0.233	0.084
3	69.77	1605.56	15.34	-3.59E-05	0.302	0.113
4	63.36	1605.59	13.94	-1.97E-05	0.366	0.141
5	57.25	1605.67	12.59	-4.91E-05	0.428	0.170
6	51.43	1605.79	11.31	-2.44E-05	0.486	0.199
7	45.79	1605.83	10.07	-2.73E-05	0.542	0.229
8	40.44	1605.76	8.89	-3.09E-05	0.596	0.261
9	35.36	1605.80	7.78	-4.42E-05	0.646	0.293
10	30.40	1605.98	6.69	-5.14E-05	0.696	0.328
11	25.65	1605.58	5.64	-4.88E-05	0.744	0.365
12	20.86	1605.63	4.59	-6.00E-05	0.791	0.407
13	16.33	1605.59	3.59	0.00E+00	0.837	0.453
14	12.10	1605.57	2.66	-1.03E-04	0.879	0.505
15	8.76	1605.58	1.93	0.00E+00	0.912	0.556
16	8.68	1605.58	1.91	0.00E+00	0.913	0.557
17	8.64	1605.55	1.90	0.00E+00	0.914	0.558
18	8.76	1605.52	1.93	0.00E+00	0.912	0.556
19	9.15	1605.81	2.01	0.00E+00	0.909	0.549
20	9.41	1605.98	2.07	0.00E+00	0.906	0.545
21	9.62	1606.03	2.12	0.00E+00	0.904	0.542
23	9.79	1606.20	2.15	0.00E+00	0.902	0.539
24	9.96	1606.35	2.19	1.09E-05	0.900	0.536

Table 29 Raw data for R at 1600°C

R at 1600°C						
Time	Mass	Sample Temp	W (Fixed carbon dry ash free)	Rapp,ave	x	$1-(1-x)^{1/3}$
hr	%	°C	g	s ⁻¹		
0.0	101.60	1596.15	20.53	-2.60E-04	-0.016	-0.005
1.0	82.40	1607.22	16.65	-1.95E-05	0.176	0.062
2.0	73.65	1607.73	14.88	-2.18E-05	0.264	0.097
3.0	65.82	1608.48	13.30	-1.95E-05	0.342	0.130
4.0	58.58	1608.43	11.84	-2.75E-05	0.414	0.163
5.0	51.43	1608.66	10.39	-2.51E-05	0.486	0.199
6.0	45.02	1608.62	9.10	-7.15E-05	0.550	0.234
7.0	38.79	1609.15	7.84	-3.32E-05	0.612	0.271
8.0	32.67	1609.08	6.60	-4.92E-05	0.673	0.311
9.0	26.98	1609.19	5.45	-5.97E-05	0.730	0.354
10.0	21.58	1609.05	4.36	-5.98E-05	0.784	0.400
11.0	16.33	1608.79	3.30	-7.89E-05	0.837	0.453
12.0	11.38	1608.28	2.30	-1.42E-04	0.886	0.515
13.0	7.15	1608.08	1.44	0.00E+00	0.929	0.585
14.0	6.71	1608.20	1.36	0.00E+00	0.933	0.594
15.0	6.85	1607.82	1.38	0.00E+00	0.932	0.591
15.3	6.90	1608.02	1.39	1.75E-05	0.931	0.590

Table 30 Raw data for R repeat test at 1600°C

R repeat test at 1600°C						
Time	Mass	Sample Temp	W (Fixed carbon dry ash free)	Rapp,ave	x	$1-(1-x)^{1/3}$
hr	%	°C	g	s ⁻¹		
0	100.00	0.00	19.04	0.00E+00	0.000	0.000
1	95.56	498.19	18.19	0.00E+00	0.044	0.015
2	92.62	795.62	17.63	-1.73E-05	0.074	0.025
3	89.37	1094.10	17.02	0.00E+00	0.106	0.037
4	85.14	1392.51	16.21	0.00E+00	0.149	0.052
5	80.45	1599.12	15.32	0.00E+00	0.196	0.070
6	74.81	1598.96	14.24	-2.57E-05	0.252	0.092
7	68.41	1599.04	13.03	-1.41E-05	0.316	0.119
8	62.45	1599.15	11.89	-1.54E-05	0.376	0.145
9	56.70	1598.96	10.80	-2.83E-05	0.433	0.172
10	51.23	1599.13	9.75	-3.76E-05	0.488	0.200
11	45.93	1599.04	8.75	-2.10E-05	0.541	0.228
12	40.76	1599.03	7.76	-3.94E-05	0.592	0.259
13	35.69	1599.11	6.80	-4.50E-05	0.643	0.291
14	30.71	1599.01	5.85	0.00E+00	0.693	0.325
15	25.88	1599.06	4.93	-4.96E-05	0.741	0.363
16	21.18	1599.10	4.03	-9.11E-05	0.788	0.404
17	16.59	1599.00	3.16	-3.87E-05	0.834	0.451
18	12.17	1599.17	2.32	-7.91E-05	0.878	0.504
19	7.88	1599.00	1.50	-1.63E-04	0.921	0.571
20	3.91	1599.07	0.74	0.00E+00	0.961	0.661
21	2.02	1599.13	0.38	-4.77E-04	0.980	0.728
22	2.01	1599.13	0.38	-1.60E-04	0.980	0.728
23	2.02	1599.03	0.38	1.59E-04	0.980	0.728
24	1.99	1599.03	0.38	-1.61E-04	0.980	0.729
25	1.99	1599.03	0.38	-3.23E-04	0.980	0.729
26	1.96	1599.02	0.37	0.00E+00	0.980	0.730
27	1.95	1599.05	0.37	3.29E-04	0.981	0.731
28	1.93	1599.06	0.37	3.33E-04	0.981	0.732
29	1.91	1598.98	0.36	3.36E-04	0.981	0.733
30	1.91	1599.12	0.36	0.00E+00	0.981	0.733
31	1.90	1457.19	0.36	3.38E-04	0.981	0.733
32	1.93	1159.45	0.37	-3.33E-04	0.981	0.732
33	1.96	866.51	0.37	0.00E+00	0.980	0.730
34	1.97	685.42	0.38	0.00E+00	0.980	0.730
35	1.98	566.68	0.38	-1.62E-04	0.980	0.729
36	1.96	476.11	0.37	1.64E-04	0.980	0.730
37	1.95	402.96	0.37	0.00E+00	0.981	0.731
38	1.93	343.47	0.37	0.00E+00	0.981	0.732
39	1.92	293.01	0.37	0.00E+00	0.981	0.732
40	1.91	251.40	0.36	6.69E-06	0.981	0.733

Table 31 Raw data for VLV at 1600°C

VLV at 1600°C						
Time	Mass	Sample Temp	W (Fixed carbon dry ash free)	Rapp,ave	x	$1-(1-x)^{1/3}$
hr	%	°C	mg	s ⁻¹		
0.0	99.92	1585.21	46.70	-3.00E-04	0.001	0.000
1.0	88.80	1610.70	41.51	-2.31E-05	0.112	0.039
2.0	83.31	1612.19	38.94	-1.40E-05	0.167	0.059
3.0	78.30	1613.34	36.60	-1.50E-05	0.217	0.078
4.0	73.64	1613.43	34.42	-1.59E-05	0.264	0.097
5.0	69.28	1612.42	32.38	-8.45E-06	0.307	0.115
6.0	65.18	1611.44	30.47	-1.80E-05	0.348	0.133
7.0	61.28	1611.46	28.64	-9.55E-06	0.387	0.151
8.0	57.53	1611.91	26.89	-2.03E-05	0.425	0.168
9.0	53.90	1611.00	25.19	-1.09E-05	0.461	0.186
10.0	50.49	1610.37	23.60	-1.16E-05	0.495	0.204
11.0	47.20	1610.61	22.06	-1.24E-05	0.528	0.221
12.0	44.04	1609.38	20.58	-2.66E-05	0.560	0.239
13.0	40.99	1609.78	19.16	-1.43E-05	0.590	0.257
14.0	38.08	1610.41	17.80	-1.54E-05	0.619	0.275
15.0	35.31	1610.82	16.50	-1.66E-05	0.647	0.293
16.0	32.63	1611.81	15.25	-1.79E-05	0.674	0.312
17.0	30.04	1611.09	14.04	-2.92E-05	0.700	0.330
18.0	27.54	1611.67	12.87	-2.13E-05	0.725	0.349
19.0	25.11	1611.83	11.74	-2.33E-05	0.749	0.369
20.0	22.76	1610.83	10.64	-2.57E-05	0.772	0.389
21.0	20.45	1612.19	9.56	-2.86E-05	0.796	0.411
22.0	18.21	1611.92	8.51	-3.21E-05	0.818	0.433
23.0	16.05	1611.00	7.50	-9.11E-05	0.840	0.457
23.4	15.13	1611.78	7.07	1.04E-05	0.849	0.467

Table 32 Raw data for SAA at 1600°C

SAA at 1600°C						
Time	Mass	Sample Temp	W (Fixed carbon dry ash free)	Rapp,ave	x	$1-(1-x)^{1/3}$
hr	%	°C	g	s ⁻¹		
0	99.97	1566.63	30.77	-1.99E-04	0.000	0.000
1	87.76	1597.29	27.01	-1.04E-05	0.122	0.043
2	84.07	1598.63	25.87	-1.09E-05	0.159	0.056
3	80.44	1598.82	24.76	0.00E+00	0.196	0.070
4	76.69	1600.81	23.60	-1.19E-05	0.233	0.085
5	73.06	1601.04	22.48	-1.25E-05	0.269	0.099
6	69.53	1600.80	21.40	-1.31E-05	0.305	0.114
7	66.21	1597.15	20.38	-1.84E-05	0.338	0.128
8	62.52	1596.12	19.24	-1.95E-05	0.375	0.145
9	58.76	1596.77	18.08	-1.56E-05	0.412	0.162
10	55.29	1595.84	17.02	-1.65E-05	0.447	0.179
11	52.06	1596.49	16.02	-1.75E-05	0.479	0.196
12	48.77	1596.82	15.01	-3.74E-05	0.512	0.213
13	45.45	1596.93	13.99	-2.01E-05	0.546	0.231
14	42.19	1596.60	12.98	-2.16E-05	0.578	0.250
15	39.45	1597.89	12.14	-2.31E-05	0.606	0.267
16	36.25	1600.23	11.16	0.00E+00	0.638	0.287
17	33.49	1595.51	10.31	-2.73E-05	0.665	0.306
18	30.57	1598.66	9.41	-2.99E-05	0.694	0.326
19	27.80	1599.29	8.56	-3.28E-05	0.722	0.347
20	25.74	1532.43	7.92	0.00E+00	0.743	0.364
21	23.34	1597.05	7.18	0.00E+00	0.767	0.384
22	20.91	1596.93	6.43	-4.37E-05	0.791	0.406
23	18.54	1596.84	5.71	-4.92E-05	0.815	0.430
24	16.21	1597.36	4.99	1.06E-05	0.838	0.455